Title
Analyses of the Response of Pavements Containing Ceramic Plugs for Vehicle Guidance

Author
Monismith, Carl L.

Publication Date
2004-08-01

CALIFORNIA PATH PROGRAM
INSTITUTE OF TRANSPORTATION STUDIES
UNIVERSITY OF CALIFORNIA, BERKELEY

Analyses of the Response of Pavements Containing Ceramic Plugs for Vehicle Guidance

Carl L. Monismith
University of California, Berkeley

California PATH Research Report
UCB-ITS-PRR-2004-28

This work was performed as part of the California PATH Program of the University of California, in cooperation with the State of California Business, Transportation, and Housing Agency, Department of Transportation; and the United States Department of Transportation, Federal Highway Administration.

Final Report for Task Order 4219

August 2004

ISSN 1055-1425

ANALYSES OF THE RESPONSE OF PAVEMENTS CONTAINING CERAMIC PLUGS FOR VEHICLE GUIDANCE

REPORT
To

California Path Program
Institute for Transportation Studies
University of California, Berkeley

By

Carl L. Monismith
Pavement Research Center
Institute for Transportation Studies
University of California, Berkeley

Final Report for MOU 4219
March 2004

EXECUTIVE SUMMARY

In studies undertaken by staff of the PATH Program concerned with automatic vehicle control (AVC) ceramic sensors (magnets) have been placed at or near the surface of both asphalt concrete (AC) and portland cement concrete (PCC) pavements. Thus far sensors have been installed at three locations: 1) AC pavement at the Richmond Field Station (RFS); 2) AC and PCC pavement on Interstate 15 in San Diego, CA; and 3) AC and PCC pavement on Interstate 80 near Donner Summit, CA. The installations at Donner Summit have been used for the guidance of snow plows during the winter months.
With increased interest in dedicated truck lanes for goods movement where vehicle guidance could have significant economic influence (1,2,3,4) as well as for uses like those at Donner Summit noted above, the question arises relative to the long-term effects of these sensors on the satisfactory performance of the pavement/sensor system. Potential reductions in pavement and/or sensor performance could result from interactions between the vehicle, the sensor and the pavement as well as from environmental effects because of the embedment of a material with dissimilar thermal characteristics to that of the pavement.

Accordingly, the purpose of this investigation has been to examine the influence of the sensor on pavement performance, specifically cracking, considering both the effects of traffic loading and temperature changes. A major effort of the study has been devoted to a series of simulations considering both the effects of a range in traffic loading conditions and temperature changes on representative pavement structures containing the type of sensor currently in use in California. To assess the reasonableness of the simulations, a limited traffic loading study was conducted on an asphalt pavement containing the sensors using the Heavy Vehicle Simulator (HVS) operated by the Pavement Research Center (PRC). The AC pavement section was subjected to more than 300,000 repetitions of a dual tire truck configuration representative of one-half of a legally loaded standard single axle.

For the analytical study an epoxy resin binder (a thermoset plastic) was used to partially bind the sensors to both an AC and a PCC pavement. The HVS test, on the other hand, used three asphalt type binders (thermoplastic materials). In the latter study, all three materials provided a bond between the sensors and the AC pavement although the overcoat remained soft and required the addition of additional material during the HVS loading.

The analytical study indicated that thermal stresses may lead to cracking in the vicinity of the sensors for cold temperature environments. However, for the case of an AC overlay placed over the cores installed in existing PCC pavement, thermal stresses for the cold temperature conditions were higher near the joints of the PCC than in the vicinity of the cores. While the analytical study incorporated an epoxy binder for the sensors at the cold temperatures used for the study, it is likely that a similar stress pattern would be developed with the three asphalt materials since the materials became essentially elastic in response at these low temperatures.

In this study only been one magnet configuration used although a number of different bonding materials have been used including the following: 1) I-15, San Diego, epoxy binder in both AC and PCC pavements; 2) I-80, Donner Summit, two types – flexible (asphalt) seals and concrete patching material; and 3) HVS test, three flexible (asphalt) materials.

No attempt has been made to optimize sensor geometry or installation procedure to minimize distress in the pavement structure. It is likely that stress concentrations in the vicinity of the sensors due to both mechanical and thermal loading can vary significantly depending on the size (diameter and length) of the sensors and the installation methods (including drilling methods, the gap between the top of the magnetic marker and the road surface, filling materials, etc.). Development of an optimized method will help reduce the stress level thus preventing the damage to the pavement structure that may result in premature failure of the pavement. Accordingly future effort should be directed to optimize the entire configuration of the sensor to minimize adverse effects to pavements.

ANALYSES OF THE RESPONSE OF PAVEMENTS CONTAINING CERAMIC PLUGS FOR VEHICLE GUIDANCE

REPORT

To

California Path Program

Institute for Transportation Studies
University of California, Berkeley

By

Carl L. Monismith
Pavement Research Center
Institute for Transportation Studies
University of California, Berkeley

Final Report for MOU 4219

March 2004

TABLE OF CONTENTS

LIST OF FIGURES

LIST OF TABLES

EXECUTIVE SUMMARY

INTRODUCTION

Ceramic sensors (magnets) for automated vehicle control (AVC) have been placed at or near the surface of both asphalt concrete (AC) and portland cement concrete (PCC) pavements. In the studies undertaken by staff of the PATH* Program for AVC, one type of sensor has been utilized and has been located longitudinally at approximately 4-ft intervals along the center line of a lane in both types of pavements. In California the sensors have been installed at three locations: 1) AC pavement at the Richmond Field Station (RFS); 2) AC and PCC pavement on Interstate 15 in San Diego, CA; and 3) AC and PCC pavement on Interstate 80 near Donner Summit, CA. The installations at Donner Summit have been used for the guidance of snow plows during the winter months.

With increased interest in dedicated truck lanes for goods movement where vehicle guidance could have significant economic influence (1,2,3,4) as well as for uses like those at Donner Summit noted above, the question arises relative to the long-term effects of these sensors on the satisfactory performance of the pavement/sensor system. Potential reductions in pavement and/or sensor performance could result from interactions between the vehicle, the sensor and the pavement as well as from environmental effects because of the embedment of a material with dissimilar thermal characteristics to that of the pavement.

Accordingly, the purpose of this investigation has been to examine the influence of the sensor on pavement performance, specifically cracking, considering both the effects of traffic loading and temperature changes. A major effort of the study has been devoted to a series of simulations considering both the effects of a range in traffic loading conditions and temperature changes on representative pavement structures containing the type of sensor currently in use in California. To assess the reasonableness of the simulations, a limited traffic loading study was conducted on an asphalt pavement containing the sensors using the Heavy Vehicle Simulator (HVS) operated by the Pavement Research Center (PRC). The AC pavement section was subjected to more than 300,000 repetitions of a dual tire truck configuration representative of one-half of a legally loaded standard single axle.

---

* PATH is the acronym for Partners for Advanced Transit and Highways

Results of the simulations, performed by Dr. S. Weissman of the Symplectic Engineering Corporation, are summarized and engineering considerations for their use in pavements for a range of environments are discussed. The Symplectic report is included as an addendum to this report. Also included are the results of the HVS test program.

Based on the information obtained from both the simulations and the limited HVS test program, a discussion is provided of pavement and materials engineering considerations which should be evaluated if more widespread use of this type of vehicle guidance system is contemplated, e.g. for use in dedicated truck lanes for goods transport.

1.0 APPROACH

The investigation reported herein included the following activities:

1. *Program Formulation*. Meetings with the PATH and Caltrans Staff were held during the project to enable the PRC Staff to obtain the requisite background knowledge and to define and obtain needed information so that the analysis and test programs could be effectively completed.
2. *Analysis Program.* Based on the discussions with the PATH Staff, an analysis program was developed. This program consisted of a series of three-dimensional finite element idealizations of pavement sections containing a series of sensors. Both PCC and AC sections were included. These sections were subjected to truck loadings in two representative temperature environments. The analyses, performed by the Symplectic Engineering Corp., are summarized subsequently in this report.
3. *HVS Loading-AC Pavement*. During the period June – August 2003 an asphalt concrete pavement containing 12 sensors (of the type used in the California pavement installations) was subjected to 322,000 repetitions of a 52 kN (10,000 lb. load) on dual tires. The sensors were installed in the pavement using three types of bonding materials. Following completion of the HVS loading, cores were taken from the pavement to permit examination of the segments of the pavement containing the sensors.

The following sections summarize the results of these activities.

2.0 PROGRAM FORMULATION

A series of meetings were held with PATH and Caltrans Staff during the course of the investigation to: 1) define the scope of the investigation; 2) insure that requisite information on sensor and bonding material characteristics as well as installation methodology were made available to the PRC Staff; 3) to obtain cores containing sensors from both AC and PCC pavements from in-service pavements (I-15 and I-80); and 4) to define the HVS test section layout for sensor locations.

Caltrans and Path Staff who participated in the various meeting and field trips included the following:

Staff	**Organization**	**Function**
Dr. Wei Bin Zhang	PATH	Program Advisor
Dr. Chin Woo Tan	PATH	Program Advisor
Mr. Asftand Siddiqui	Caltrans – Div. R & I	Program Manager
Mr. David Evans	Caltrans – District 11, Pavement Engineer	I-15 core sampling
Mr. Lin Barton	Caltrans – District 11, Traffic Engineer	I-15 core sampling
Mr. John Eicholtz	Caltrans – District 11, Driller	I-15 core sampling
Mr. Michael Jenkinson	Caltrans – Div. R & I	Core locations, I-80 near Donner Summit

Formulation of the analysis program to be accomplished by Symplectic evolved in a series of stages. Initially the plan was to examine sensor size and placement as well as truck axle location relative to the sensor for two temperature environments. As the finite element simulations were formulated and the initial results were obtained and discussed with PATH and Caltrans Staff, the decision was made to narrow the program because of funding limitations. Accordingly, one sensor type and installation, representative of the I-15 installation was selected for use.

The initial finite element simulations as well as the remaining analyses were based on information from cores obtained by District 11 Staff on 13 January 2001 from the I-15 freeway in San Diego, CA. A representative sketch of the sensor installation is shown in Figure 1a and a photograph of the core which has been saw cut to expose the sensor in Figure 1b. Appendix A

contains a sketch showing the approximate locations from which the four cores were obtained as well as photographs taken during the core sampling program.

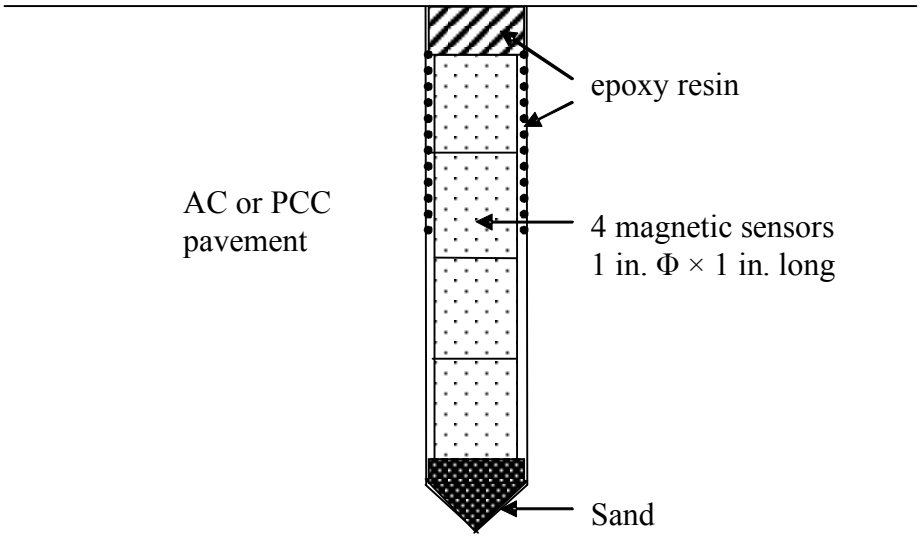

a. Cross section through pavement in vicinity of magnetic sensors.

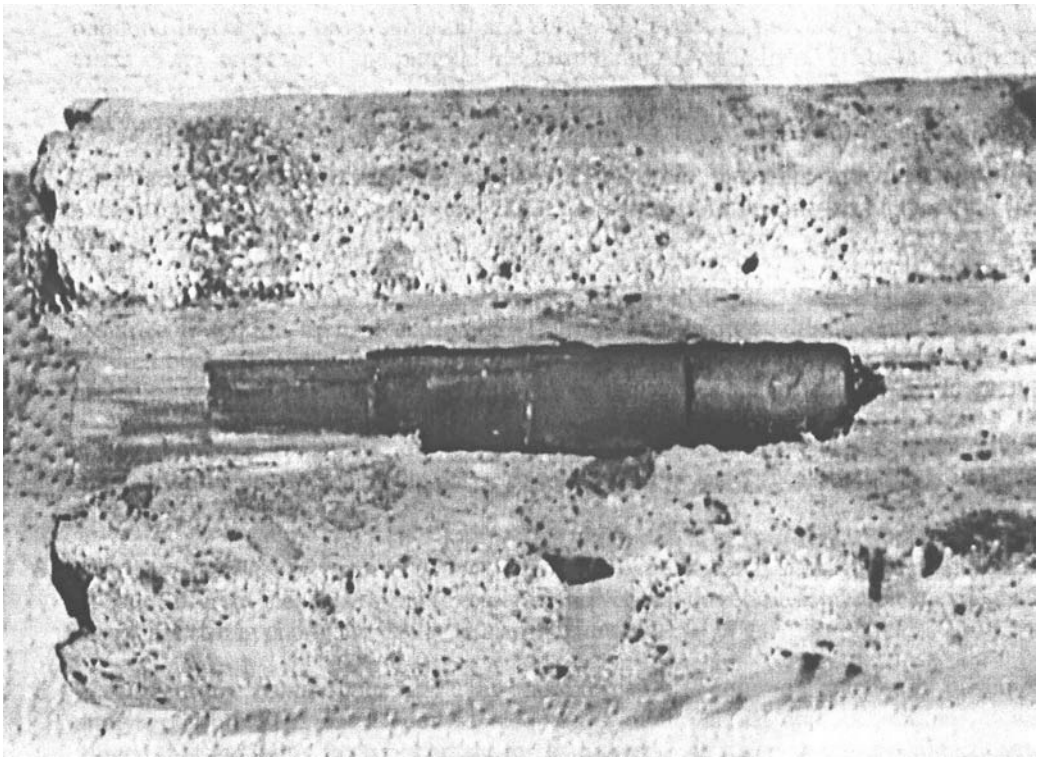

b. Photograph of core from I-15 PCC pavement sawcut to show magnetic sensors.

Figure 1. Sensor installation, I-15 San Diego, CA

Near the conclusion of the analytical studies at a meeting with the PATH and Caltrans Staff, the decision was made to obtain cores from the I-80 pavements near Donner Summit in order to provide information on the behavior of pavement sections with a "cold" winter. The intent of these cores was to provide information on the effects of thermal stresses on potential cracking of the pavement adjacent to the holes drilled to contain the magnetic sensors.

C.L. Monismith together with Caltrans Staff visited I-80 near Donner Summit on 31 October 2002 to select sites for cores in both the AC and PCC pavement sections. The sites and number of cores were as follows:

1. Westbound in #2 lane from Donner Lake interchange in PCC pavement, one core, flexible (black) sealant.
2. Westbound in #2 lane in AC overlay (6-12 in. thick):
   a. Two cores: one from cracked area and one from uncracked area, flexible sealant
   b. Two cores: from representative sections, concrete patch material sealant
3. Eastbound at Norden overcrossing in new PCC pavement, one core.

Based on the timing of the site visit, it was decided that there would be insufficient time to obtain cores and install new sensors prior to the onset of snow in amounts requiring the use of the snow plows. (The sensors are used to guide the snow plows so that they can operate under even severe "white out" conditions). By late Spring 2003 budget stringencies precluded obtaining the cores. *While the project has been completed, it would be very desirable to obtain these cores for evaluation by the PRC and PATH/Caltrans Staffs when funds permit.*

3.0 ANALYTIC STUDIES

The analytical studies were performed by Dr. Shmuel Weissman of the Symplectic Engineering Corporation. His report on this phase of the project is attached as *Addendum 1*. This section contains a brief summary and interpretation of the results of the report.

3.1 Analysis Parameters

Five different pavement structures were analyzed. Table 1 contains a summary of the pavement structures including compositions and layer thicknesses. Three dimensional finite element models were used to represent these structures, details of which are included in *Addendum 1*.

Two temperature profiles were utilized: 1) a cold weather profile based in the mean low temperatures observed at Fairbanks, Alaska during the period December 1997 to January 2001; and 2) a hot weather profile based on mean temperatures observed at Palmdale, California during the period April 1998 to January 2001.

Traffic loading was simulated by a single axle with 2 sets of dual tires. A tire pressure of 690 kPa (100 psi) and a dual tire load of 52 kN (10,000 lb) were assumed. The tire-pavement contact stress distribution used for these conditions was based on measurements reported in Reference (5) and included the horizontal longitudinal and transverse stress components as well as the vertical stress distribution. To simulate traffic wander and longitudinal positioning of the tires relative to the sensor, the tires were moved between 9 different lateral and three different longitudinal positions for a total of 27 positions evaluated.

Table 1. Pavement Systems

Material	Pavement System, Layer thicknesses, mm (in.)				
	1	**2**	**3**	**4**	**5**
Overlay	-	-	-	-	50.8 (2.0) (AC)
Surface course	203 (8.0) (AC)	305 (12.0) (AC)	229 (9.0) (PCC)	305 (12.0) (PCC)	203 (8.0) (PCC)
Untreated Aggregate Base	203 (8.0)	203.8 (8.0)	152 (6.0)	152 (6.0)	152 (6.0)
Untreated Aggregate Subbase	305 (12.0)	305 (12.0)	305 (12.0)	305 (12.0)	305 (12.0)
Subgrade 1	Infinite	Infinite	Infinite	Infinite	Infinite

All materials were assumed to behave elastically although the stiffness moduli of the AC layer and the epoxy binder used to bind the magnetic sensors to either the AC or PCC layer were assumed to be temperature dependent. *Addendum 1* contains a detailed discussion of the stiffness (Young's) moduli and Poisson's Ratio used for the analyses.

The finite element idealization of the pavement in the vicinity of the magnetic sensor is shown in Figure 2. This configuration resulted from the information obtained from the cores taken from the I-15 pavement, e.g. Figure 1.

Prior to performing the detailed analyses for each of the five pavement systems, a finite element analysis was conducted for a structure similar to No. 1 in Table 1 in which three sensors were located 1.1 m (4.0 ft) apart. Results of the analysis indicated that the stress concentration present near a tire load and near a plug exhibited a rapid decay with distance. As a result, it was concluded that the presence of adjacent sensors has only a marginal effect on the stress distribution at any given sensor. Accordingly only a single sensor was used in the succeeding analyses of the five structures.

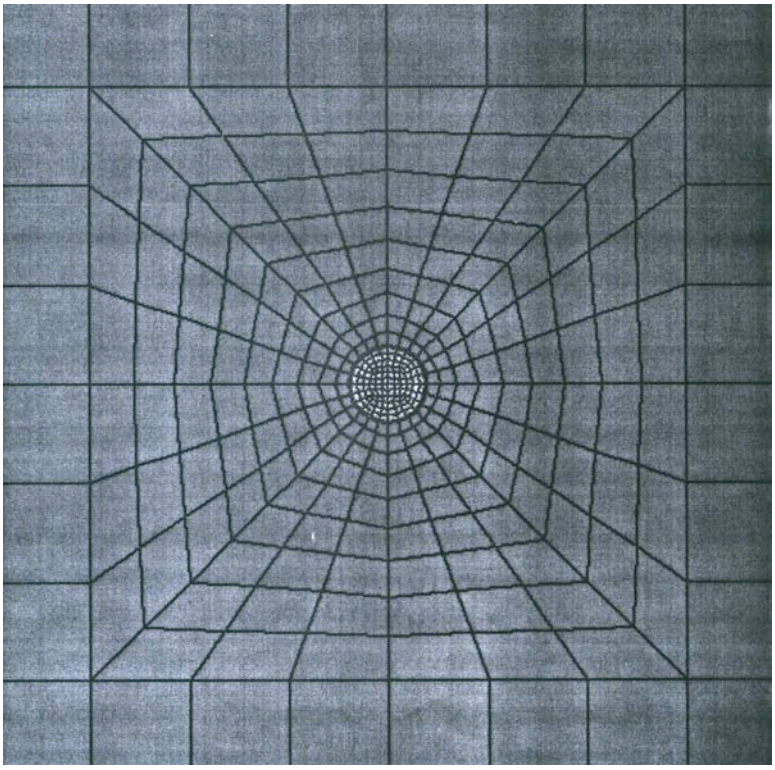

a. Plan view of the mesh near the magnetic plug

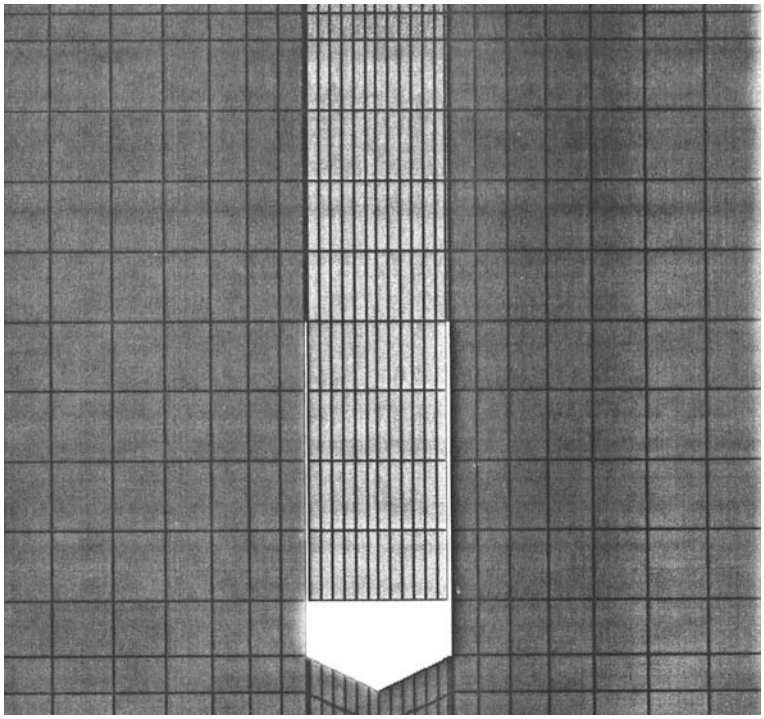

b. Transverse vertical section through the center of the plug

Figure 2. Mesh configuration in the vicinity of the magnetic sensor.

3.2 Summary of the Analyses

In general, the results of the finite element simulations indicate that the stresses near the sensors may be as much as three times as high as those away from the sensors. This finding is consistent with classical results of stress concentrations near a circular hole. Accordingly, the presence of the magnetic reasons may have an adverse effect in pavement service life.

Traffic load and thermal effects were evaluated independently. For traffic loading, the stresses near the sensors are significantly smaller than those in the vicinity of the tires when the truck is driving in a lane (i.e. the sensors are aligned with the transverse center of the vehicle). Thus, even when the stress concentration resulting from the presence of the magnetic sensors is considered, the sensors will likely have no influence on pavement service life. When a truck changes lanes, however, one set of tires may come close or traverse over the sensor. For this situation, the higher stresses may have an adverse effect on the pavement. Consideration of fatigue cracking in AC or PCC, which results from repetitive stress (or strain) applications, may have to be evaluated by assessing the probability of lane changes during the expected period of pavement performance.

The presence of magnetic plugs is more relevant to the effects of stresses resulting from low temperatures resulting in thermal stresses of significant magnitude. With the exception of structure 5 (the AC overlay on the PCC pavement with the sensor embedded in the PCC), the highest stresses are obtained at the interface between the pavement and the magnetic sensors (i.e. along the walls of the drilled hole). It is likely that thermal cracking would initiate near the sensor. This finding suggests the desirability of optimizing the sensor-epoxy installation both in terms of geometry and materials. Moreover it would appear necessary to analyze the pavement/sensor system for a range of temperature environments since the optimal design may be dependent on the temperature environment.

4.0 HVS TEST PROGRAM

A limited traffic loading program was accomplished using the Heavy Vehicle Simulator (HVS). Figure 3 contains a diagram and specifications for this equipment purchased from the Council for Scientific and Industrial Research (CSIR) of South Africa in 1994.

Wheel loads of up to 200 kN (45,000 lb.) are applied on a half axle using dual, standard-size truck tires or a single aircraft lane. The loads move in either a bi-directional (for fatigue cracking evaluation) or a unidirectional (for permanent deformation evaluation) mode at speeds up to 10 km/h. (6.2 MPH). At this rate, up to 18,000 load repetitions can be applied per day in the bi-directional mode. Longitudinal wheel travel is 8.0 m (26.2 ft.) and lateral travel is programmable over 1.5 m. (4.9 ft.) (6).

For this investigation, a 52 kN load was applied to the dual radial tire configuration and repetitive loading was applied in the bi-directional mode.

Overall weight:		59,646 kg (131,500 lbs.)
Load weight of the test wheel		20-100 kN (4,500-22,500 lbs.) with truck tire 20-200 kN (4,500-45,000 lbs.) with aircraft tire
Tire Pressure		690 kPa
Dimensions of tested area of pavement		1.5 m × 8 m (4.9 ft × 26.2 ft) maximum
Velocity of the test wheel		10 km/h (6.2 mph) maximum
Maximum trafficking rate		1000 repetitions/hr
Average trafficking rate		750 repetitions/hr
Average daily repetitions		16,000 (including daily maintenance)
Engines:	Hydraulic plant	10-cylinder diesel
	Electrical plant/hydraulic control	6-cylinder diesel
Dimensions:	Length	22.56 m (74 ft
	Width, overall	3.73 m (12 ft)
	Height	3.7 m (12 ft)
	Wheel base	16.7m (55 ft)
Number of axles		3 (1 in rear, 2 in front)

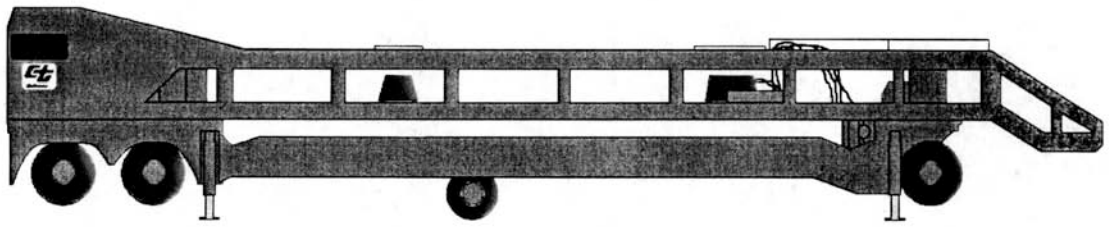

Figure 3. Diagram and specification of HVS.

4.1 Materials and Test Section

Based on conversations with W.B. Zhang and correspondence with Caltrans staff, three materials were selected for providing sealing and bonding of the magnet sensors in the HVS test section. These materials are:

1. Asphalt emulsion sealant, State Specification 8040-41A-15; obtained from Reed and Graham, San Jose.
2. Dotstick; obtained from Henry Co., Elk Grove
3. Flexible Dotstick; obtained from Henry Co., Elk Grove

No physical tests were performed to identify these three materials. Presumably the material termed Dotstick meets Caltrans Standard Specification, Section 85-1.055.

The test section is part of a pavement constructed in Building 280 at the Richmond Field Station according to Caltrans specifications and used to study the response of new and overlay AC pavements to repeated trafficking. This pavement section consisted of an asphalt rubber hot mix (gap graded) (ARHM-GG) placed as an overlay on an AC pavement consisting of a dense-graded asphalt concrete (DGAC) layer on top of asphalt-treated permeable base (ATPB), untreated aggregate base and subbase, and a clay subgrade.

Layout of the test pavement for loading by the HVS is shown in Figure 4; this section is 8 m. (26.2 ft.) long by 1 m. (3.28 ft.) wide. The 1 m. (3.28 ft.) sections at each end (grey areas in Figure 4) are where the load reverses direction; pavement performance is observed/measured in the remaining 6 m. (19.7 ft.) length. It will be noted that it is within this area that the magnetic sensors were installed. One set of sensors was installed along the center line of travel of the dual truck wheel while the other was installed just outside (0.86 m.) the wander pattern of the HVS load (±0.5 m.).

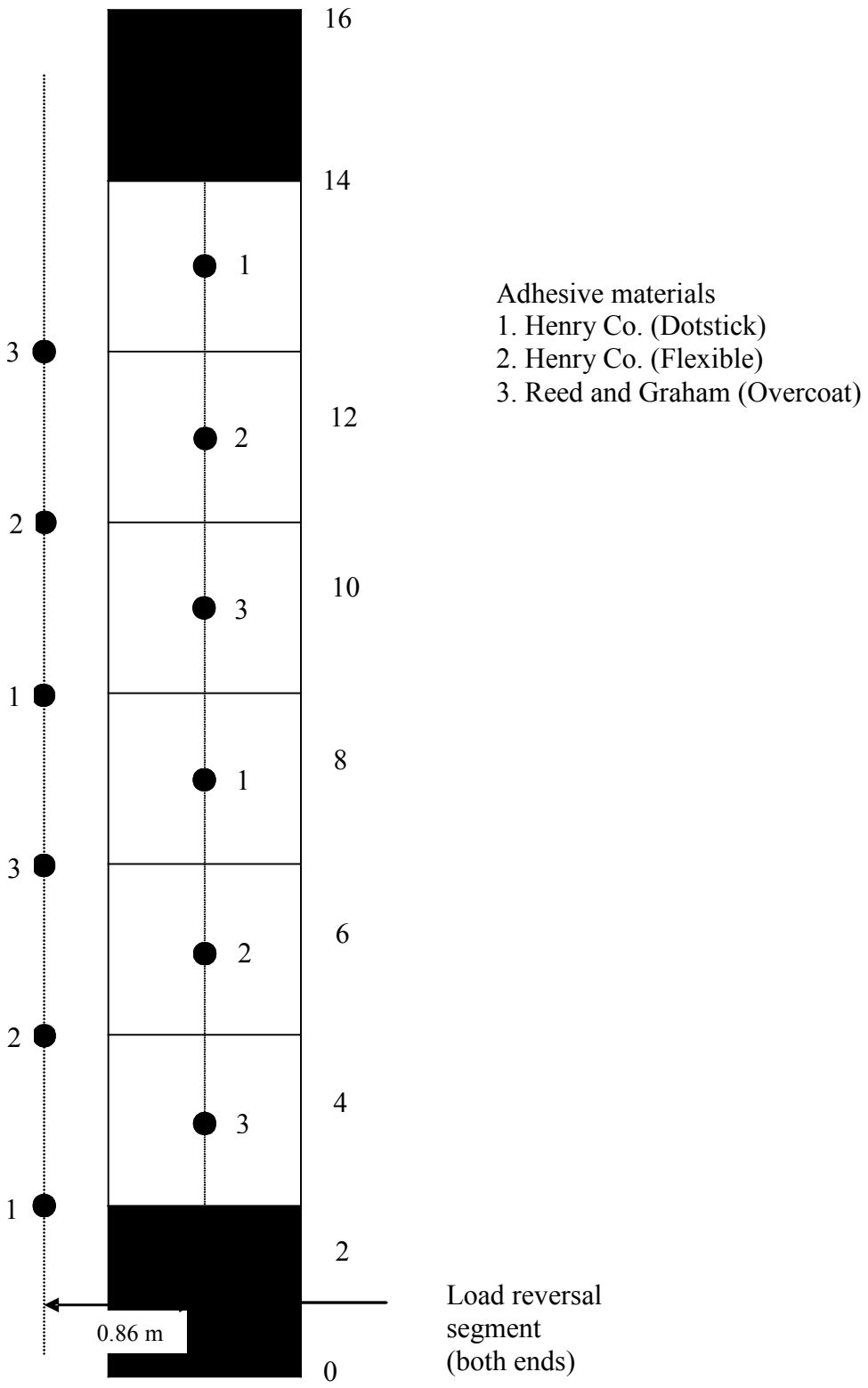

Figure 4. HVS Test Section Layout.

The wander pattern used in HVS testing has been designed to simulate observed traffic wander in the wheel path (5). The 0.86 m. distance was selected to simulate the location of a sensor just outside the traveled way to observe the performance of sensors representative of those located in the center of the lane. (N.B. clearance and pavement width limitations precluded this set of sensors being created a larger distance, 2.6 m., from the center line of travel of one set of dual wheels).

To install the sensors, 1 in. diameter by 5 ½ in. deep holes were drilled in the AC followed by placement of a ½ in.-layer of sand in the bottom of the hole. Sealant was then placed in the hole followed by insertion of three magnets. The Overcoat material was poured at the ambient temperature while the 2 Dotstick materials were heated to 149ºC (300ºF) prior to placement.

In placing the cores, it was observed that cleaning the holes prior to placement was essential; otherwise the sealants would not bond to the AC.

4.2 HVS Loading

Repetitive loading was conducted with the HVS for a total of 322,000 repetitions. Loading was applied as follows:

1. 22,000 repetitions with the standard wander pattern over the 1 m. width of the section at a wheel speed of 9.3 km. per hr.
2. 300,000 repetitions without wander (channelized loading) with one wheel of the dual tire configuration traversing directly over the gages on the center line of the test section at a speed of 6.5 km. per ht. (some equipment problems required that the loading pattern be changed and the speed reduced in order for the project to be completed within the available window of time).

At the conclusion of the HVS loading, six 6 in. diameter cores were taken from the trafficked area. The cores were drilled so that the magnetic sensors were at or near the core centers. These cores were then sawed to observe the core/pavement interfaces. Photographs of the cores with the magnets exposed were included in Appendix B.

4.3 Evaluation

The materials used to bind the magnets in the AC were different than that which had been used in the I-15 pavements (a thermoset plastic) and used in the analyses prepared by Dr. Weissman (included in A*ddendum 1* of this report). The Dotstick materials were thermoplastic materials which required heating so that they would be fluid enough for magnet installation; they solidified upon cooling. The Overcoat material, normally used as a crack sealer was fluid at ambient temperature (an asphalt emulsion) at the time of placement of the magnets; the water gradually evaporated leaving a solid asphalt residue.

While the Dotstick materials required heating in order to be poured into the drilled holes, when the magnets were inserted there occurred only a slight sinking which required placing a small amount of additional material on the surface. With the Overcoat material, on the other hand, considerable sinking of the magnets was observed and required several "fillings" at the pavement surface.

Visual observations of the cores indicate no apparent crackings in the vicinity of the sensor holes after the 300,000 plus repetitions. This would tend to support the analyses reported by Dr. Weissman for traffic loading at moderate temperatures. It must be emphasized that while the traffic loading was severe, the environmental conditions were not conducive to the development of high thermal stresses in this loading test.

5.0 SUMMARY AND DISCUSSION

This study has included a detailed analytical study of one type of magnetic sensor in both AC and PCC pavements as well as in a PCC pavement which has been overlaid with AC. It has also included a limited loading study using the HVS to test an AC pavement containing the magnetic sensors using three different materials to bind the sensors to the pavement.

For the analytical study an epoxy resin binder (a thermoset plastic) was used to partially bind the sensors to both an AC and a PCC pavement. The HVS test, on the other hand, used three asphalt type binders (thermoplastic materials). In the latter study, all three materials provided a bond

between the sensors and the AC pavement although the overcoat remained soft and required the addition of additional material during the HVS loading.

The analytical study indicated that thermal stresses may lead to cracking in the vicinity of the sensors for cold temperature environments. However, for the case of an AC overlay placed over the cores installed in existing PCC pavement, thermal stresses for the cold temperature conditions were higher near the joints of the PCC than in the vicinity of the cores. While the analytical study incorporated an epoxy binder for the sensors at the cold temperatures used for the study, it is likely that a similar stress pattern would be developed with the three asphalt materials since the materials became essentially elastic in response at these low temperatures.

Vehicle guidance may have a series of roles to play in transportation systems operations. This has already been demonstrated by the successful application to snow plow operations on I-80 near Donner Summit and more recently for precision docking of buses (7). The potential for vehicle guidance in dedicated bus and truck lanes also may lead to substantial savings in both guideway design, and in the case of trucks primarily, to savings in vehicle operating costs - particularly fuel costs (4).

Thus far there has only been one magnet configuration used. A number of different bonding materials have been used including the following: 1) I-15, San Diego, epoxy binder in both AC and PCC pavements; 2) I-80, Donner Summit, two types – flexible (asphalt) seals and concrete patching material; and 3) HVS test, three flexible (asphalt) materials.

No attempt has been made to optimize sensor geometry or installation procedure to minimize distress in the pavement structure. It is likely that stress concentrations in the vicinity of the sensors due to both mechanical and thermal loading can vary significantly depending on the size (diameter and length) of the sensors and the installation methods (including drilling methods, the gap between the top of the magnetic marker and the road surface, filling materials, etc.). Development of an optimized method will help reduce the stress level thus preventing the damage to the pavement structure that may result in premature failure of the pavement.

Accordingly effort should be directed to optimize the entire configuration of the sensor to minimize adverse effects to pavements.

6.0 REFERENCES

1. Fischer, M.J., D.N. Ahanotu, and J.M. Waliszewski, [2003], "Planning Truck-Only Lanes: Emerging Lessons from the Southern California Experience," *Transportation Research Board, 2003 Annual Meeting CD-ROM.*

2. Holguin-Veras, J., D. Sackey, S. Hussain, and V. Ochieng, [2003], "On the Economic and Financial Feasibility of Toll Truckways," *Transportation Research Board, 2003 Annual Meeting CD-ROM.*

3. Samuel, P., R.W. Poole, Jr., and J. Holguin-Veras, [2002], "Toll Truckways: A New Path Toward Safer and More Efficient Freight Transportation," Reason Foundation: Public Study.

4. Yin, Y., M.A. Miller, S.E. Shladover, "Assessment of the Applicability of Cooperating Vehicle-Highway Automation Systems of Freight Movement in Chicago," *Transportation Research Board*, January 2004.

5. de Beer, M. and C. Fisher. *Contact Stresses of Pneumatic Tires Measured with the Vehicle-Road Surface Pressure Transducer Army (VRSPTA) System for the University of California at Berkeley (UCB) and the Nevada Automotive Test Center (NATC)*. Vols. 1 and 2., Transportek, CSIR, South Africa, June 1997.

6. Harvey, J.T., J. Roesler, N.F. Coetzee, and C.L. Monismith. *Caltrans Accelerated Pavement Test (CAL/APT) Program, Summary Report, Six Year Period: 1994-2000.* Pavement Research Center, U.C. Berkeley. 2000.

7. Tan, Han-Shue, [2003], "Develop Precision Docking Function for Bus Operation," University of California: Institute of Transportation Studies, California PATH Program. UCB-ITS-PRR-2003-11.

APPENDIX A: CORE SAMPLING, I-15 FREEWAY, SAN DIEGO, CA, 13 JANUARY 2001

- Core Locations
- Photographs, Coring Operations

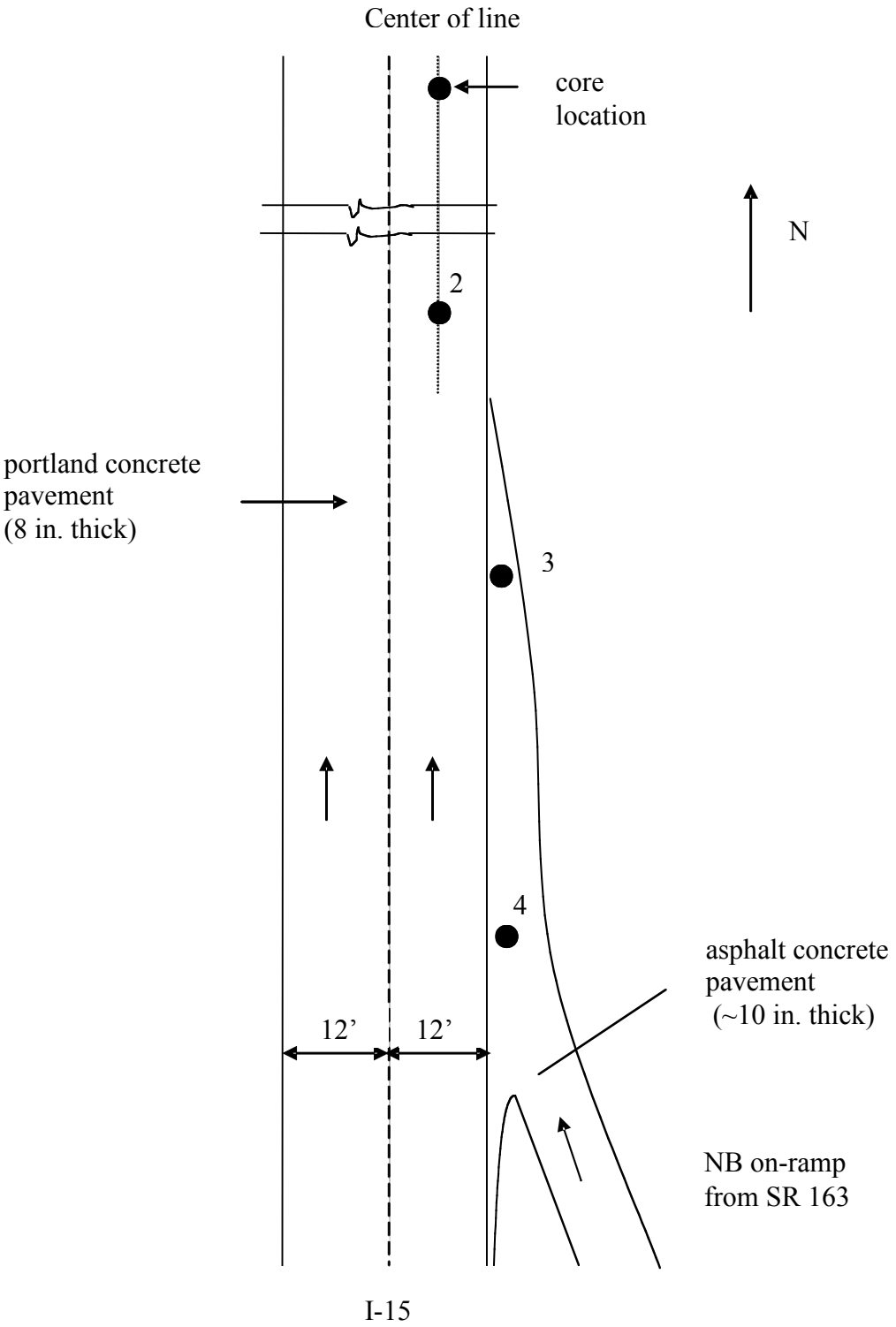

Figure A1. Core locations, I-15.

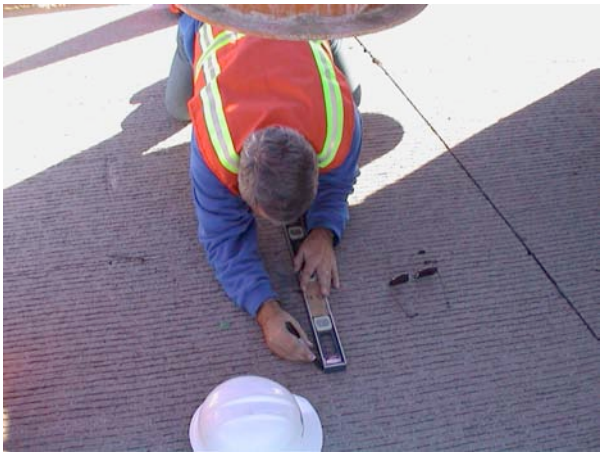

a. Marking line location, concrete pavement

b. Coring rig

c. Core extraction, concrete pavement

d. Asphalt pavement surface, magnet location prior to coring

Figure A2. Coring Operations

APPENDIX B: CORES CONTAINING MAGNETS, HVS TEST PROGRAM

a. Cores with magnets

b. magnets 2S, side view

c. Magnet 2S, top view

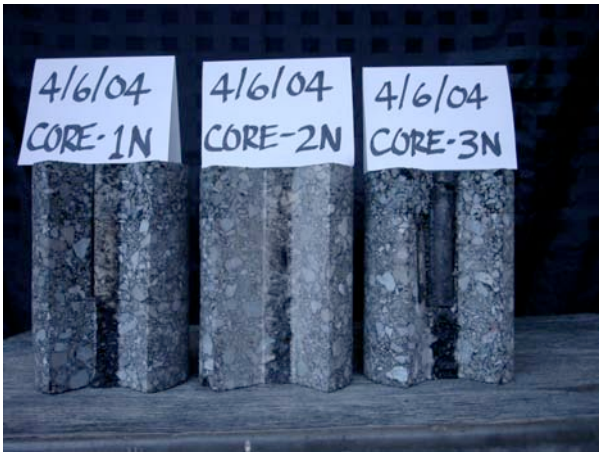

d. Cores with magnets

e. Magnet 1N, side view

f. Magnet 1N, top view

Figure B1. Core photographs.

g. Magnet 3N, side view

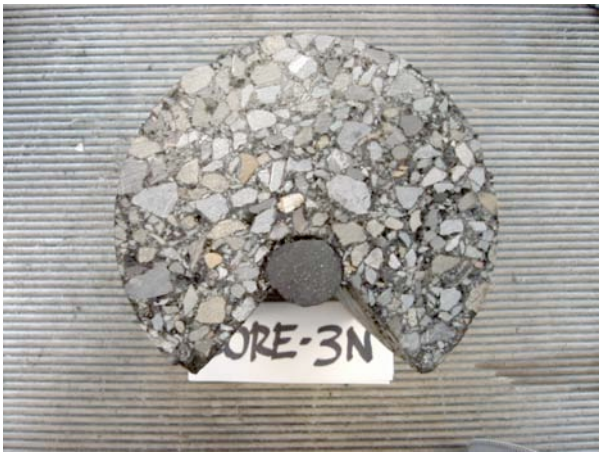

h. Magnet 3N, top view

Figure B1. Core photographs, continued.

ADDENDUM 1

Analytical Study of Pavements Containing Magnetic Sensors Subjected to Truck Loading in "Hot" and "Cold" Environments

Prepared for the Pavement Research Center

by

Symplectic Engineering Corporation

Berkeley, CA

June 2002

THREE-DIMENSIONAL FINITE ELEMENT ANALYSES OF TRAFFIC- AND THERMAL-INDUCED STRESSES IN THE VICINITY OF MAGNETIC PLUGS EMBEDDED IN ASPHALT CONCRETE AND PORTLAND CEMENT CONCRETE PAVEMENTS

By
Shmuel L. Weissman

ACKNOWLEDGMENT AND DISCLAIMER

This work was performed as part of the California PATH Program of the University of California, in cooperation with the State of California, Business, Transportation, and Housing Agency, Department of Transportation; and the United States Department of Transportation, Federal Highway Administration.

This Final Report is in support of Task No. 4219 (Agreement No. SA2993) under Master Interagency Agreement No. 65A0071.

The contents of this report reflect the views of the authors who are responsible for the facts and accuracy of the data presented herein. The contents do not necessarily reflect the official views or policies of the State of California. This report does not constitute a standard, specification, or regulation.

2901 Benvenue Ave., Berkeley, California 94705
telephone (510) 528-1251 • fax (510) 528-7102 • www.symplectic.com

Table of Contents

Table of Figures

Table of Tables

Executive Summary

The objective of this study is to quantify the stress concentrations that magnetic plugs cause in pavements when subjected to traffic and thermal loading. This information is required in order to assess the impact of the magnetic plugs on the service life of the hosting pavement. A series of three-dimensional finite element simulations is undertaken to this end, and the results are documented in this report and the accompanying CD.[1]

The systems studied are subjected to both traffic and thermal loading. The results indicate that for a vehicle driving in a lane, the stresses in the vicinity of the plugs are much smaller than those near the tires, and thus the plugs do not greatly affect the longevity of the pavement. However, when the vehicle changes lanes, the tires may move close enough to the plugs, such that the stress concentrations there exceed (by a factor of roughly three) the normal stresses in the pavements and therefore, statistical analysis should be used to investigate the accumulating damage resulting from the presence of the magnetic plugs, and its effect on the service life of the hosting pavement.

In the case of thermal loading, it was found that for both Portland cement concrete (PCC) pavements and asphalt concrete (AC) pavements, the extreme stresses in the pavement are near their interface with the plugs. Thus, thermal cracks are expected to initiate near the magnetic plugs. The only exception is found in PCC pavements with an AC overlay that bridges thermal joints (separating the PCC slabs). For overlay pavements the extreme stresses are located near the thermal joints and therefore, the presence of the plugs does not affect the performance of the pavement.

Finally, the results reported herein pertain to a single plug geometry and type of installation. It is quite possible that the magnetic plug and installation procedure can be optimized in terms of the device geometry and materials to reduce stress concentrations and thus, extend the lifespan of the pavement-plugs system. A finite element study where each desired property is changed independently, while keeping all others constant, is recommended as a way to achieve the optimized design.

[1] The accompanying CD provides animated “walks” through the models displaying various stresses and stress invariants. Detailed instructions for using the CD are provided in Section 6.1 of this report.

1. Introduction

Partnered for Advanced Transit and Highways (PATH) researchers designed a vehicle guidance and control system that depends on magnetic markers that are embedded in the pavement structure to achieve its goal. This system is described in Figure 1.1.

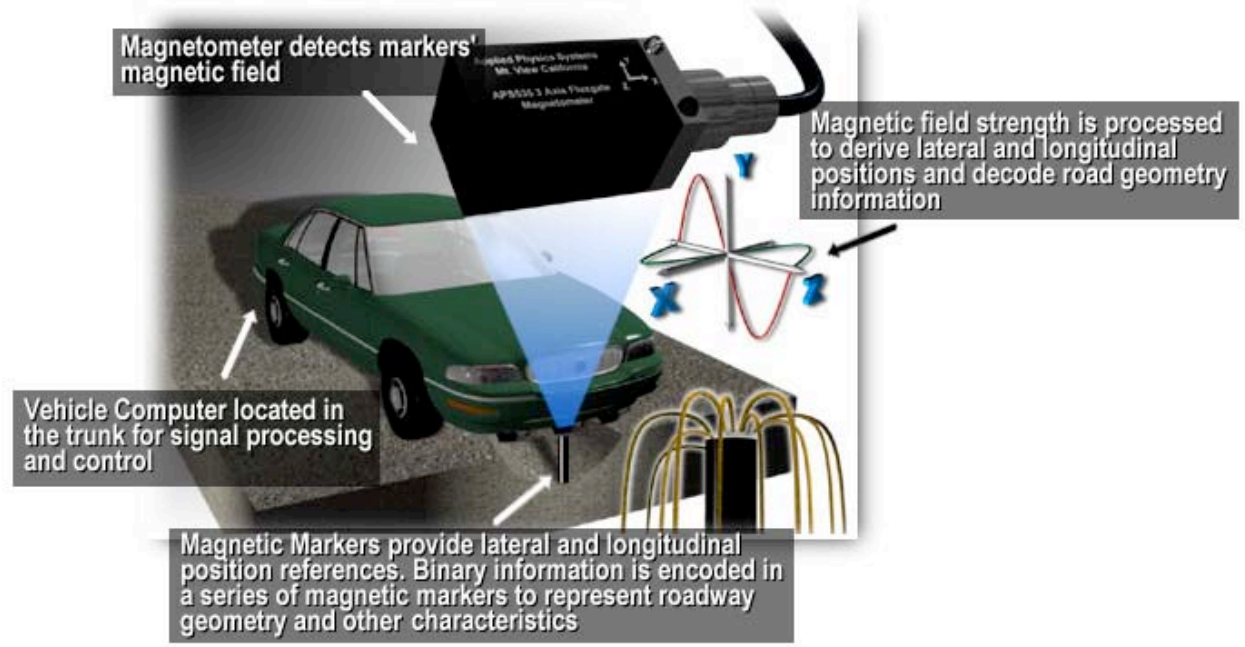

Figure 1.1: Description of the Magnetic Reference Sensing and Guidance System.[1]

The objective of the present study is to consider the impact of the magnetic markers, or "plugs," on the service life of pavements. To this end, a series of finite element simulations was undertaken to quantify the expected stress concentration in the vicinity of the plugs. The analysis described herein considered both thermal expansion and contraction, and traffic loading.

An outline of the report follows. Section 2 provides the attributes of the pavements studied. The plug installation is reviewed in Section 3, and Section 4 lists the major assumptions taken in constructing the finite element models. The finite element meshes, boundary conditions, and traffic and thermal loading are described in Section 5, and the simulation results are reviewed in Section 6. Conclusions and recommendations are contained in Section 7.

[1] Figure 1.1 is taken from http://www.path.berkeley.edu/PATH/Research/magnets.

2. Pavement systems analyzed

Five different pavement structures, labeled S1 through S5, are considered in this study as possible hosts for the magnetic plugs. The first two include asphalt concrete (AC) as the surface layer. The next two contain Portland cement concrete (PCC) as the surface layer. The last system includes a thin AC overlay over the original PCC surface. The layout of the five structures is provided in Table 2.1.

Table 2.1 structural layers configurations (thickness in meters)

Layer	S1	S2	S3	S4	S5
Overlay	--	--	--	--	0.0508 (AC)
Surface	0.2032 (AC)	0.3048 (AC)	0.2286 (PCC)	0.3048 (PCC)	0.2032 (PCC)
base	0.2032	0.2032	0.1524	0.1524	0.1524
Subbase	0.3048	0.3048	0.3048	0.3048	0.3048
Subgrade	infinite	infinite	infinite	infinite	infinite

3. Installation of the Magnetic Plugs

The magnetic plugs are cylindrical in shape, with a diameter of 0.0250 meters and a height of 0.1016 meters. To install the magnetic plugs a hole is drilled into the pavement that is about 0.12 meters deep, and about 0.0265 meters in diameter. Because the drill bit used has a cone shaped head the bottom of the hole retains this cone shape. This cone is sometimes filled with sand, but may also be left empty. The magnetic plug is inserted into the drilled cavity and is capped with epoxy, which fills also some of the gap between the magnet and the cavity walls. Figure 3.1 shows a cut through a sample plug installed in a PCC pavement.

Figure 3.1: A cut through a plug installed in a PCC pavement.

4. Modeling Assumptions

The following assumptions are made in simulations conducted in this study:

1. *Linear elastic material behavior*. All materials are assumed to exhibit linear elastic behavior. This assumption is not very good for the base, subbase and subgrade materials that are known to have very limited capacity to sustain tension. It is also not a very good approximation for AC, which is known, at elevated temperatures, to exhibit rate-dependence and large residual deformations (*i.e.*, plastic-like behavior). Unfortunately, it proved impossible to account for these properties within the time and budget confinements of this project. However, because of the highly localized zone of interest, which is the surface layer near the plugs, the importance of the nonlinear behavior of the unbound layers (*i.e.*, base, subbase, and subgrade layers) is probably secondary to the effect of the presence of the plug on the surrounding surface layer. Also, the properties selected for the surface layer do take rate effects into account (*i.e.*, properties were used that correspond to the effective properties at a normal highway speed).

2. *Temperature-dependent material properties*. All the materials modeled, with the exception of the magnetic plugs and PCC, are assumed to depend on temperature (see Section 5.2 below).

3. *Thermal expansion*. Only the surface layers (AC and PCC), the plug, and the epoxy are assumed to exhibit thermal expansion. Thermal expansion of the unbound layers was ignored because no data was made available regarding this effect, and it was judged that including it would have only a secondary effect on the stress distributions near the plugs.

4. *No interaction between the plugs*. The stress distribution at any given magnetic plug is assumed to be unaffected by the presence of adjacent plugs. This assumption is validated in Section 6.1 below.

5. *The magnetic plug is assumed as one continuous unit*. The actual magnetic plug is made of four different magnets strung together in the vertical direction. However, the magnetic forces are strong enough to justify this approximation.

6. *The layers are bonded together*. This approximation is common practice in pavement analysis. While it is not a good representation of the actual contact problem, it was judged that modeling the true contact forces between the layers would not significantly alter the results, but would require a much larger computational effort that could not be accommodated under the budget constraints of the current project.

7. *Full bonding between plug and epoxy, and between epoxy and pavement*. This representation is justified by Figure 3.1, which shows a core, taken out of a pavement in service, where the epoxy is fully bonded to both the PCC and the plug.

5. The Finite Element Models

The different finite element meshes used to predict the stress distributions near the magnetic plugs are described in this section. The geometrical attributes of the meshes, including the specification of the boundary conditions are provided in Section 5.1. The (temperature-dependent) material properties are listed in Section 5.2, and the temperature profiles considered are tabulated in Section 5.3. The applied traffic loading is detailed in Section 5.4.

5.1 Geometrical models

Three-dimensional finite element models were used to determine the stress distributions in the vicinity of the magnetic plugs, resulting from both traffic and thermal loading. Each of these meshes contains roughly 90,000 elements and nodes, and about 270,000 degrees-of-freedom.[2] Two types of meshes are used. First, a mesh where the surface layer extends infinitely in the direction of driving, but is bounded in the lateral direction. This class of meshes, denoted "M1," is used in the simulations of traffic loading, and for structures S1 and S2 also for the simulation of stresses due to thermal expansion/contraction. A perspective view of an M1 mesh is shown in Figure 5.1.

A second class of meshes, denoted "M2," is used to model thermal expansion/contraction for structures S3, S4, and S5. In the M2 class, the PCC layer is modeled as slabs separated by thermal joints and therefore, thermal stresses are significantly diminished. The M2 class meshes include only one slab with free lateral and longitudinal edges. A perspective view of an M2 class mesh is shown in Figure 5.2.

Table 5.1 summarizes the planer dimensions and boundary conditions. Also, the bottom surface of the subgrade layer is fixed in the vertical direction. In all meshes, the plug is located in the center in both the lateral and longitudinal directions.

Table 5.1: Planned dimensions and boundary conditions.

		Dimensions (m)		Edge boundary conditions	
Mesh	Layer	Longitudinal	Lateral	Longitudinal	Lateral
M1	bounded[3]	9.7908	6.7908	symmetry[4]	free
	unbounded[5]	9.7908	9.7908	symmetry	symmetry
M2	AC overlay	4.5840	3.6576	symmetry	free
	PCC	4.5720	3.6576	free	free
	unbounded	7.5720	6.6576	symmetry	symmetry

[2] The exact number of nodes, elements, and degrees-of-freedom depends on the number of layers in the system (*i.e.*, four layers for S1 through S4 structures, and five for the S5 structure).
[3] Layers with a free edge in the lateral direction (*i.e.*, AC, PCC, and the AC overlay).
[4] A symmetry boundary condition in direction X implies no motion in that direction.
[5] Layers that extend indefinitely in the lateral direction (*i.e.*, base, subbase, and subgrade).

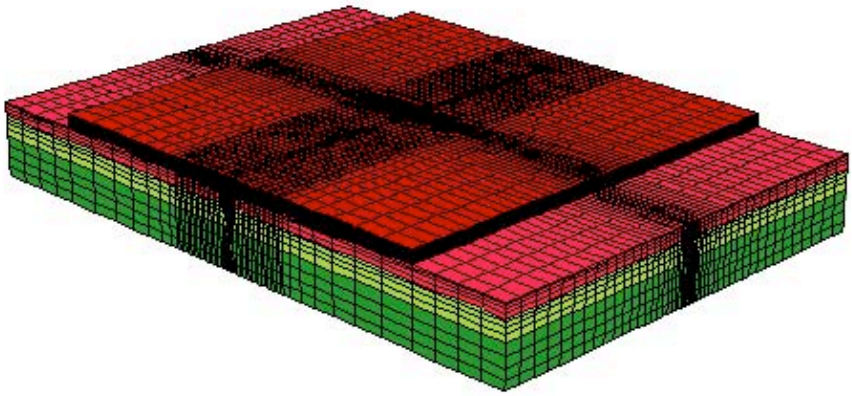

Figure 5.1: A perspective view of an M1-class mesh.

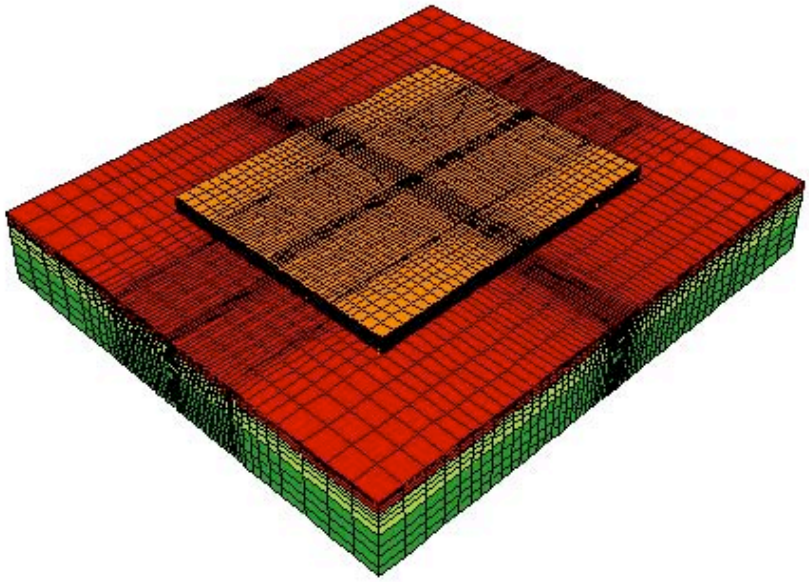

Figure 5.2: Perspective view of an M2-class mesh.

Figures 5.1 and 5.2 also show that the meshes are constructed in such a way that they are significantly refined in the vicinity of the magnetic plugs. Figure 5.3 offers a plan view of the mesh in the vicinity of the magnetic plug clearly illustrating the mesh refinement in that area.

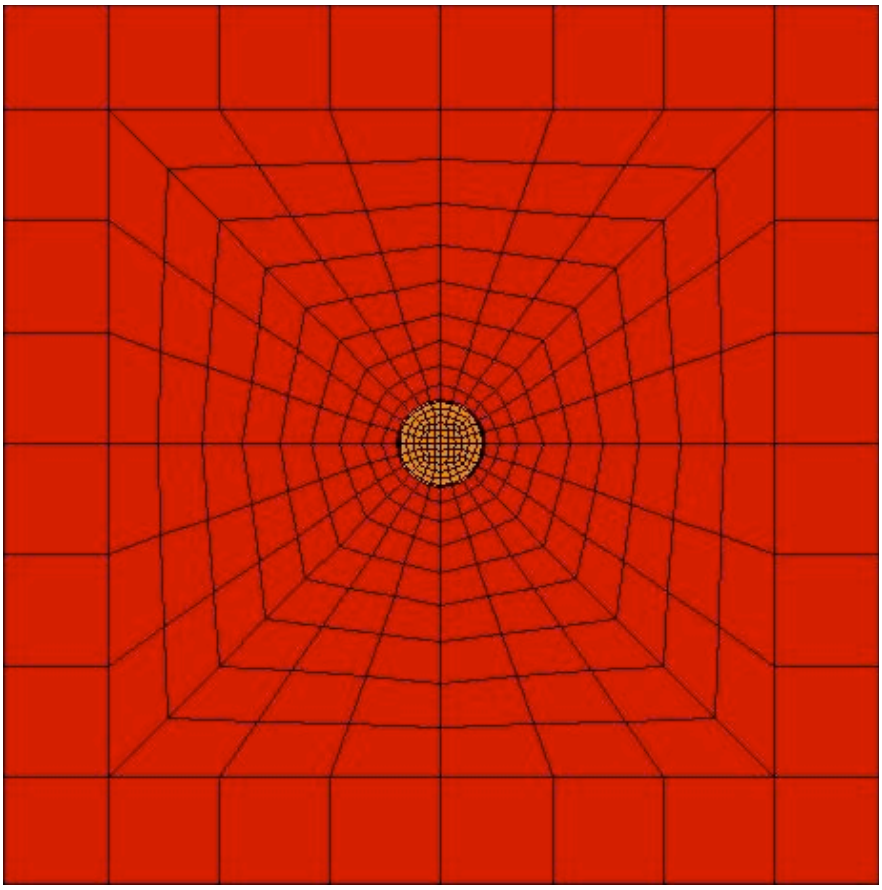

Figure 5.3: Plan view of the mesh near the magnetic plug.

Figure 5.4 shows the transverse-vertical section through the center of the magnetic plug. Some important details of the mesh construction are revealed in this image. First, the epoxy is assumed to form a cap encapsulating the upper half of the magnetic plug, and connecting it to the sides of the drilled cavity walls. The lower half of the magnetic plug is modeled as being suspended in the air. Second, it is assumed that there is no sand fill under the plug (this being a more conservative case). Third, the angle of the cone, which forms the bottom part of the drilled cavity, is taken as 30° with the horizon. Fourth, the diameter of the drilled cavity is assumed to be 0.0265 meters (*i.e.*, 0.00075 meters of epoxy or air separate the magnetic plugs from the cavity walls). Fifth, it is assumed that there is a gap of 0.01 meters between the bottom of the magnetic plug and the top of the cone.

5.2 Material Properties

All the materials in the mesh are modeled as linear elastic. However, their properties may be temperature-dependent. If a certain property is assumed to increase with temperature, then its value at a specified temperature "T" is given by the following general form:

$$P(T) = F(T) \cdot P_{max} \tag{5.1}$$

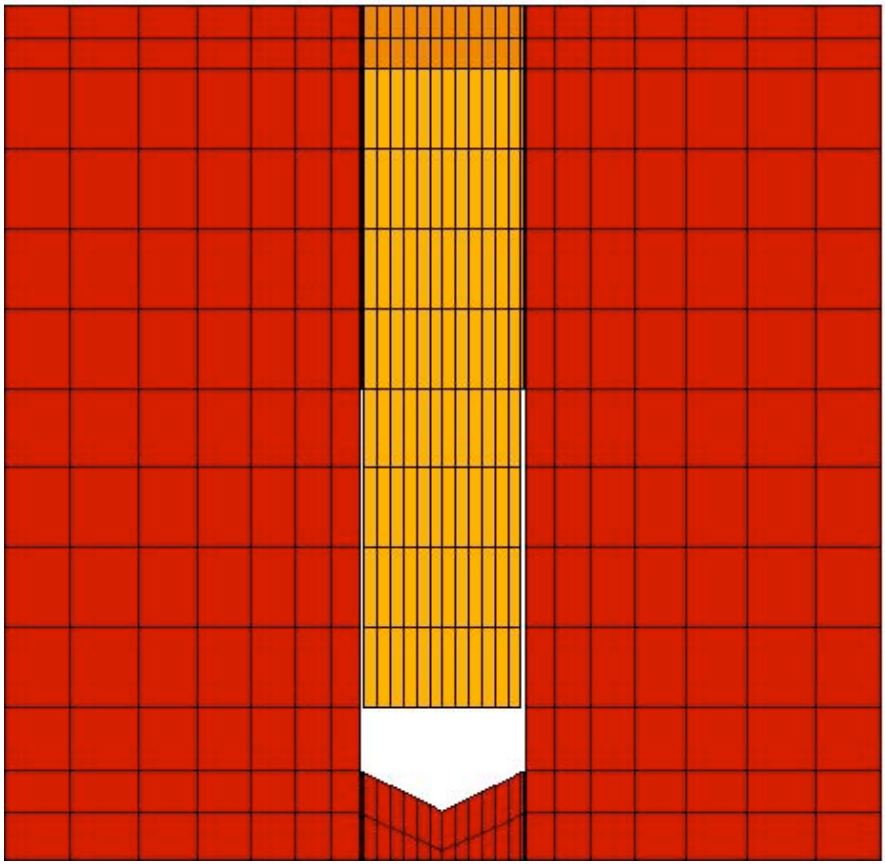

Figure 5.4: Transverse-vertical section through the center of the plug.

where P is the property, T is the temperature in degrees Kelvin, P_{max} is the asymptotic value of P as T increases, and F(T) is given by:

$$F(T) = \delta + \frac{1}{2\gamma} + \frac{1}{\pi\gamma}\operatorname{atan}\left[\alpha(T-\beta)\right] \tag{5.2}$$

where α, β, γ, and δ are material properties. Similarly, properties whose value decreases with temperature are computed using

$$P(T) = G(T) \cdot P_{max} \tag{5.3}$$

where P_{max} is now the asymptotic value of P as the temperature is reduced, and G(T) is given by:

$$G(T) = 1 - \frac{1}{2\gamma} - \frac{1}{\pi\gamma}\operatorname{atan}\left[\alpha(T-\beta)\right] \tag{5.4}$$

5.2.1 Asphalt concrete properties

The material properties of asphalt concrete exhibit a strong dependency on temperature. Young's modulus, E, decreases with temperature increase and therefore is modeled by Equation (5.3). The

Poisson's ratio, ν, on the other hand, increases with temperature increase and therefore is modeled by Equation (5.1). On the other hand, α, the thermal expansion coefficient, is taken to be constant across the range of temperatures of interest and its value is given by 2.0E-5.[6] The coefficients used to define E and ν are given in Table 5.2. Figure 5.5 shows the E-match obtained by this model against data provided by the University, and figure 5.6 depicts the ν-match.

Table 5.2: AC properties.

Property	Max Value	α	β	γ	δ
E (MPa)	27,646	0.09	270	1	--
ν	0.48	0.15	305	1.75	0.48

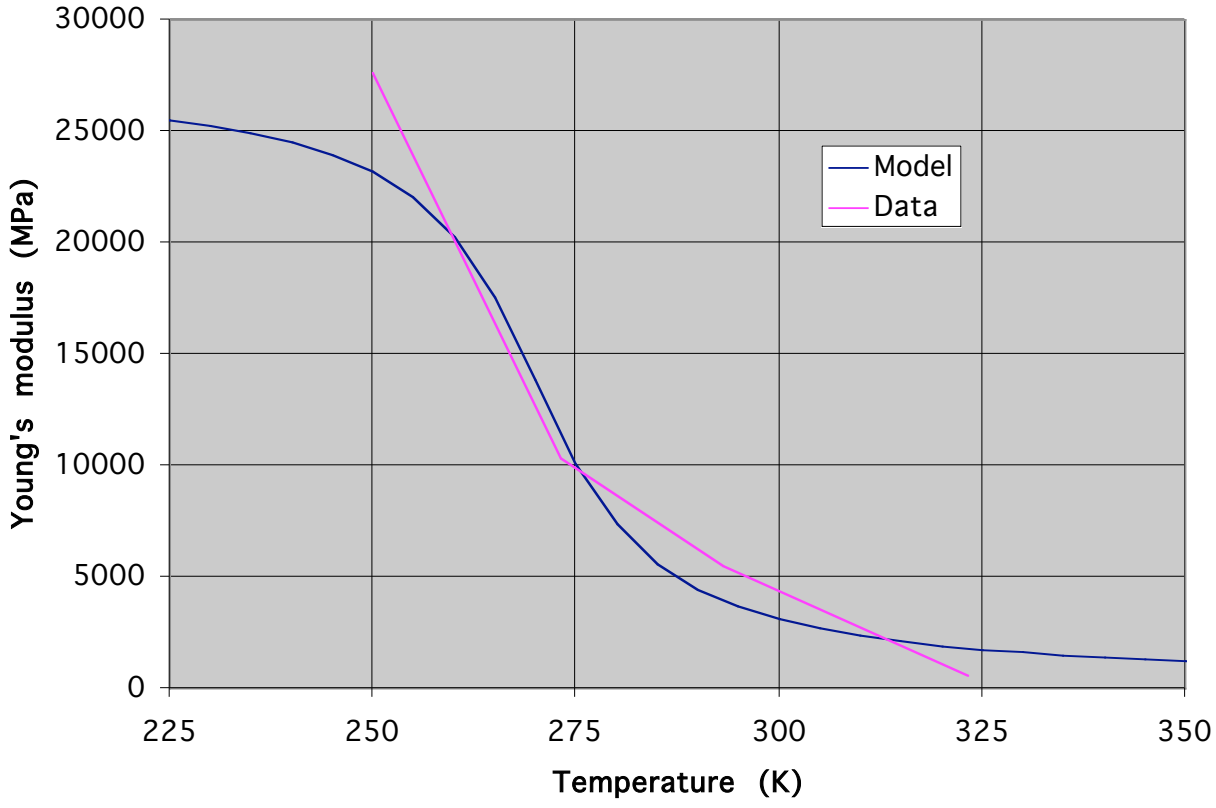

Figure 5.5: Asphalt concrete – Young's modulus fit.

[6] α, the thermal expansion coefficient, is different from the α used in equations (5.2) and (5.4). The meaning of α should be evident from the context in which it is being used.

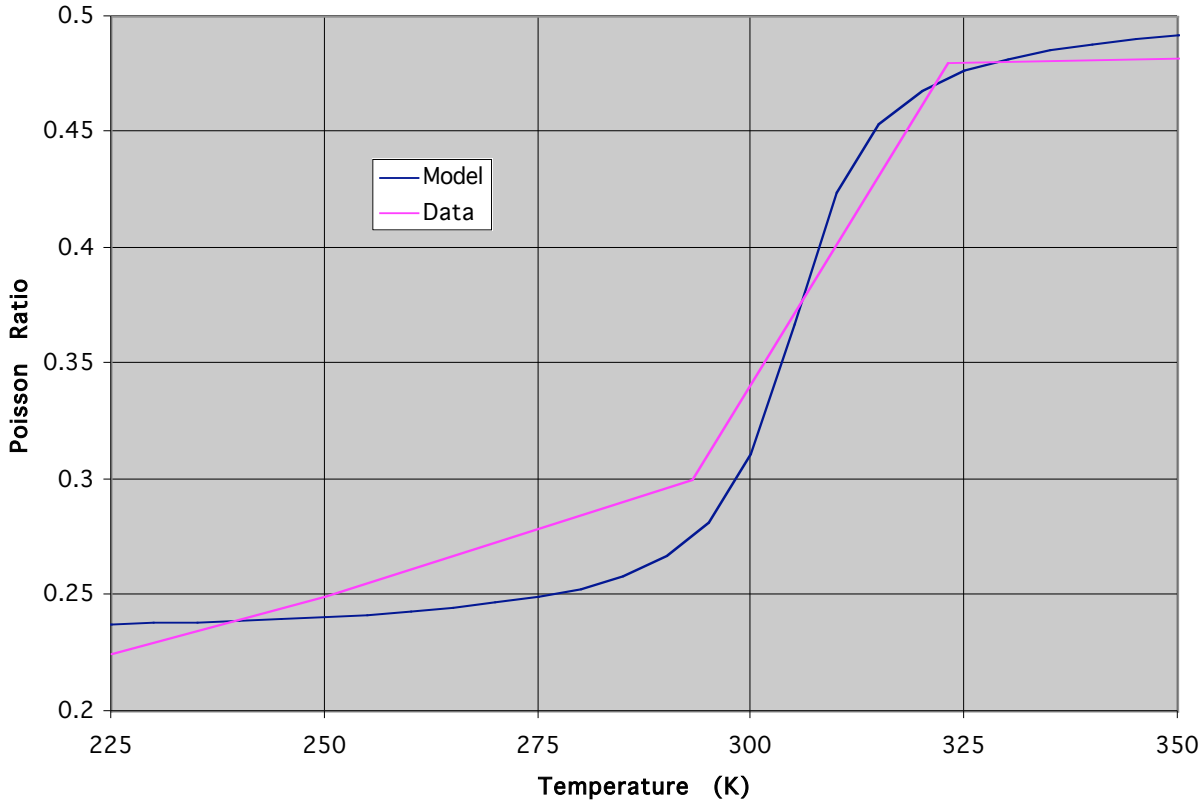

Figure 5.6: Asphalt concrete – Poisson's ratio fit.

5.2.2 Epoxy properties

The properties of the epoxy, too, exhibit strong dependence on temperature. In this case, the value of Poisson's ratio is constant across the range of temperatures of interest, and its value is 0.25. The values of the Young's modulus and thermal expansion coefficient depend on the temperature, and the values used in the fit functions are provided in Table 5.3. The fit obtained for E against data is shown in Figures 5.7. The fit obtained for α provides a smooth jump approximation to the step function data with a value of 1.02E-6 below 313.2°K and the value 1.34E-6 above 313.2°K.

Table 5.3: Epoxy properties.

Property	Max Value	α	β	γ	δ
E (MPa)	1,935	0.11	280	1	--
α	1.34E-6	1000	313	4.25	0.76

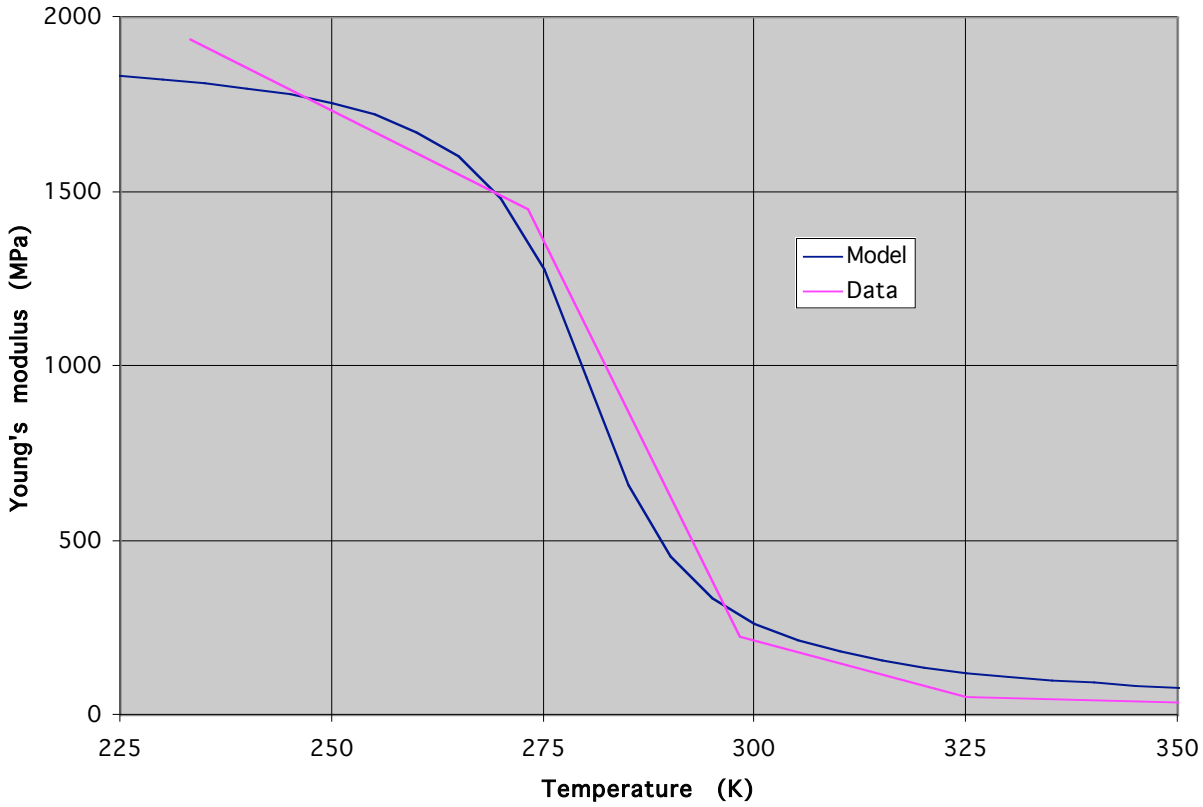

Figure 5.7: Epoxy – Young's modulus fit.

Remark: In case of a free body (*i.e.*, in the absence of any constraints), the strain due to thermal expansion is computed through the following integration:

$$\boldsymbol{\varepsilon} = \int_{T_1}^{T_2} \alpha(T)\mathrm{d}T\ \mathbf{1} \tag{5.5}$$

where $\mathbf{1}$ is the rank 2 identity tensor. For the case where α is constant, Equation (5.5) reduces to

$$\boldsymbol{\varepsilon} = \alpha\left(T_2 - T_1\right)\mathbf{1} \tag{5.6}$$

which is the conventional linear expansion. Equation (5.6) is used for all materials with the exception of the epoxy, where the integration indicated in Equation (5.5) is carried out.◆

5.2.3 Properties of magnetic plug, PCC, and unbound materials

The properties of the magnetic plug and PCC materials are assumed to be independent of temperature. The properties of the bounded layers are assumed to exhibit different properties above and below freezing and consequently, two sets of values are provided for the unbound layers. Table 5.4 provides a summary of the properties employed in the simulations.[7]

Table 5.4: Material properties for the magnetic plug, PCC and unbound layers

Material	E (MPa)	ν	α
Magnetic plug	13,823	0.25	1.2e-5
PCC	27,646	0.15	1.0e-5
Base (AC) (cold)	346	0.35	0
Base (AC) (hot)	173	0.35	0
Base (PCC)	1,036	0.30	0
Subbase (cold)	346	0.35	0
Subbase (hot)	138	0.35	0
Subgrade (cold)	346	0.40	0
Subgrade (hot)	69	0.40	0

5.3 Temperature profiles

Each of the five pavement systems, S1 through S5, is analyzed for two temperature profiles. A cold profile based on the mean low temperatures measured at Fairbanks, Alaska, between December 1997 and January 2001, and a hot profile based on the mean temperatures measured in Palmdale, California, in the period of April 1998 and January 2001 (Monismith [2002]). These measured temperatures, reported in degrees Kelvin, are listed in Table 5.5 below.

To conduct the analysis, a reference temperature must be set. For the purpose of the current study, the reference temperature is set to 293.2°K. This temperature was arbitrarily picked based on the following rationale. Much of pavement construction takes place during the dry season, which in California corresponds to the warm season. The selected reference temperature is representative of the average temperature in a given twenty-four hour period for much of the state of California.

[7] Note that thermal expansion is ignored for the unbound layers (*i.e.*, $\alpha = 0$).

Table 5.5: Temperatures (˚K)

	Fairbanks, Alaska – mean low				Palmdale, California – mean high			
Depth (m)	S1	S2	S3	S4 and S5	S1	S2	S3	S4 and S5
0.0000	232.54	232.03	232.67	230.24	312.34	312.42	312.57	312.62
0.0254	234.69	233.96	233.96	231.45	311.42	311.53	311.74	311.82
0.0508	236.83	235.89	235.26	232.64	310.50	310.66	310.91	311.02
0.0762	238.97	237.81	236.53	233.84	309.59	309.78	310.09	310.23
0.1016	241.09	239.72	237.79	235.02	308.69	308.93	309.28	309.45
0.1270	243.18	241.61	239.02	236.18	307.81	308.09	308.49	308.69
0.1524	245.24	243.48	240.22	237.32	306.95	307.26	307.71	307.94
0.1778	247.26	245.33	241.38	238.44	306.08	306.44	306.95	307.21
0.2032	249.25	247.14	242.49	239.51	305.24	305.64	306.19	306.49
0.2286		248.92	243.57	240.56		304.86	305.46	305.78
0.2540		250.68		241.56		304.08		305.09
0.2794		252.41		242.53		303.32		304.41
0.3048		254.09		243.45		302.58		303.74
0.3810			243.64				304.81	
0.4064	250.18				304.65			
0.4318				243.52				303.14
0.5080		254.75				302.05		

5.4 Traffic loading

A single axle with dual-tire configuration provides the traffic loading. The distance between the centers of the dual-tires in the lateral direction is 2.5908 meters, and the lateral distance between the centers of two adjacent tires is 0.3048 meters. The applied tire-pavement contact stress distribution corresponds to that reported tire in Volume 1 of de Beer and Fisher [1997] for a Goodyear G159A 11R22.5 radial truck tire with internal pressure of 690 KPa and loaded by a 26 KN per tire.

The reported measurements are for a slow moving vehicle, and do not include the added traction required to overcome vehicle-air friction. To compensate for this shortcoming, a uniformly distributed force of 1 KN was added in the longitudinal direction. Contour plots of the lateral, longitudinal, and vertical components of the tire-pavement contact stress distribution for a dual-

tire configuration are shown in Figures 5.8, 5.9, and 5.10, respectively.[8] Also, as is evident from the plots, the load rests heavier on one side of each tire. For this reason, the two dual-tires are positioned in such a way that the inner side of each tire carries more load than the outer part.

The location of the applied loading (*i.e.*, the positioning of the tires relative to the location of the plugs) considerably effects the stress distributions in the vicinity of the plugs. Therefore, the tires are positioned in a few locations. First, the tires are positioned so that the plug is halfway between the two sets of dual-tires in the lateral direction, and also the plug is aligned with the center of the tires in the longitudinal direction. This case is referred to as "Case C."

Next, one dual-tire set is placed in the vicinity of the plug, while the other set is near the lateral edge of the pavement. To evaluate the impact of the loading locations, the tires are moved between nine different positions in the lateral directions, and three different positions in the longitudinal directions. Thus, a total of twenty-seven different locations are studied. In the following, these cases are designated as Sij cases, where the index i assumes the values of one, two, or three indicating the longitudinal position, and the index j assumes values between one and nine and indicates the lateral position. The nine lateral stations are designated in Table 5.6. These stations represent a traffic wander that is typical of highway traffic (Monismith [2000]). The expected percentage of traffic in each position is also reported in Table 5.6.[9] The three longitudinal stations are explained in Table 5.7. The accompanying CD contains an animation of the traffic moving between the 27 locations, where the vertical stress component is used to track the location of the tires.

Table 5.6: Lateral positions and percentage of traffic.

Position (j)	Offset[10] (m)	% of total traffic
1	-0.51	3.5
2	-0.38	6.5
3	-0.25	12.5
4	-0.13	17.5
5	0	20.0
6	0.13	17.5
7	0.25	12.5
8	0.38	6.5
9	0.51	3.5

[8] Figures 5.8 through 5.10 are stress plots resulting from the finite element approximation, and not of the applied tractions. Therefore, stresses not immediately under the tires may not be zero.
[9] The percentage of traffic is applicable to in-lane driving. The case where one set of dual-tires is near a magnetic plug represents a vehicle changing lanes. However, in the absence of better data, these percentages offer an approximation that can be used in evaluating the evolution of damage.
[10] The offset is the lateral distance between the center of the plug and the midpoint between the two tires.

Table 5.7: Longitudinal positions

Position (i)	Offset[11] (m)
1	-0.1672
2	0.0000
3	0.1672

Finally, the applied in-plane tractions in the longitudinal direction are significantly larger if the vehicle is braking. To simulate this event, a uniformly distributed force of 7KN per tire is subtracted from the longitudinal tractions measured in de Beer and Fisher [1997]. The loads are applied in a pattern similar to the case S25, and is designated "S7."

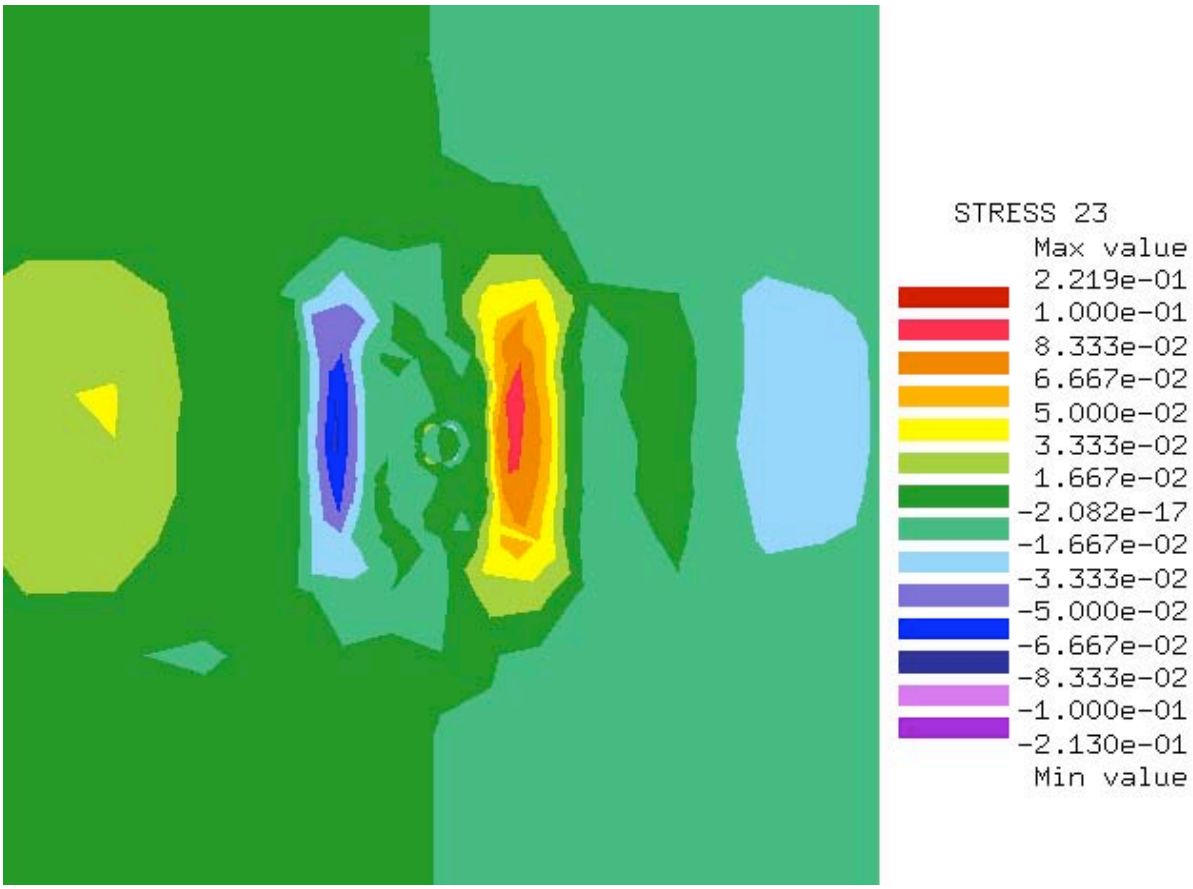

Figure 5.8: Tire-pavement contact stress distribution – lateral component.

[11] The offset represents the longitudinal distance between the center of the plug and the longitudinal center of the tire (the tire length is 0.2835 meters). Thus, when j = 1 the leading edge of the tire just arrives at the plug; when j = 2 the tire is (longitudinally) centered above the plug; and when j = 3 the trailing edge of the tire just left the plug.

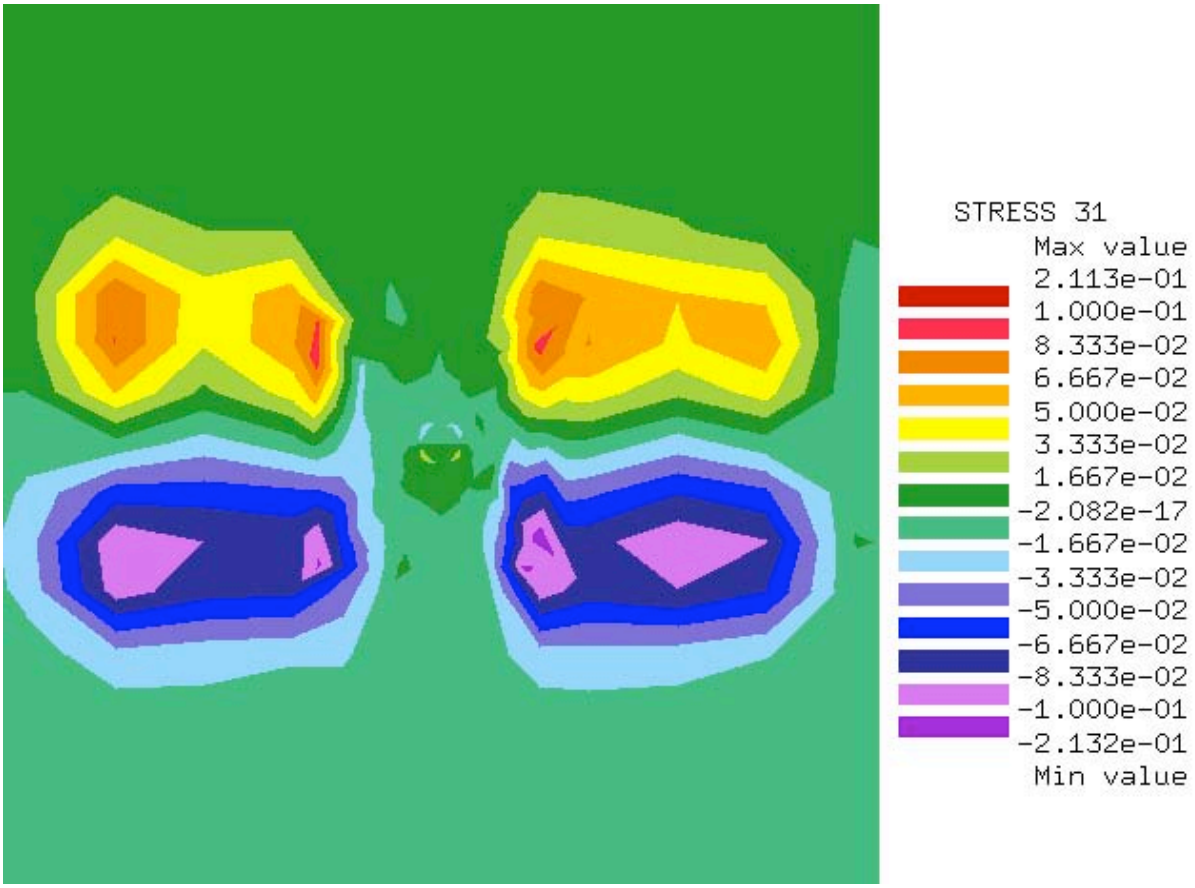

Figure 5.9: Tire-pavement contact stress distribution – longitudinal component.

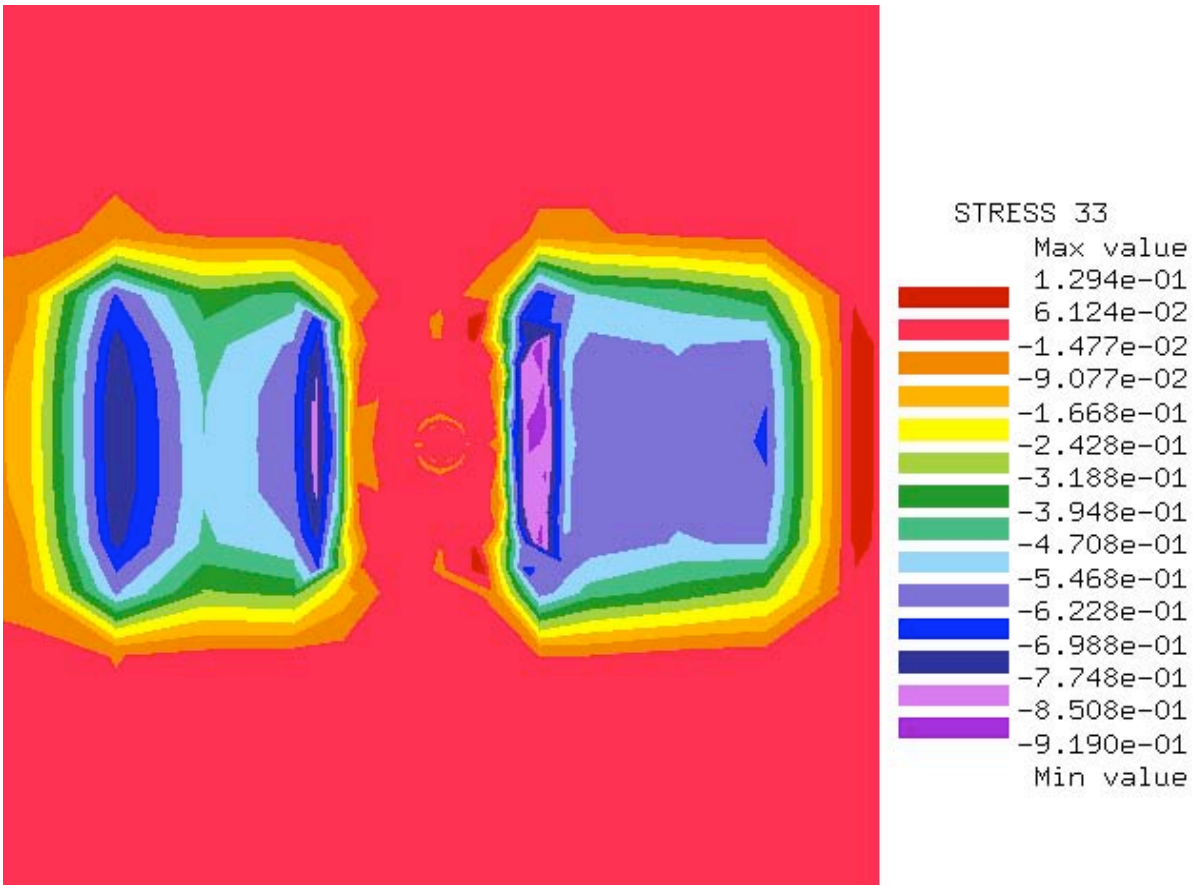

Figure 5.10: Tire-pavement contact stress distribution – vertical component.

6. Simulation Results

The best approach to investigate the large data generated by three-dimensional finite element simulations is to view graphical representations, including virtual "walks" through the models. In this report, the data is illuminated primarily through animated walkthroughs that are contained in the accompanying CDs. The rest of this section highlights some of the results, and provides a guide as to how to view the animations contained on the CD. Also, results of the analysis of a pavement containing three adjacent plugs is included to demonstrate that the presence of adjacent plugs has only a second-order effect on the stress distributions at any given plug, thus justifying including only one plug in the remainder of the analyses.

All finite element simulations in this study are carried out using Symplectic Engineering's CoMeT™ proprietary finite element package. All simulations are carried out on a Sun Ultra60 workstation.

6.1 CD organization

Two CDs accompany this report: "plugPave1" and "plugPave2." The former contains animations of the results for structures S1 through S4, while the latter contains the animations for the S5 structure. The plugPave2 CD also contains an animation of the moving load, and two files entitled "finalReport.pdf" and "resSum.exe." finalReport.pdf is a copy of the final report in pdf format. resSum.exe, in MS-Excel format, contains a summary of the minimum and maximum values of the different stress components and the first stress invariant as well as the second stress deviator invariant.[12] Additionally each file contains a file entitled "animateContinous.zip" that contains the Java applet required to run the animations.

To view the animations for a specific structure, insert the appropriate CD (*i.e.*, plugPave1 to view the animations for structures S1 through S4 and plugPave2 to view S5 animations). Then, open the "viewRes.htm" file from within any Java-enabled web browser such as Netscape Navigator or Internet Explorer. You can do that by selecting "Open" from the "File" menu within the browser, and navigating through the file system to the CD and selecting "viewRes.htm."[13] You'll be faced with a choice of structures S1 through S4 or S5 and moving load. You can access any one of these options by clicking on the desired one.

When choosing one of the structures you'll be faced with a choice of Palmdale (high-temperature profile) or Fairbanks (low-temperature profile). Upon selecting the desired locale, you can choose the material to examine. The options are, depending on the structure, AC, PCC, epoxy, plug, and all. For each of these options you'll be given an array of animations to view (you'll see

[12] By definition, the second invariant of the stress deviator has a non-negative value. Therefore, only the maximum value is provided.

[13] An alternative that will shorten the time required to load the animations is to copy all the files to the hard drive. In this case copy all files to the same folder, and proceed to open the "viewAllRes.htm" from within the Java-enabled web browser. Proceed in the same way as described in the text.

a link followed by a brief description of what is displayed). Choose one of them, and your browser will load all the images and run through them in a continuous loop.

All images are of stresses and stress invariants. The legend that appears on the right side of the contour plots consists of a title and a range for each color. The title for stress plots is "STRESS" followed by a two-digit number that identifies the stress component. Table 6.1 explains the notation used. Two stress invariants are presented. The first stress invariant, denoted "I_1," is the sum of the normal stresses (*i.e.*, $I_1 = \sigma_{11} + \sigma_{22} + \sigma_{33}$), and its value is equal to the negative of three times the pressure. The second stress invariant, denoted "J_2," provides a measure of the effective stress deviator.[14]

Table 6.1: Stress labeling notations

Stress component	Plane acting on	Orientation	Type
σ_{11}	longitudinal[15]	longitudinal	normal
σ_{22}	transverse	transverse	normal
σ_{33}	vertical	vertical	normal
σ_{12}	longitudinal	transverse	shear
σ_{23}	transverse	vertical	shear
σ_{31}	vertical	longitudinal	shear

The images can also be accessed individually. To do that, open the image folder and keep opening the desired folder, in a sequence similar to that described above for navigating using the browser, until you arrive at the desired folder containing the images. Double-click on the desired image and your operating system should open an image viewer displaying the desired image. In each image folder you will find the image files designated with a .gif suffix, a .htm file that is used in running the animation, a .zip file that contains the Java applet code, and a readme file that contains an explanation of the images in that folder. Finally, each image name ends with a number, which indicates in which frame it is found in the animation. For example, s31_11.gif is the eleventh frame. This number can also be used to identify the location of the surface displayed in the image in the three-dimensional model. As an illustration, suppose that s31_11.gif is the eleventh frame in a sequence of 100 images that starts at the surface above the center of the plug, and moved in the vertical direction downwards a total of 0.1 meters. Then, the surface displayed in that image is located at a depth of 0.1 * (10/99) = 0.0101 below the surface.

[14] $J_2 = \frac{1}{2} s_{ij} s_{ij}$, where the usual summation convention applies, and s_{ij} are the components of the stress deviator, given by: $s_{ij} = \sigma_{ij} - \frac{1}{3} I_1 \delta_{ij}$.

[15] The orientation of a plane is defined by the direction of the normal to it.

6.2 Interaction between adjacent plugs

An underlying assumption in constructing the finite element meshes described in Section 5 is that the stress distributions in the vicinity of a magnetic plug are unaffected by the presence of adjacent plugs (see Section 4). Analyzing a mesh that includes three plugs that are spaced 1.1 meters apart in the longitudinal direction now validates this assumption. A uniformly distributed circular pressure of 0.7 MPa, with a radius of 0.1 meters is applied centered above the middle plug. A perspective view of the mesh is shown in Figure 6.1. The structure is similar to that described for the S1 pavement. The difference lies in that the surface layer is assumed to extend indefinitely in both longitudinal and lateral directions; the drilled cavity is assigned a simpler geometry (see Figure 6.2); and the lateral circumference of the plug is assumed to be fully connected to the drilled cavity walls (the epoxy is ignored). The mean minimum temperature profile measured at Fairbanks, Alaska, is applied (this being the more conservative case in terms of possible interaction). However, thermal expansion is not considered.

Figure 6.3 shows a plan view of the pavement surface depicting the vertical component of the displacement. Figures 6.4 and 6.5 offer plan views of the pavement's surface depicting the first invariant of the stress tensor and the second invariant of the stress deviator tensor, respectively. Stress contours of the normal components of the stress as well as the longitudinal-vertical shear component plotted on a transverse plane through the centers of the three plugs are shown in Figures 6.7 through 6.10, while Figure 6.6 shows the location of the different materials on the same plane in order to provide an easy identification of the location of the plugs.

An analysis of the results presented indicates that the stress concentration present near a tire load and near a plug exhibit rapid decay with distance. As a result, the presence of adjacent plugs has only a marginal effect on the stress distribution at any given plug and thus, accurate predictions of stress concentrations near a plug can be achieved even when the model includes only a single plug. This practice is followed in the remainder of this work.

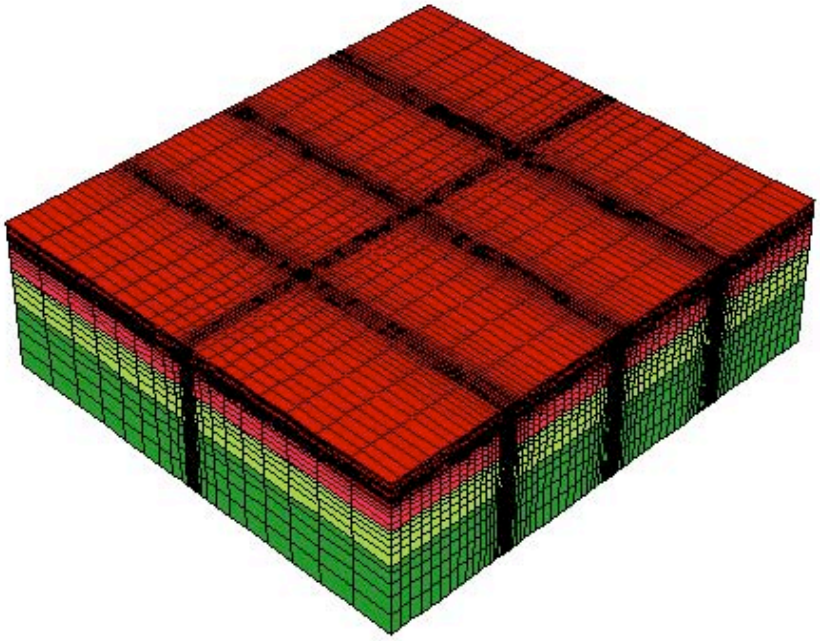

Figure 6.1: Perspective view of the 3-plug mesh.

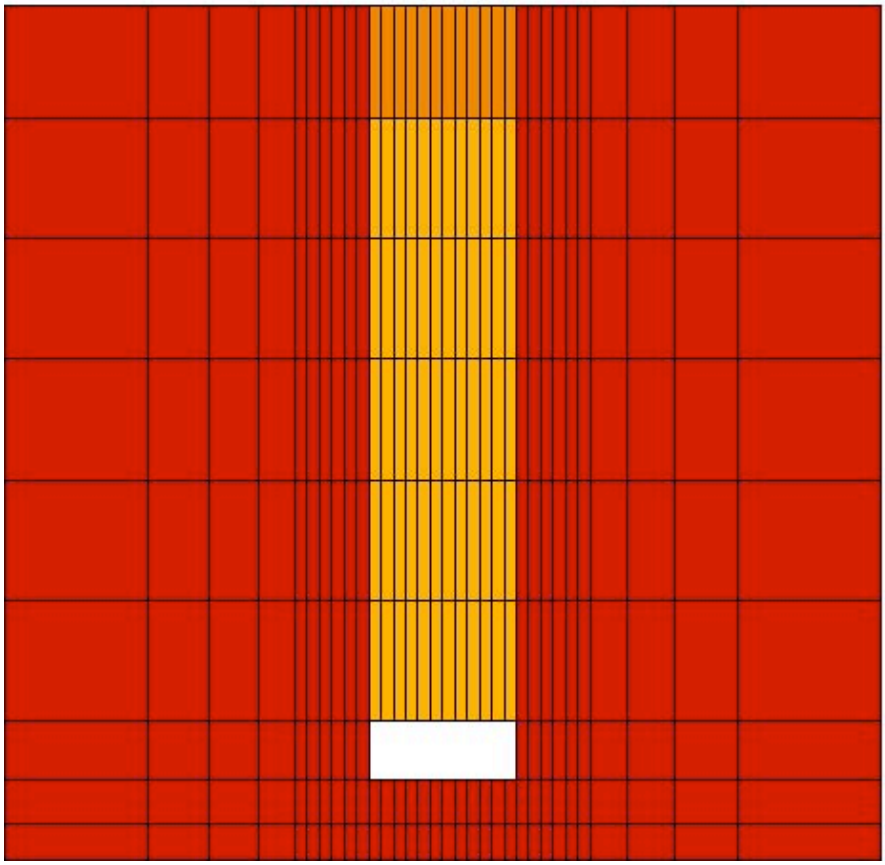

Figure 6.2: Transverse-vertical section through the center of a plug.

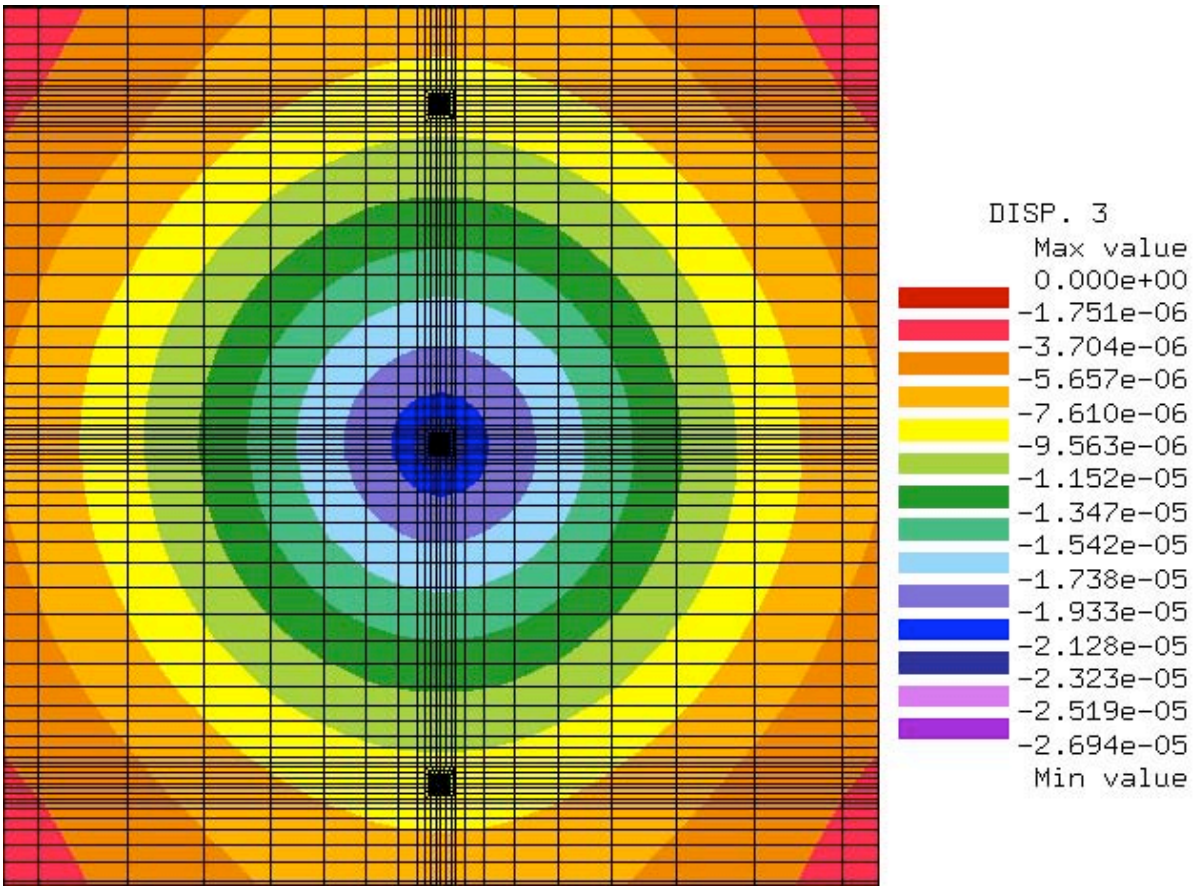

Figure 6.3: Contours of the vertical component of the displacements; AC surface, plan view.

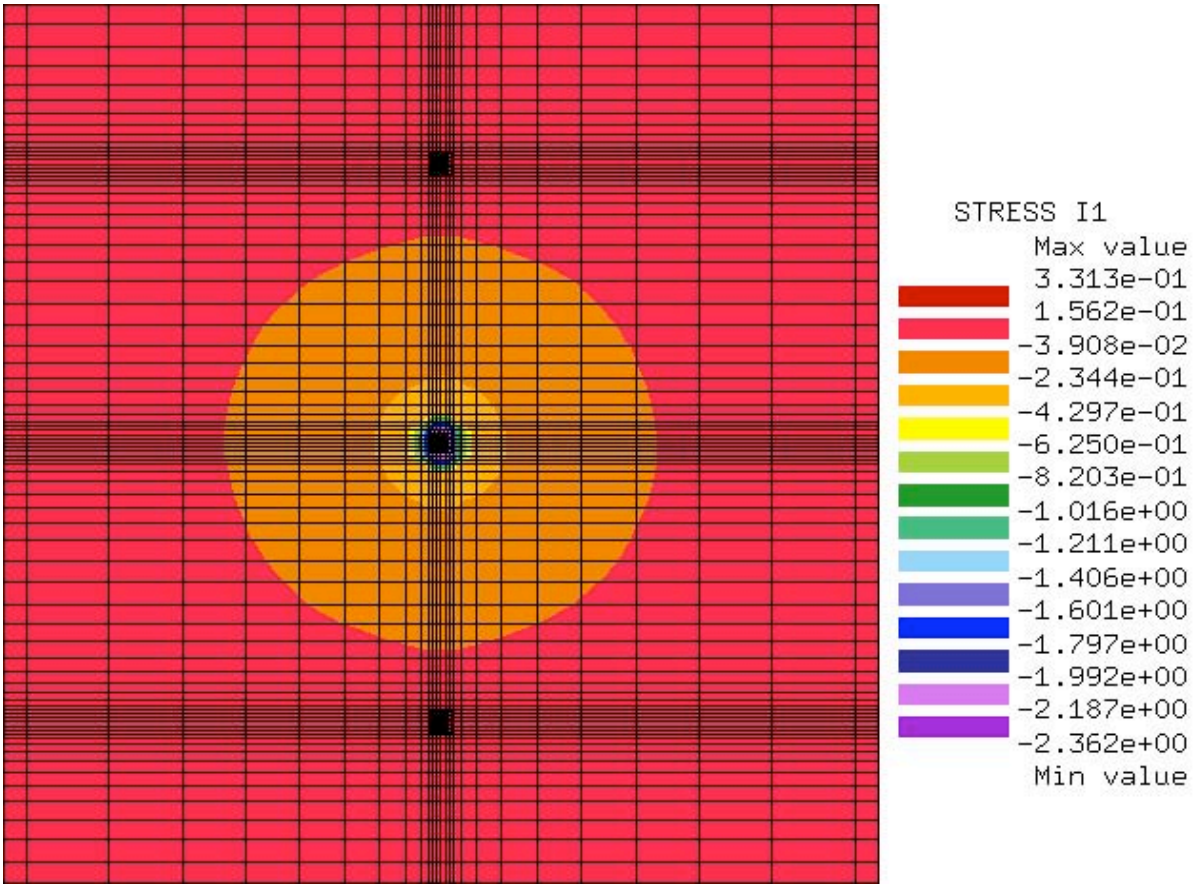

Figure 6.4: First invariant of the stress; AC surface, plan view.

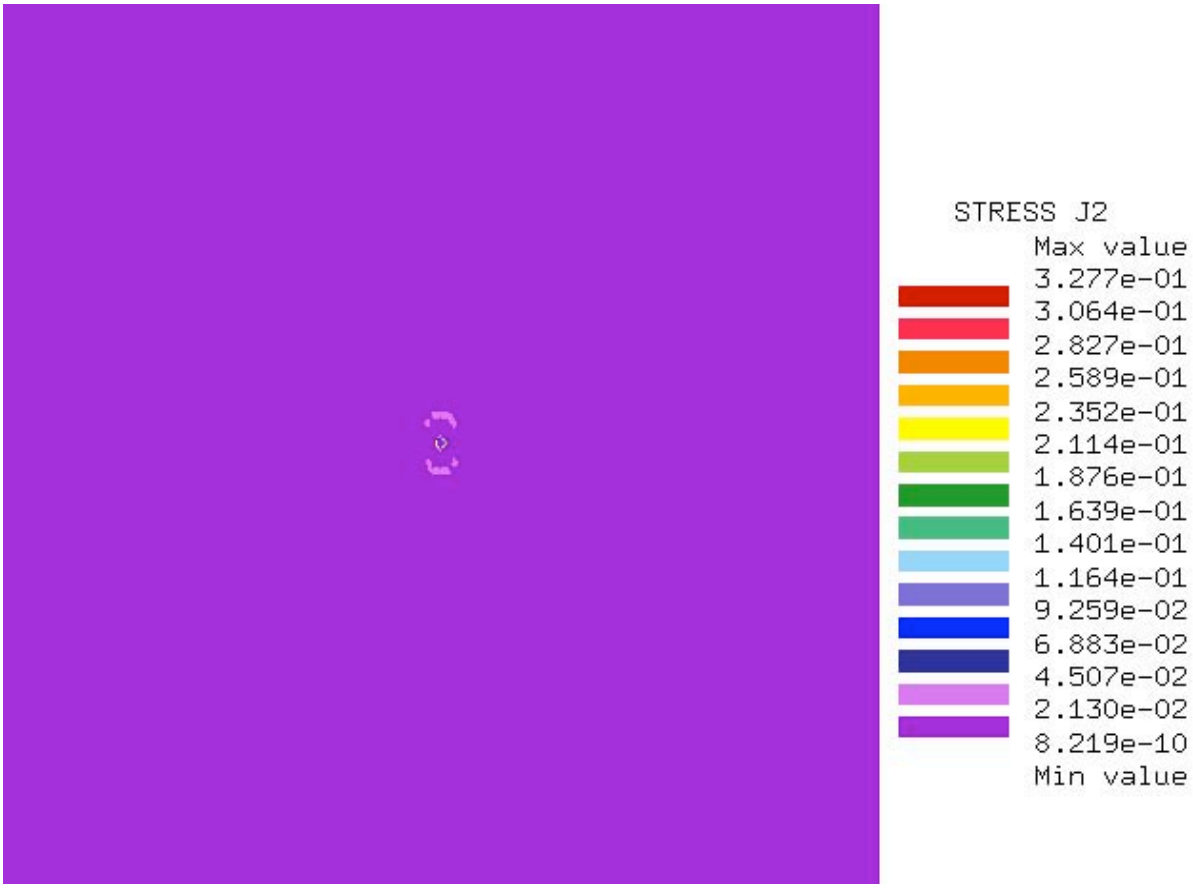

Figure 6.5: Second invariant of the stress deviator; AC surface, plan view.

Figure 6.6: Transverse (longitudinal-vertical) plane through the center of the magnetic plugs.

Figure 6.7: Normal longitudinal stress component; transverse plane through the plugs' centers.

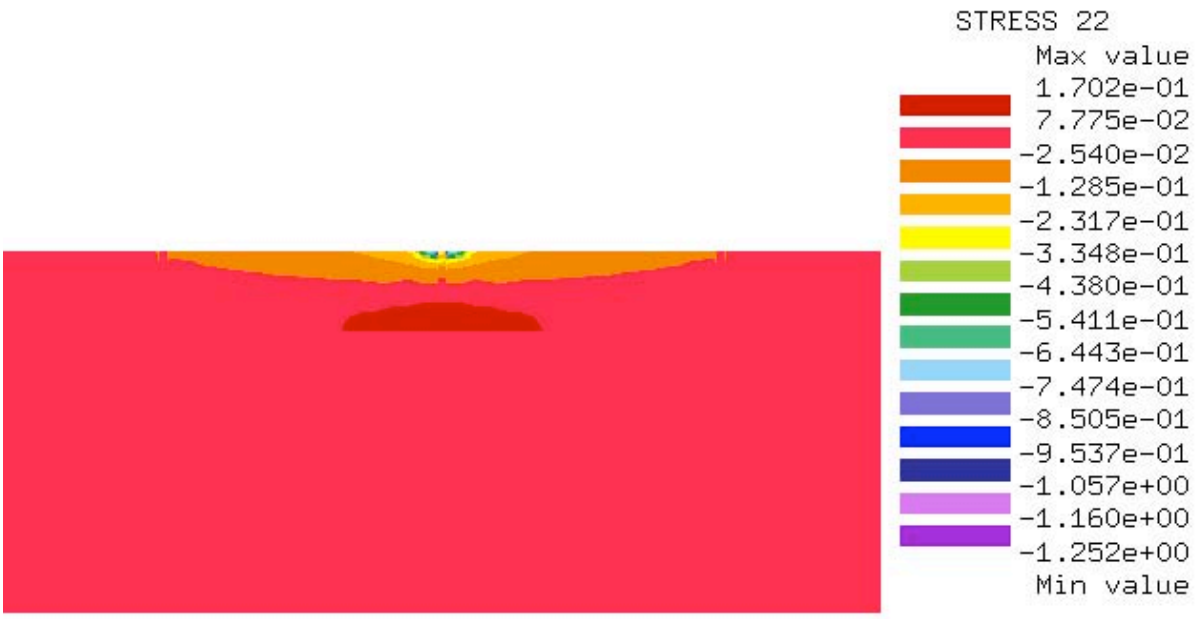

Figure 6.8: Normal transverse stress component; transverse plane through the plugs' centers.

Figure 6.9: Normal vertical stress component; transverse plane through the plugs' centers.

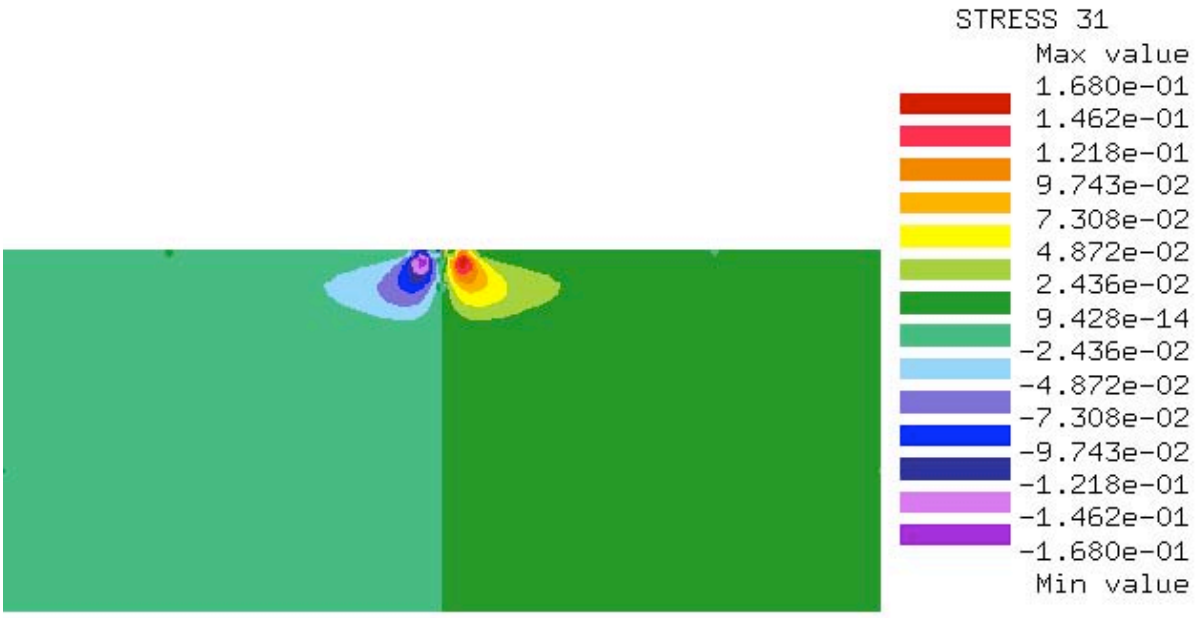

Figure 6.10: Longitudinal-vertical shear stress; transverse plane through the plugs' centers.

6.3 S1 pavement system

Any motion can be decomposed into volume- and shape-preserving components.[16] Because of the fundamental nature of this decomposition, it is most instructive to evaluate stress quantities that directly relate to these two components. Furthermore, it is desirable to examine quantities that are independent of the particular coordinate system used. Therefore, through the remainder of Section 6, the response of the pavements is primarily evaluated by examining line plots of I_1 and J_2 stress invariants, where I_1 relates to the change of volume and J_2 to shape distortion. These plots show the change in the invariants with depth at three positions along the drilled cavity circumference: 0°, 45°, and 90°.[17] The stress invariants plotted are on the pavement side so that for structure S1 they represent the state in the AC material at the specified locations.

Figures 6.11 through 6.14 provide line plots of I_1 and figures 6.15 through 6.18 are J_2 line plots. Four cases are examined: (1) constrained thermal expansion and contraction for Fairbanks, Alaska; (2) constrained thermal expansion and contraction for Palmdale, California; (3) traffic loading at position S23, where the highest J_2 is attained for Fairbanks temperature profiles (see the Excel spreadsheet resSum.exe on the accompanying CD); and (4) traffic loading at position S23, where the highest J_2 is attained for Palmdale temperature profiles (again, see the Excel spreadsheet resSum.exe).

[16] In the following, volume-preserving motion will be referred to as "volumetric motion," and shape-preserving motion will be referred to as "deviatoric motion."

[17] The location along the circumference is relative to a cylindrical coordinate system with its origin at the center of the plug, and having the z coordinate aligned with the vertical direction and 0° aligned with the longitudinal axis.

Figures 6.11 through 6.18 reveal a few characteristics. First, there is an order of magnitude difference in the level of predicted stress between stresses due to thermal contraction under the cold profile, and all other cases. This is attributed to the large temperature change from the reference temperature. The level of stresses encountered for the Fairbanks local (Figures 6.11 and 6.15) are so high that thermal cracking, initiating at the surface at the 90˚ location, must be expected. The initiation point is selected because I_1 attains almost its maximal value, and as shown in Figures 6.19 J_2 exceeds by far its value at any other point along the circumference.

Figures 6.19 and 6.20 clearly illustrate the stress concentration near the plug (note the rapid decay in the values of J_2 and I_1 when moving away from the drilled cavity, which appears in these figures as a circular hole at the center of the figures). Stress concentrations near the cavity are present in all cases studied, and are clearly visible in the stress and stress invariant plots. The amplification factor due to the presence of the plug (*i.e.*, the ratio of the stress near the plug to that without a plug) is roughly three, which is in full agreement with the theoretical amplification factor (see *e.g.*, Timoshenko and Gooiear [1970]).

The stress values due to traffic loading (both hot and cold temperatures) and the thermal expansion stresses predicted for the Palmdale locale are all of the same order of magnitude, thus indicating that the thermal stresses must be included in the analysis for all locals. These stresses, while much smaller than those reported for thermal contraction at the Fairbanks locale, are high enough to cause concern regarding the expected service life of the pavement.

It is also of interest to look at the displacement patterns. Because of the boundary conditions, the displacement field for the thermal expansion/contraction cases result in nearly plane strain states, with a local disturbance around the plug. Figures 6.21 through 6.24 present the vertical and lateral components of the displacements for the pure constrained thermal expansion/contraction cases. The displacement contours are plotted on a longitudinal plane through the center of the plug. (Recall that by the convention used in this report, a plane is defined by the direction of the normal to it and thus, a longitudinal plane coincides with the transverse-vertical surface.)

Contour plots of the three components of the displacement, resulting from traffic loading, are presented in Figures 6.25 through 6.30. The contours are plotted on the top surface of the pavement (*i.e.*, plane view). Finally, the reader is reminded that much more information is available on the accompanying CD.

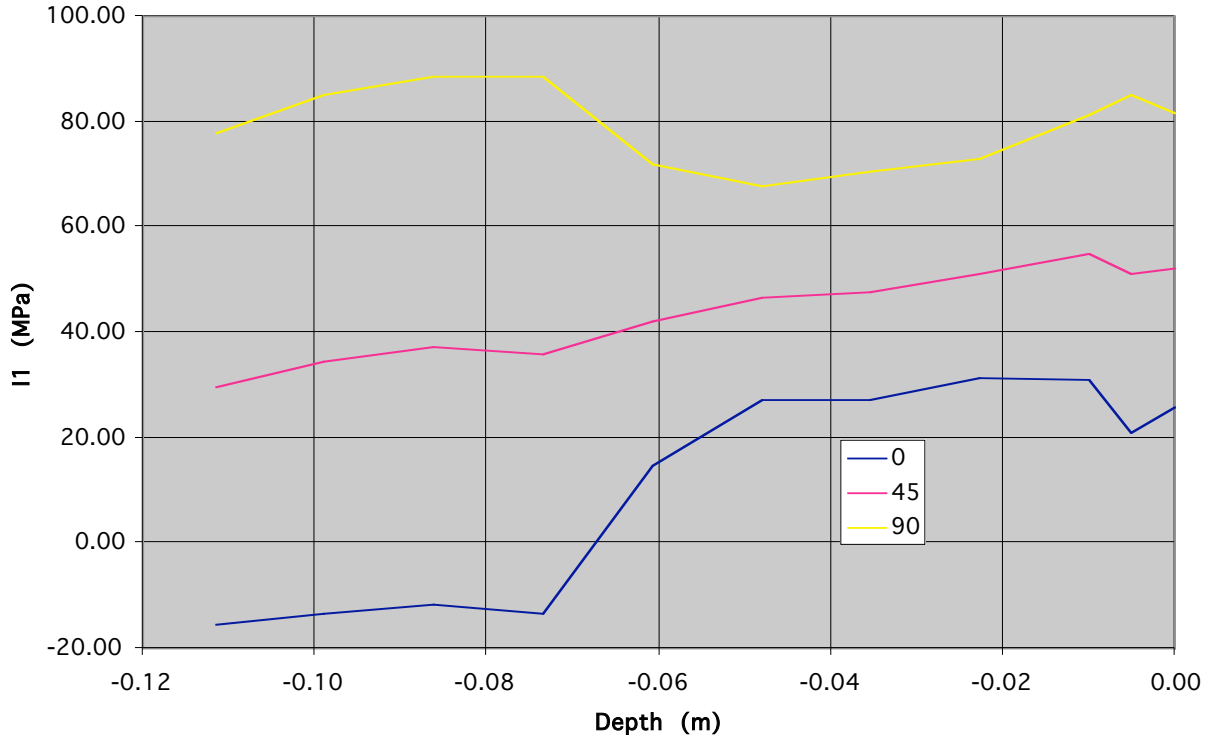

Figure 6.11: I_1 vs. depth; thermal loading; Fairbanks locale; S1.

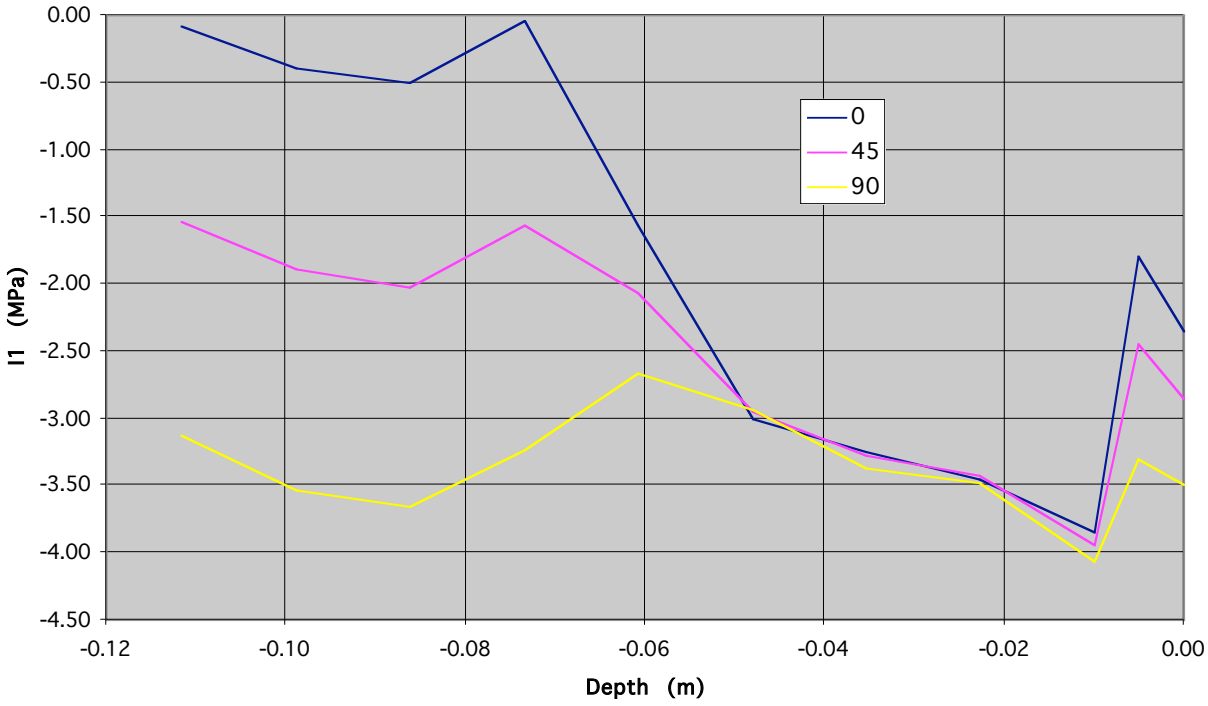

Figure 6.12: I_1 vs. depth; thermal loading; Palmdale locale; S1.

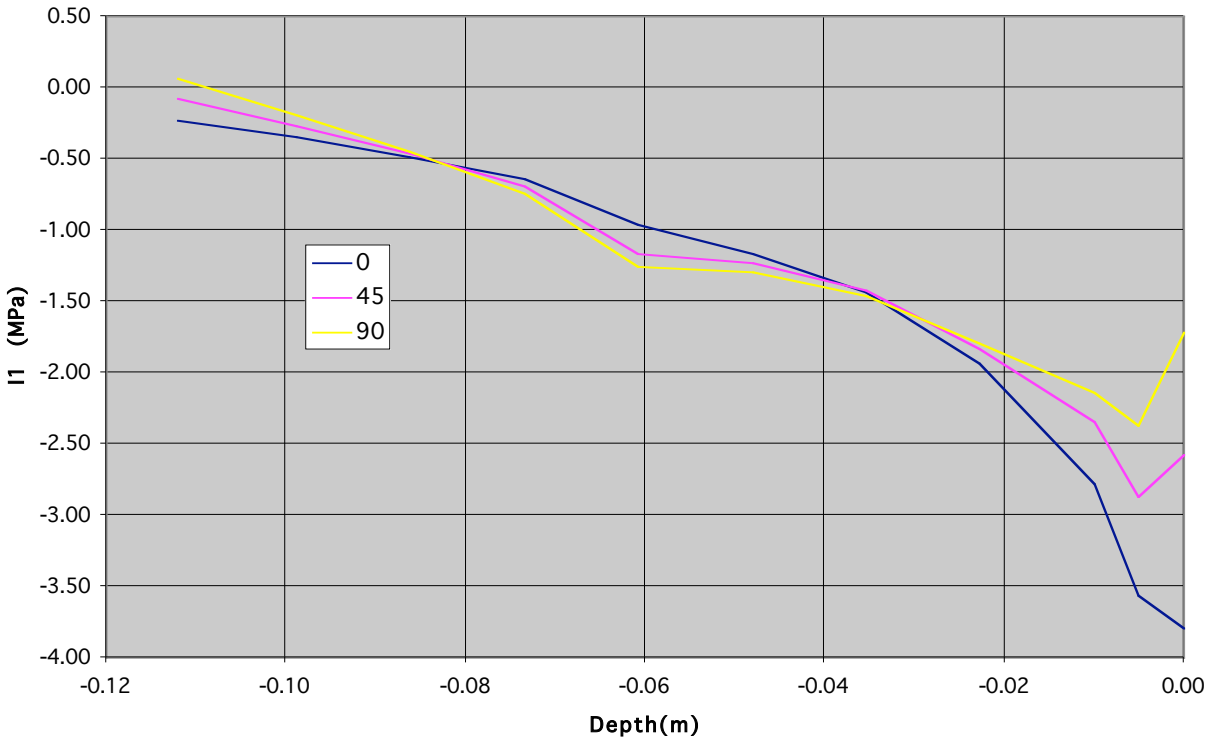

Figure 6.13: I_1 vs. depth; traffic loading (S23); Fairbanks locale; S1.

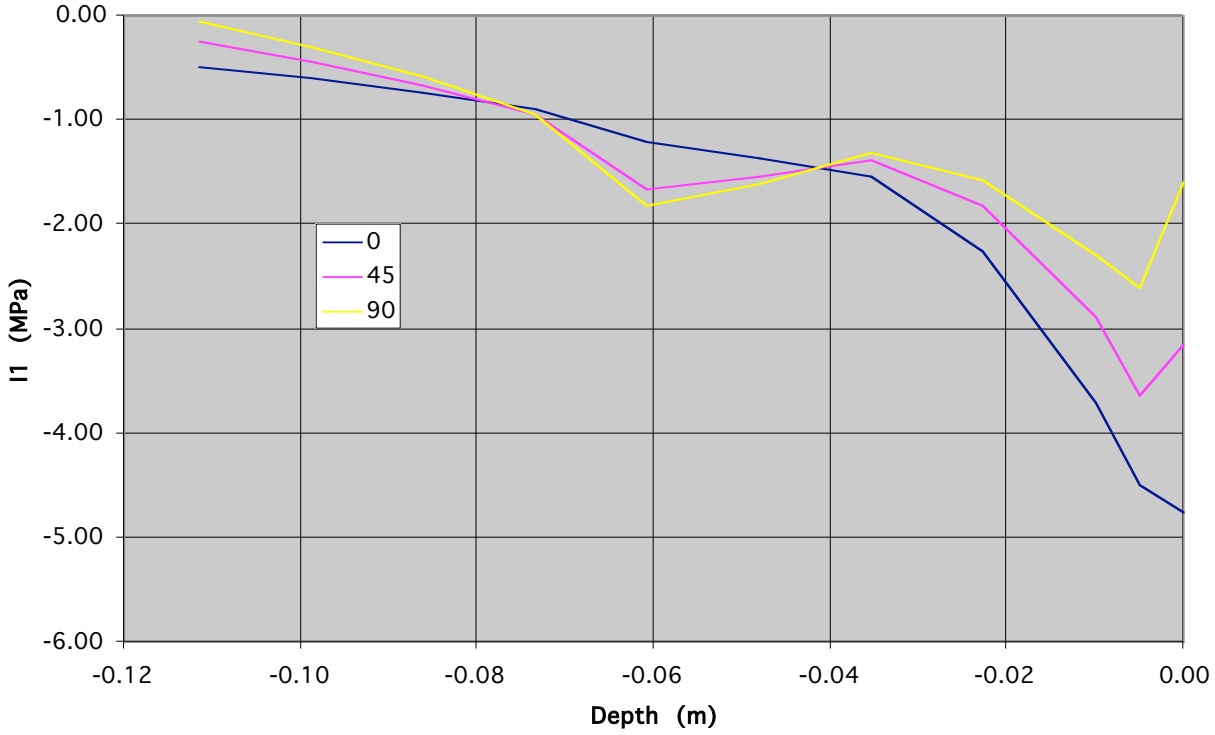

Figure 6.14: I_1 vs. depth; traffic loading (S23); Palmdale locale; S1.

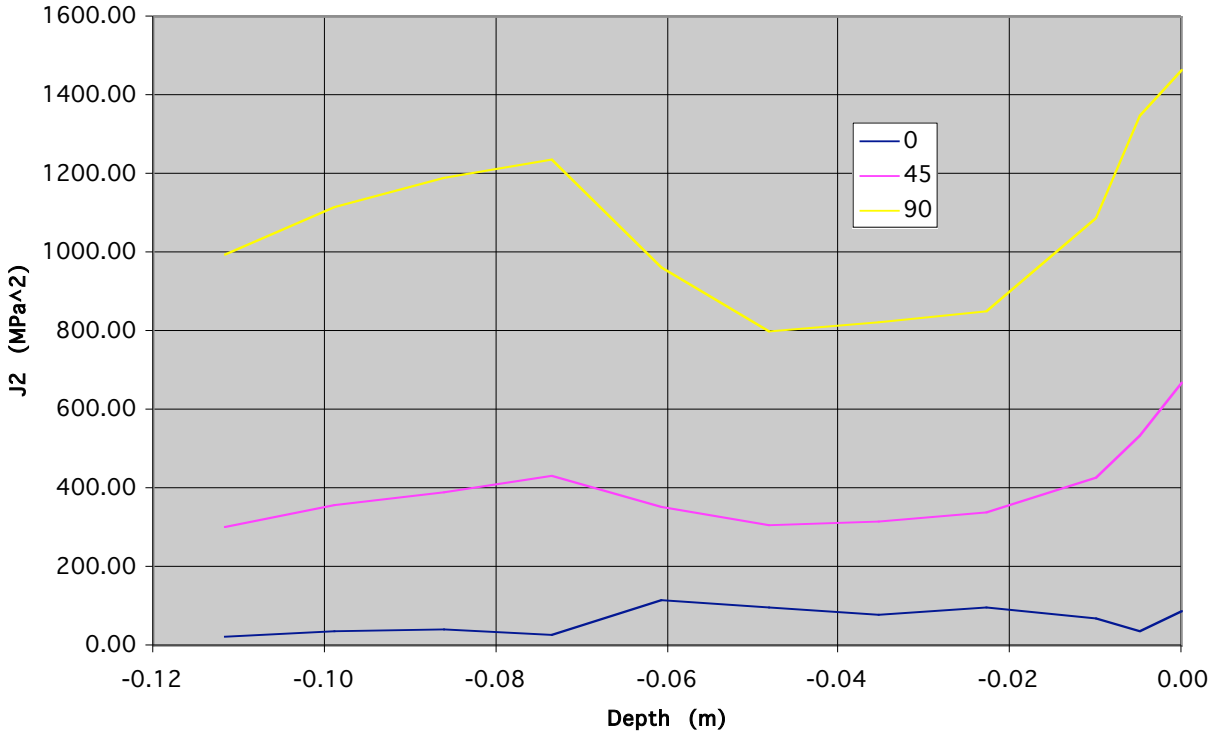

Figure 6.15: J_2 vs. depth; thermal loading; Fairbanks locale; S1.

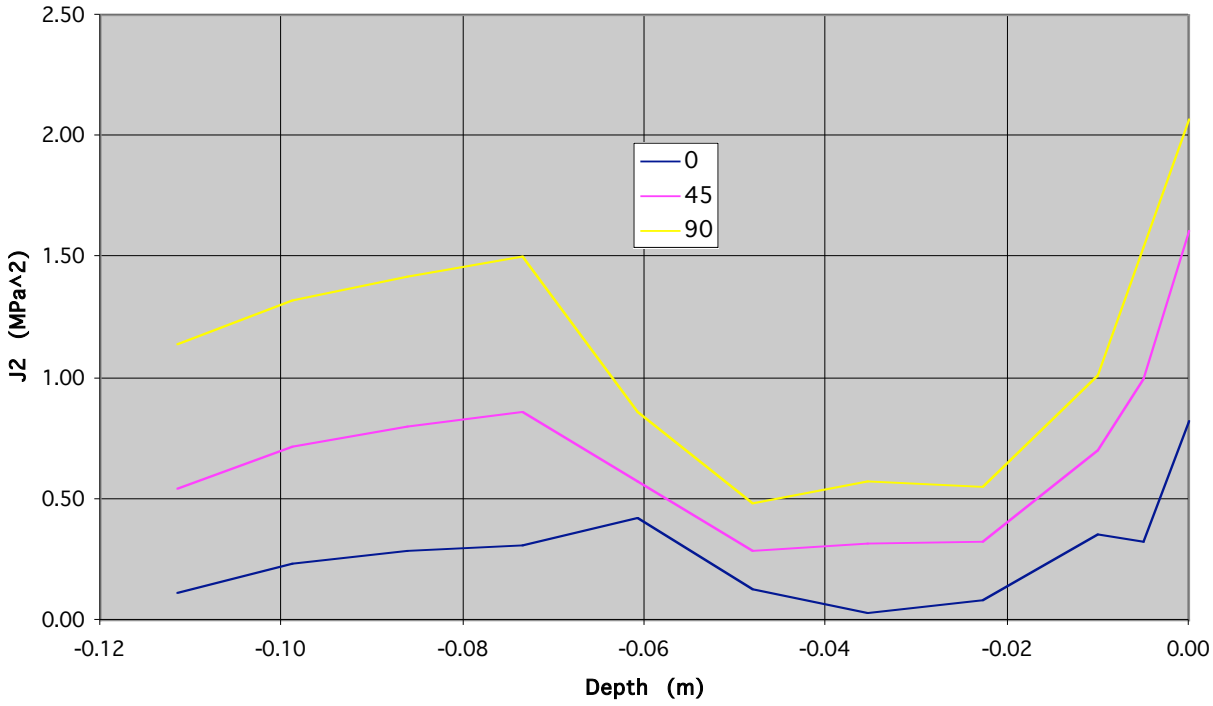

Figure 6.16: J_2 vs. depth; thermal loading; Palmdale locale; S1.

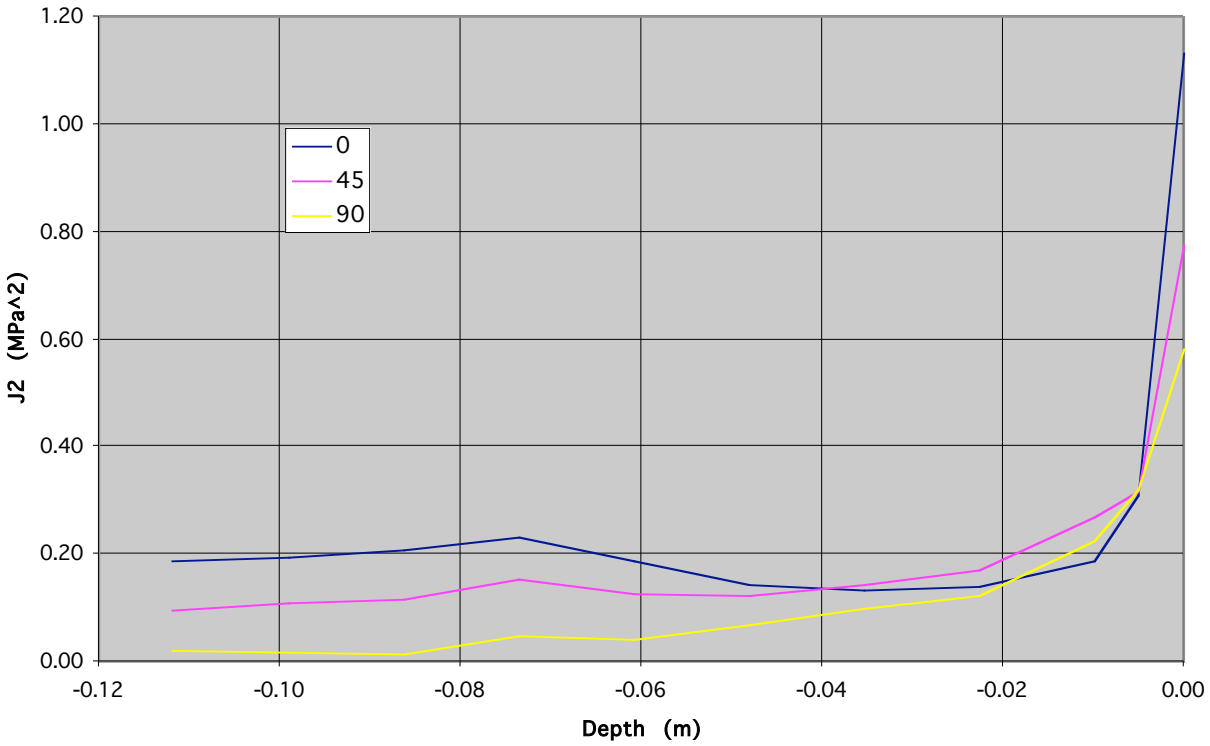

Figure 6.17: J_2 vs. depth; traffic loading (S23); Fairbanks locale; S1.

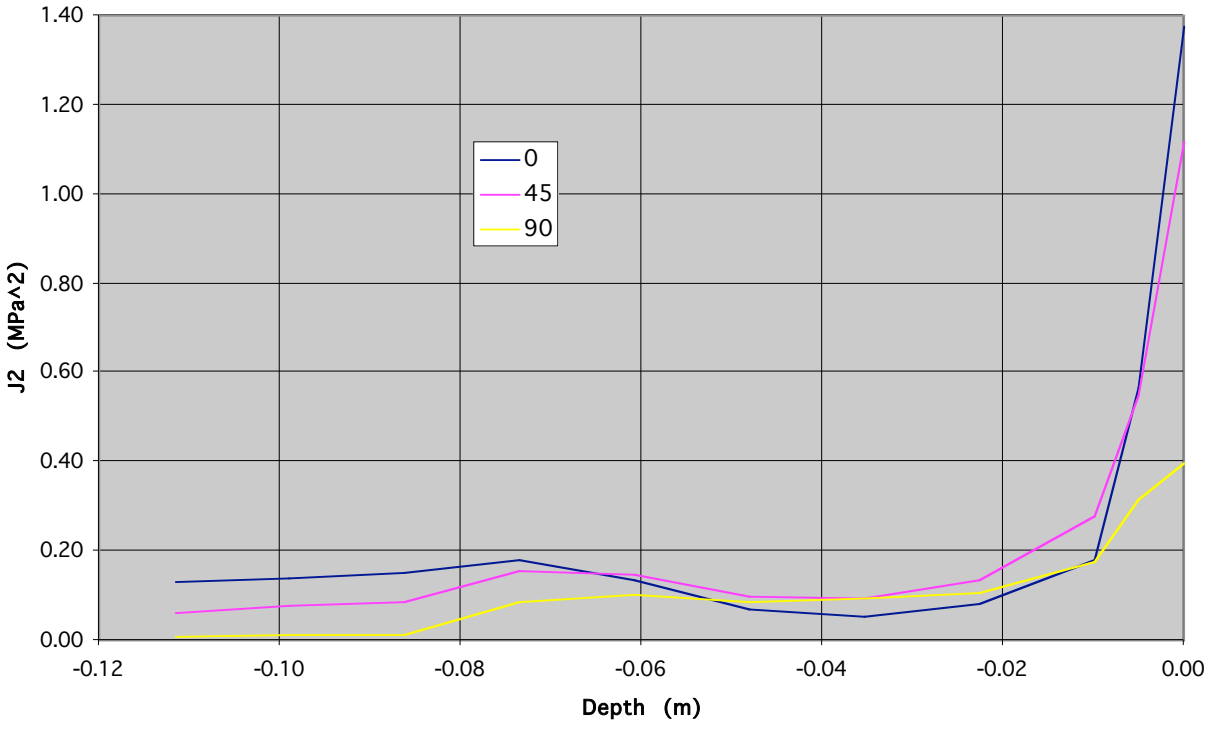

Figure 6.18: J_2 vs. depth; traffic loading (S23); Palmdale locale; S1.

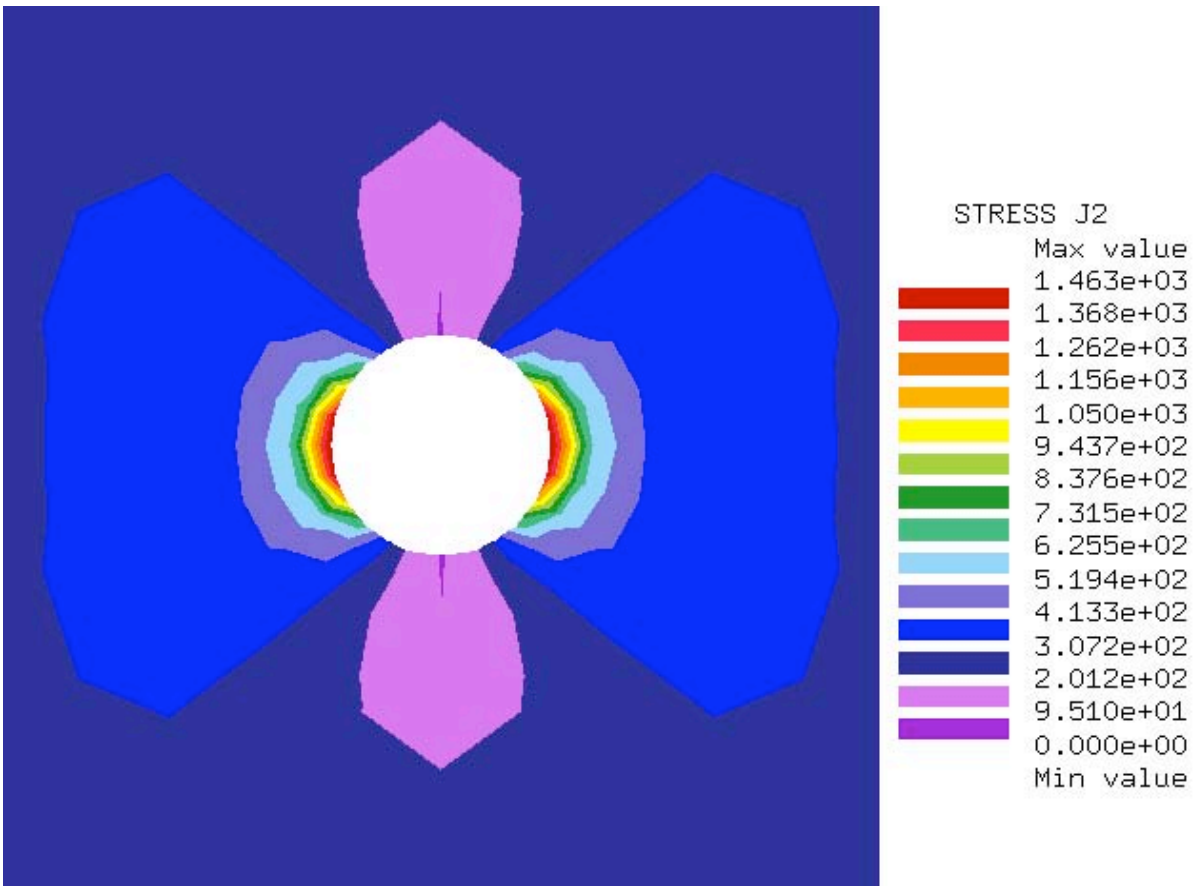

Figure 6.19: J_2 contours on the surface of the AC layer; thermal loading; Fairbanks; S1.

Figure 6.20: I_1 contours on the surface of the AC layer; thermal loading; Fairbanks; S1.

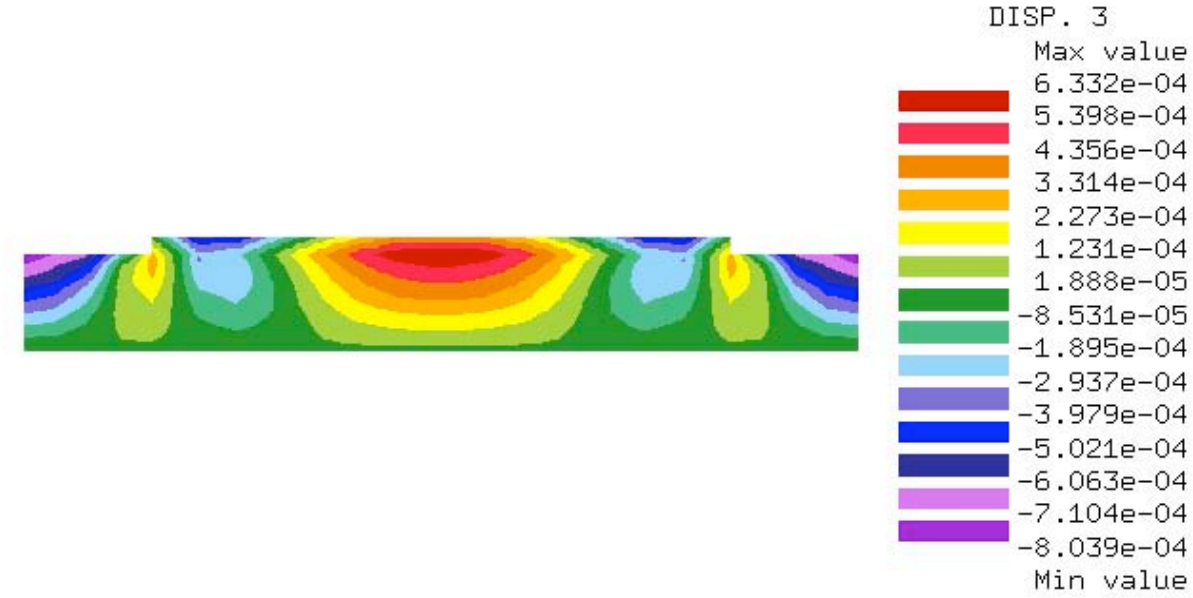

Figure 6.21: Vertical displacement contours; longitudinal plane; thermal loading; Fairbanks; S1.

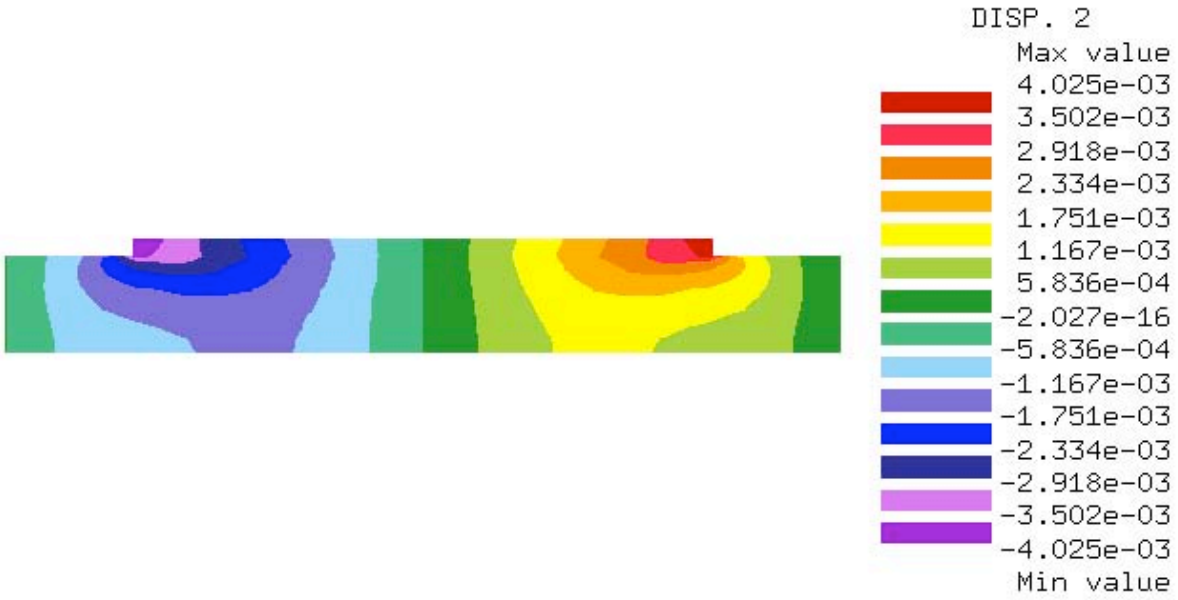

Figure 6.22: Lateral displacement contours; longitudinal plane; thermal loading; Fairbanks; S1.

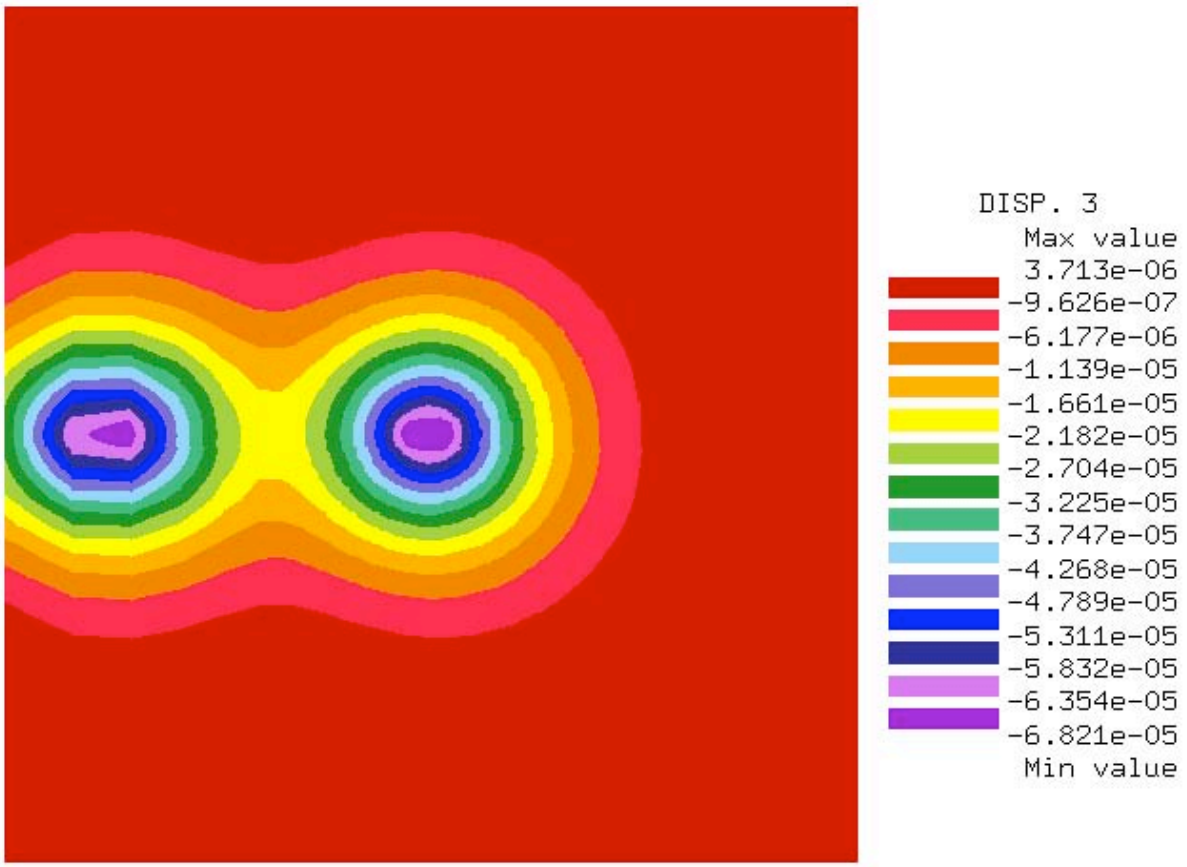

Figure 6.23: Vertical displacement contours; AC surface; traffic loading (S25); Fairbanks; S1.

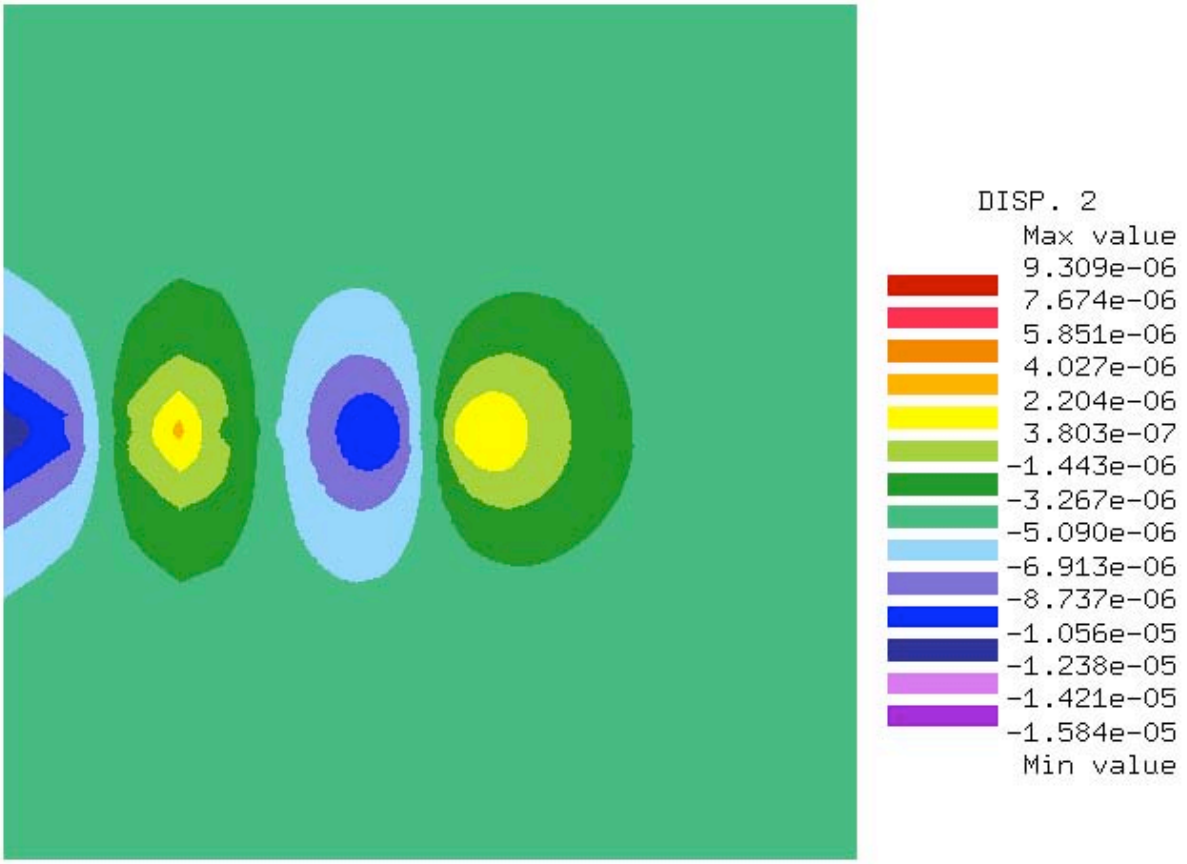

Figure 6.24: Lateral displacement contours; AC surface; traffic loading (S25); Fairbanks; S1.

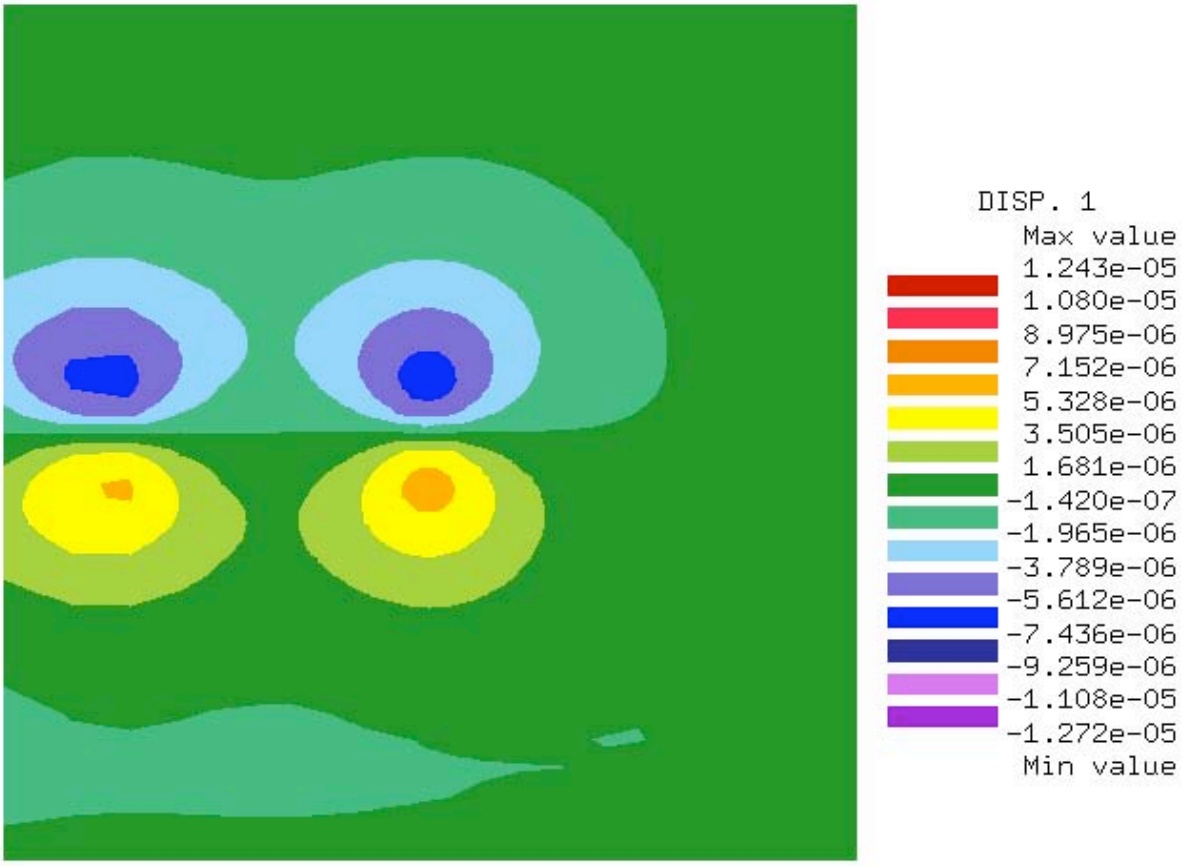

Figure 6.25: Longitudinal disp. contours; AC surface; traffic loading (S25); Fairbanks; S1.

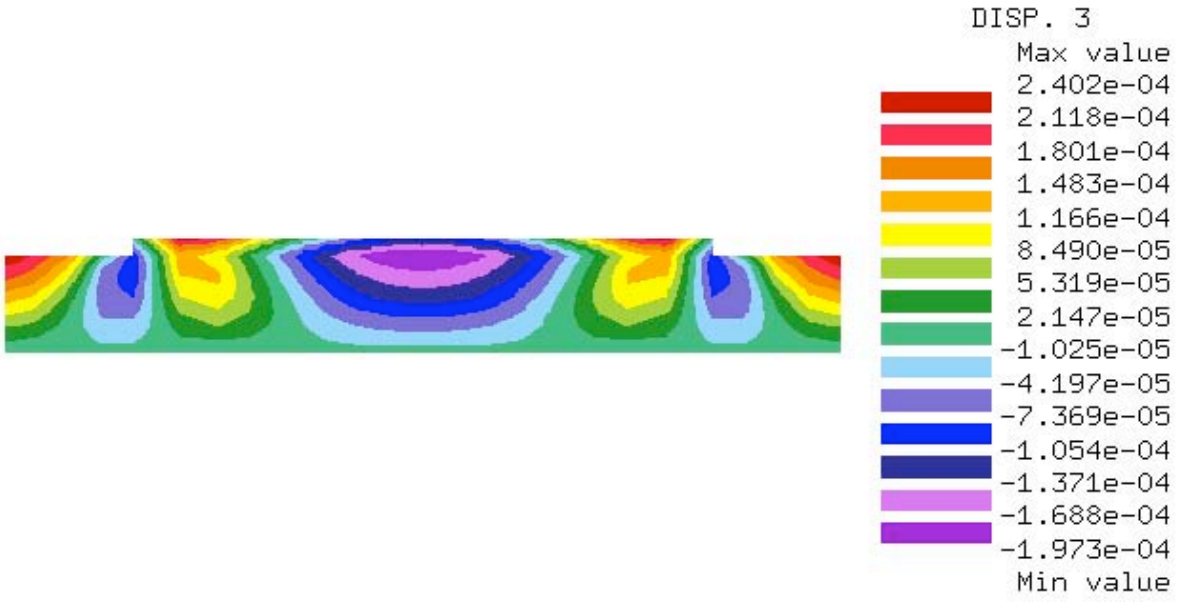

Figure 6.26: Vertical displacement contours; longitudinal plane; thermal loading; Palmdale; S1.

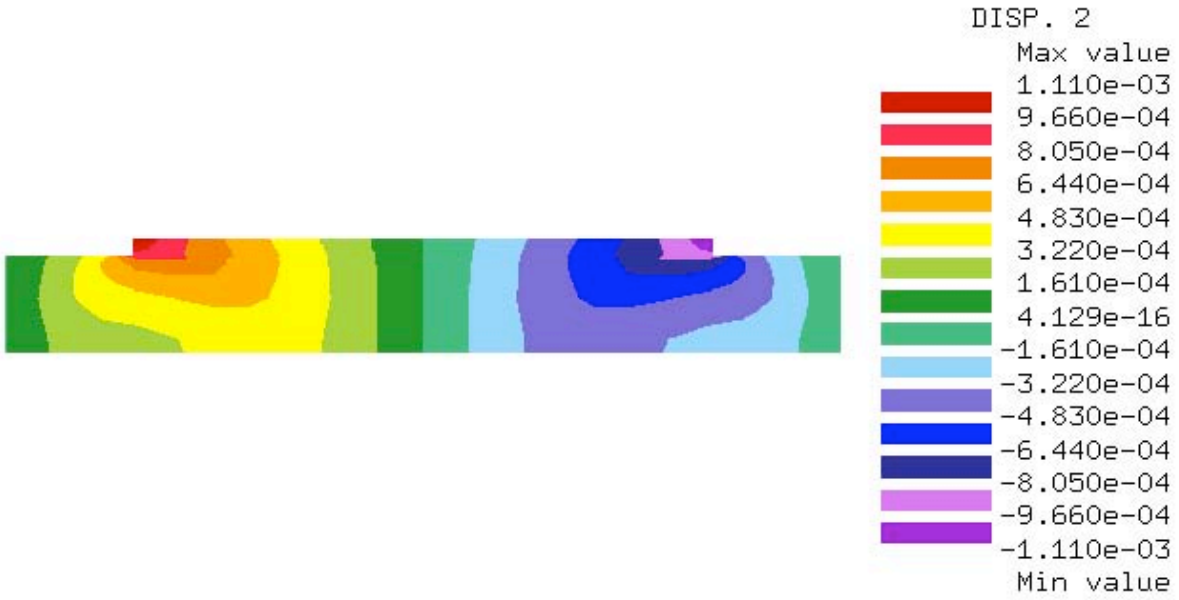

Figure 6.27: Lateral displacement contours; longitudinal plane; thermal loading; Palmdale; S1.

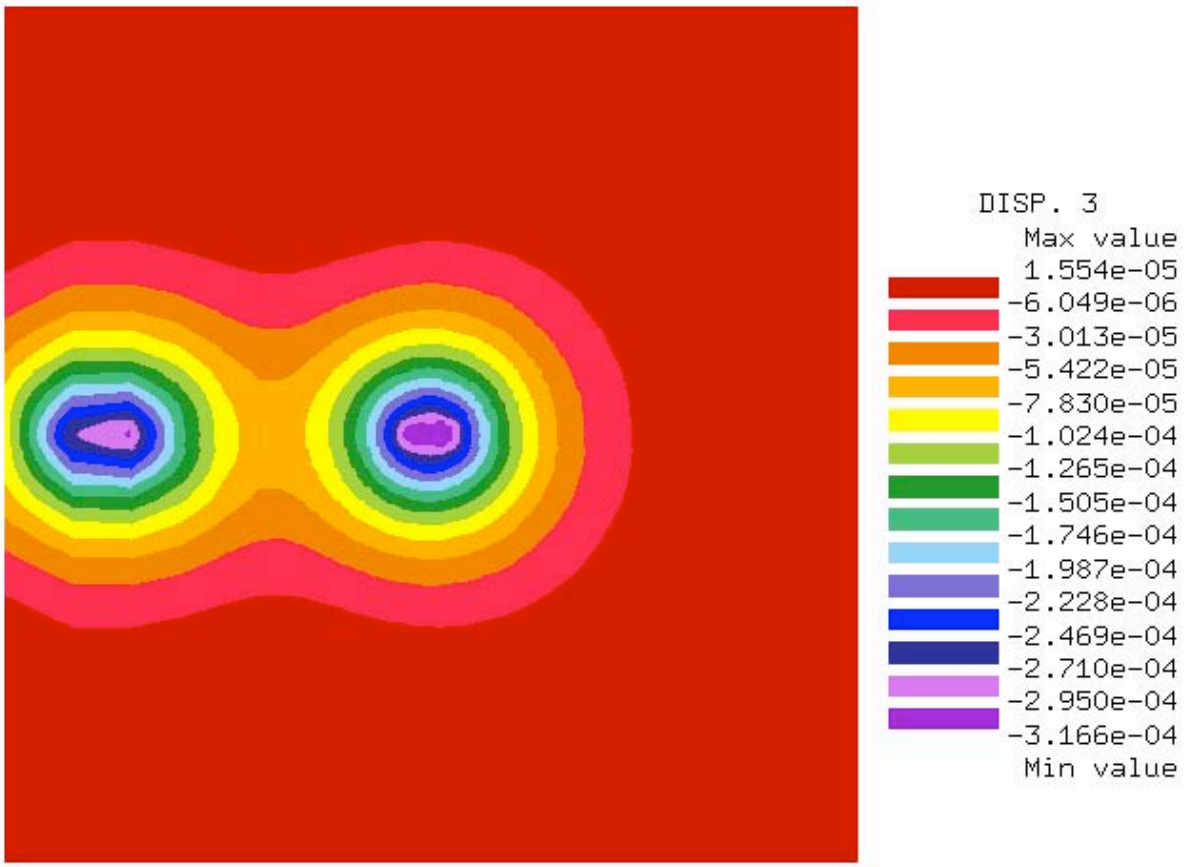

Figure 6.28: Vertical displacement contours; AC surface; traffic loading (S25); Palmdale; S1.

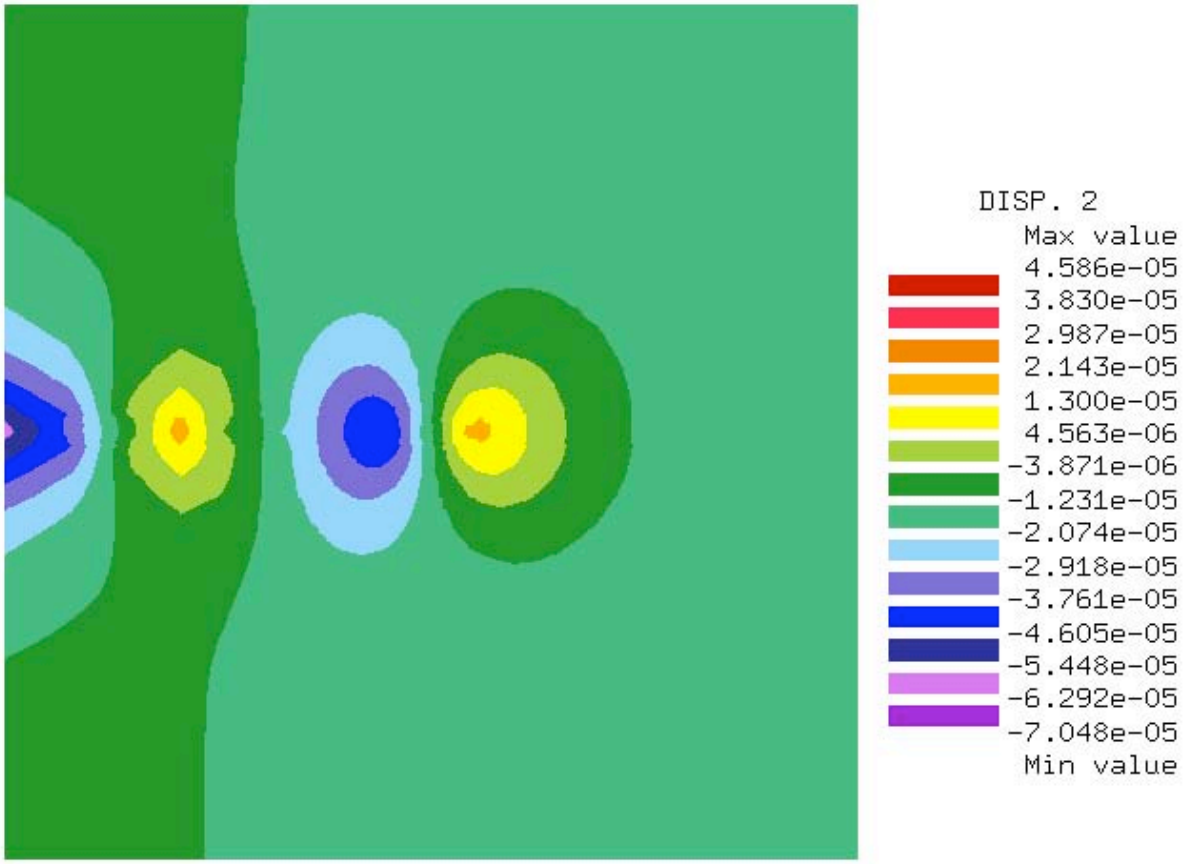

Figure 6.29: Lateral displacement contours; AC surface; traffic loading (S25); Palmdale; S1.

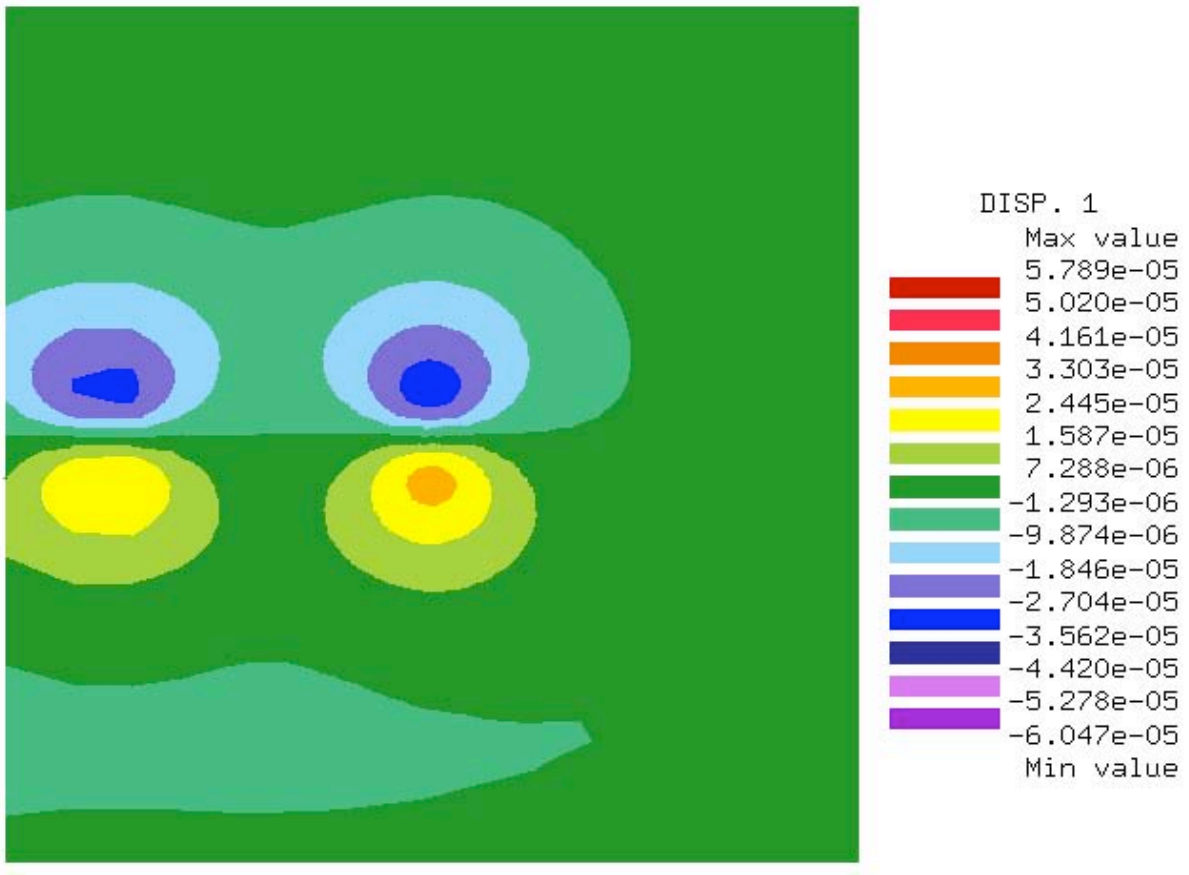

Figure 6.30: Longitudinal disp. contours; AC surface; traffic loading (S25); Palmdale; S1.

6.4 S2 pavement system

The results obtained for the S2 structure are similar in nature to those discussed above for the S1 structure. Therefore, only I_1 and J_2 line plots are reported for this case. These plots are shown in Figures 6.31 through 6.38. The reader is referred to the accompanying CD for contour plots of different stress components and stress invariants.

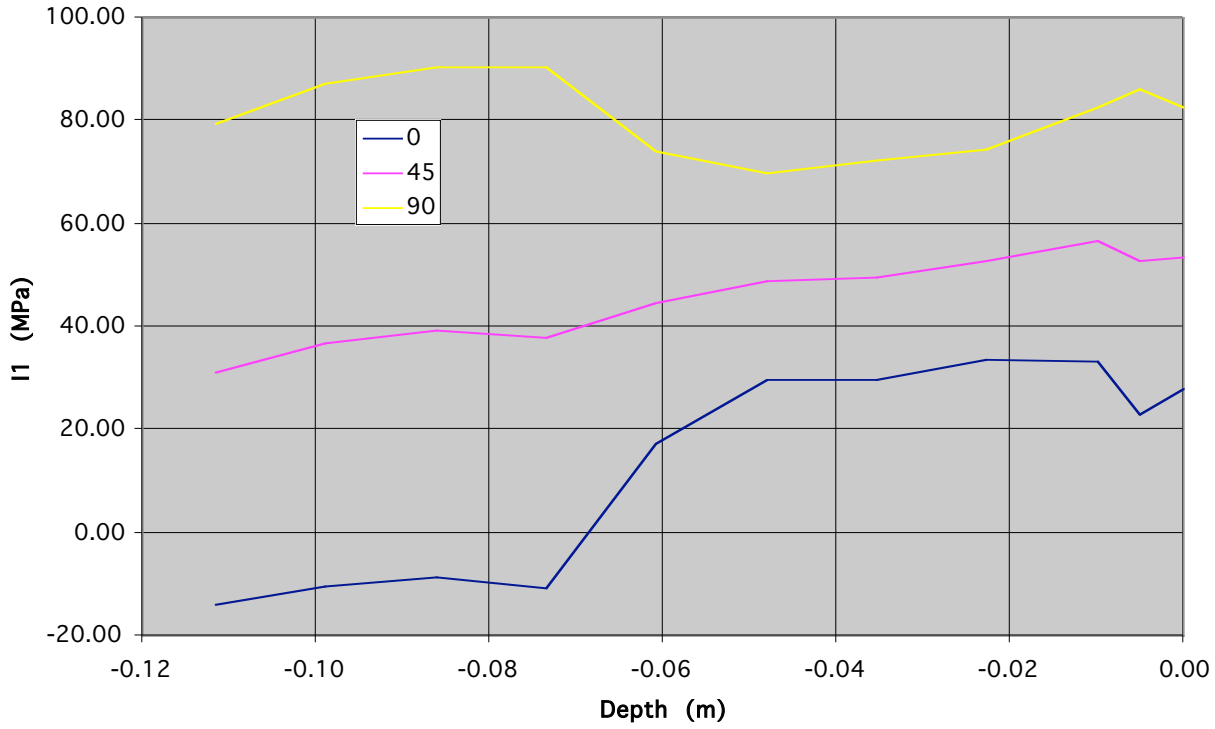

Figure 6.31: I_1 vs. depth; thermal loading; Fairbanks locale; S2.

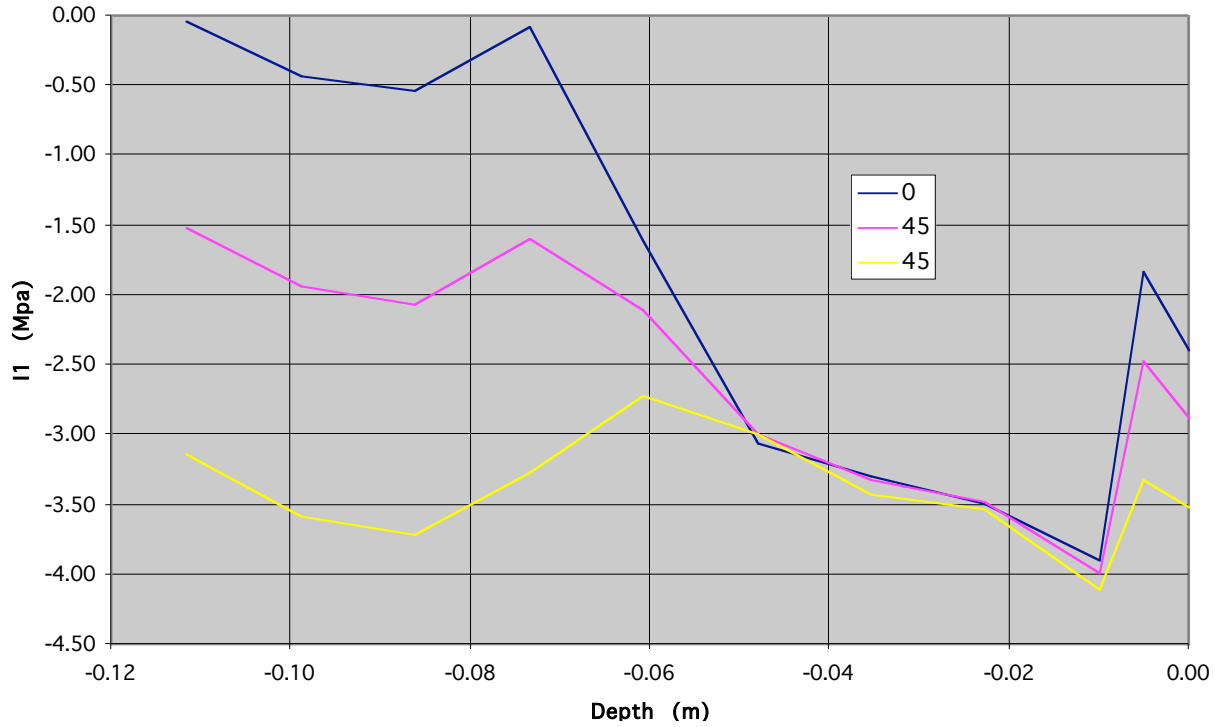

Figure 6.32: I_1 vs. depth; thermal loading; Palmdale locale; S2.

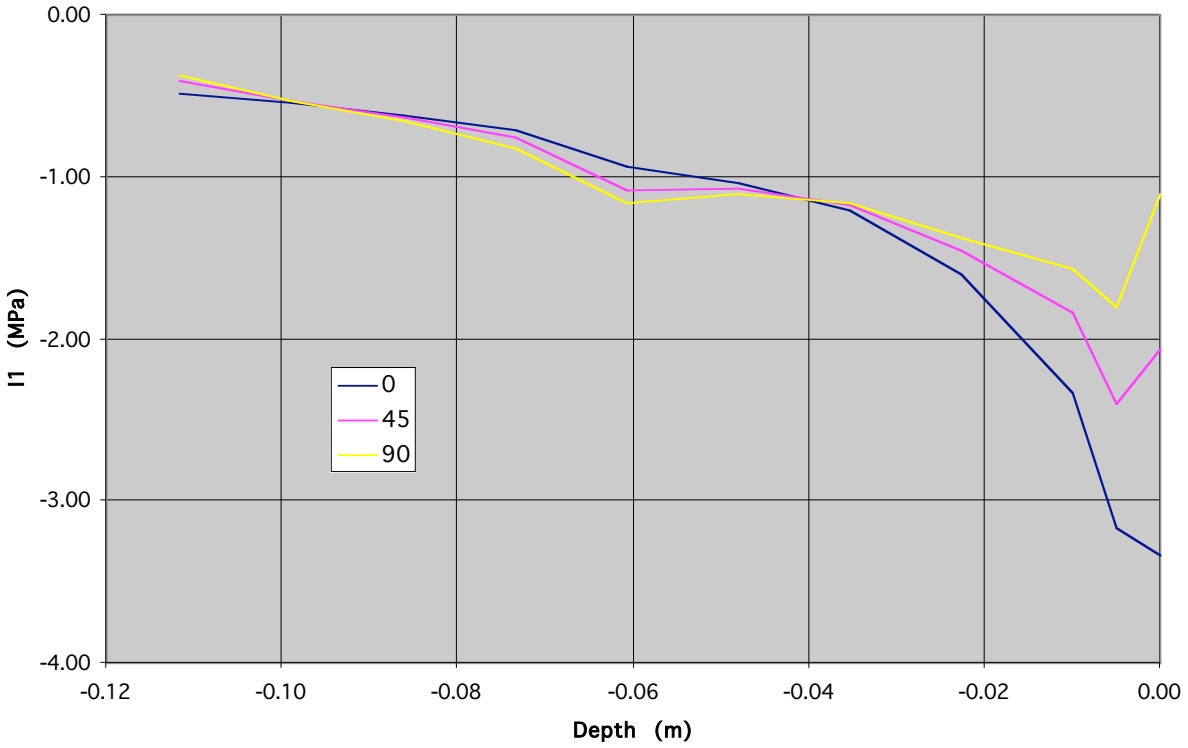

Figure 6.33: I_1 vs. depth; traffic loading (S23); Fairbanks locale; S2.

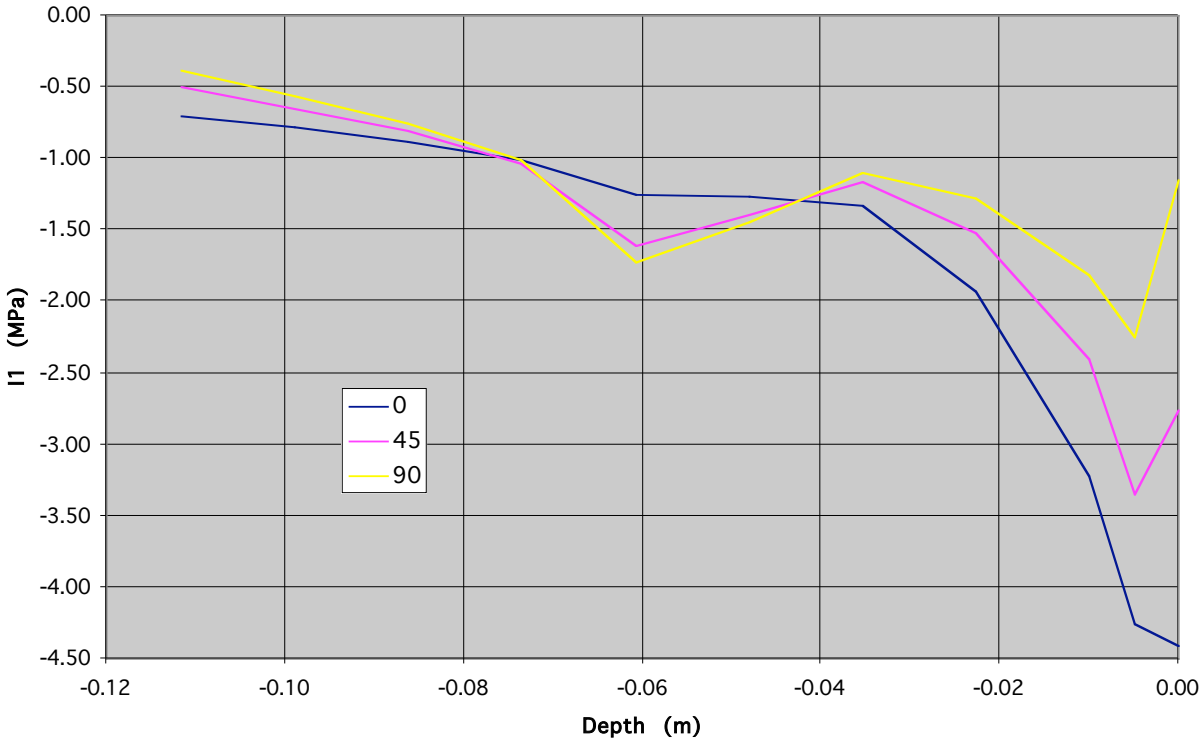

Figure 6.34: I_1 vs. depth; traffic loading (S23); Palmdale locale; S2.

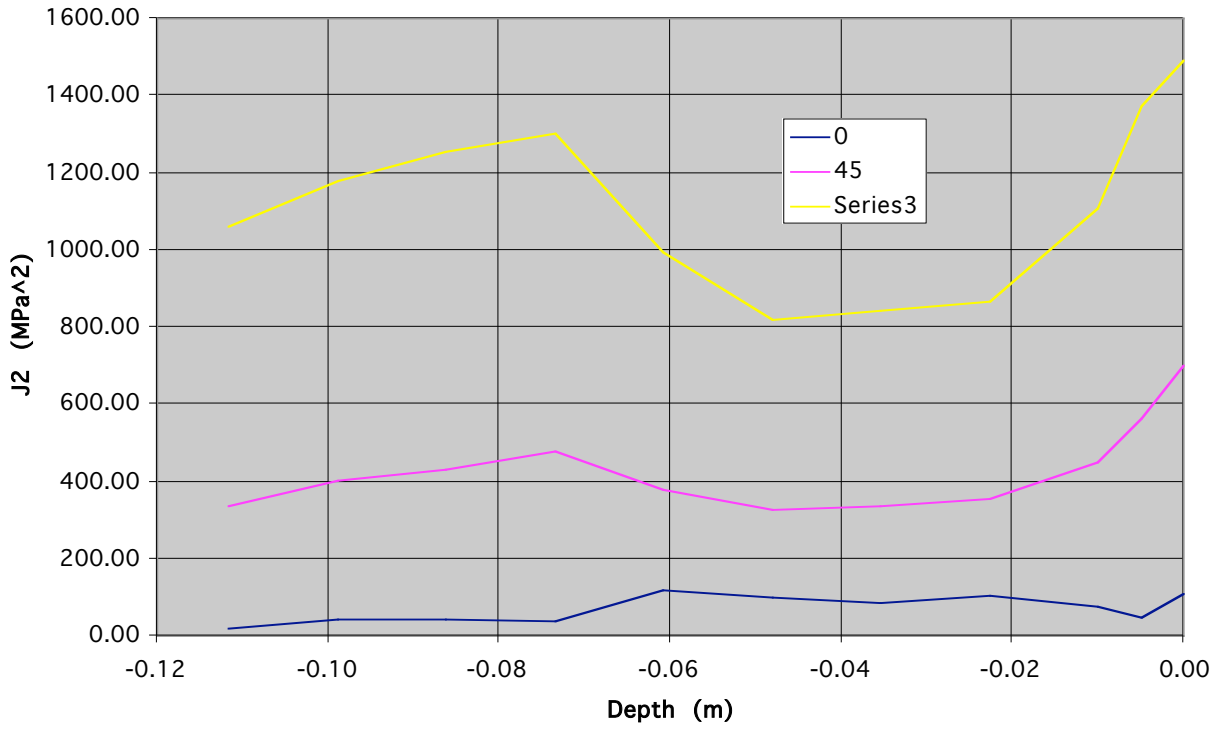

Figure 6.35: J_2 vs. depth; thermal loading; Fairbanks locale; S2.

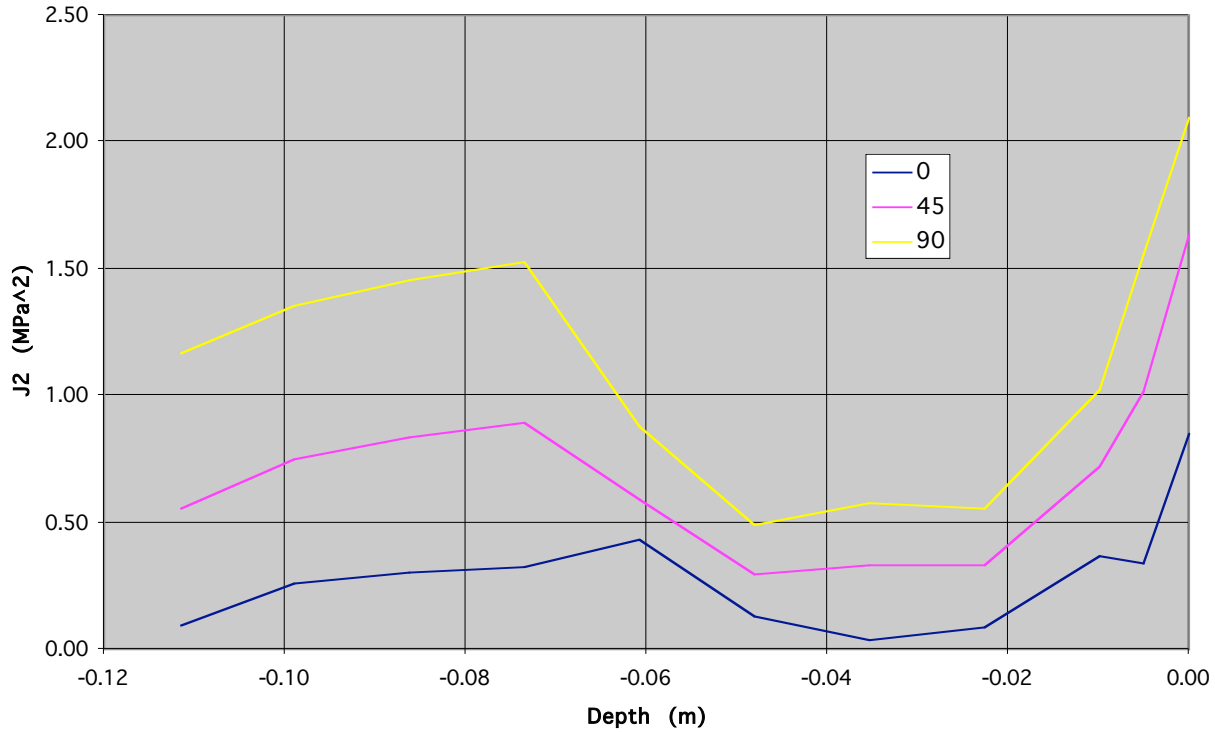

Figure 6.36: J_2 vs. depth; thermal loading; Palmdale locale; S2.

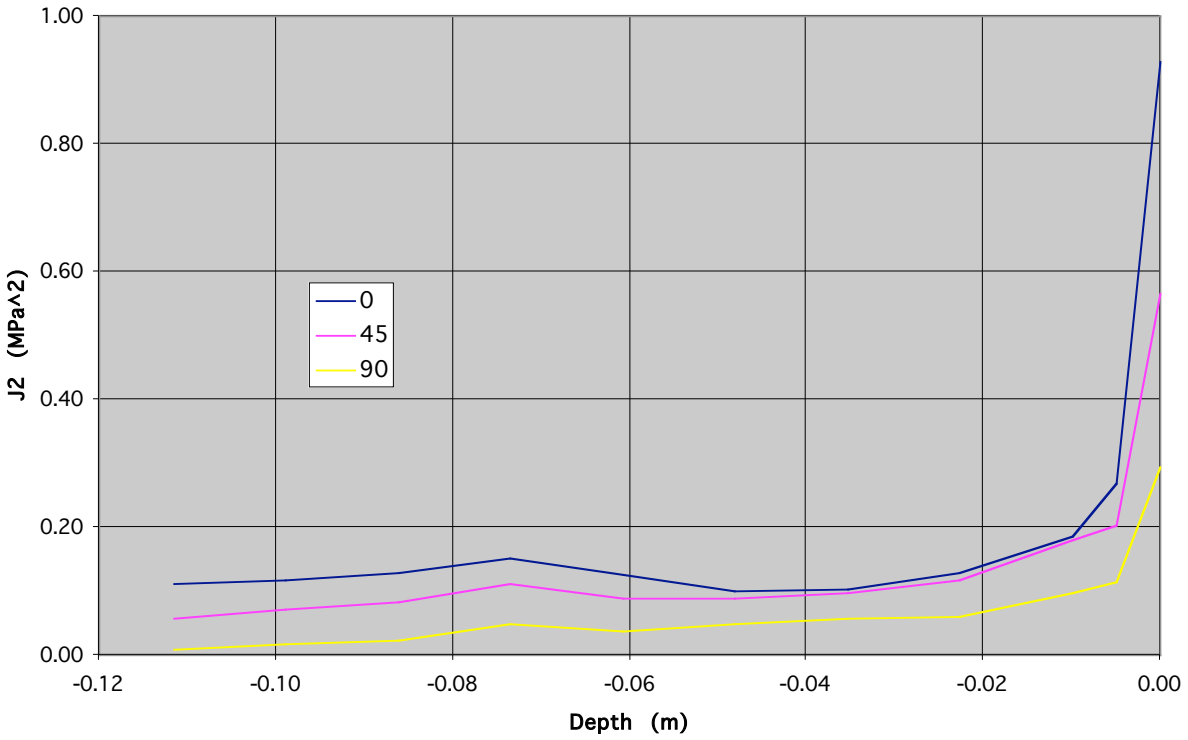

Figure 6.37: J_2 vs. depth; traffic loading (S23); Fairbanks locale; S2.

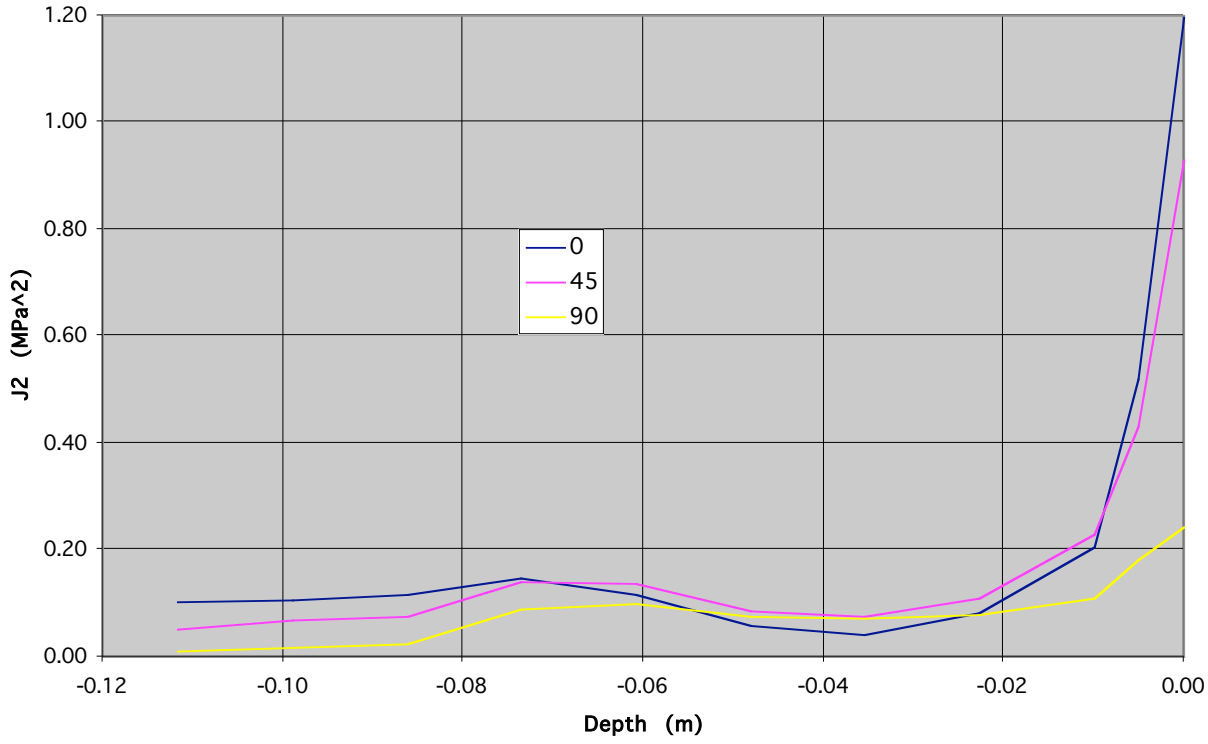

Figure 6.38: J_2 vs. depth; traffic loading (S23); Palmdale locale; S2.

6.5 S3 pavement System

For traffic loading, the results obtained for the S3 pavement structure are in line with those previously discussed for the S1 and S2 pavements. However, as a result of the presence of thermal joints, very different results are observed for thermal loading. This difference is clearly demonstrated by examining the displacement fields. Figures 6.39 (Fairbanks local) and 6.40 (Palmdale locale) show contour plots of the vertical component of the displacements, plotted on the surface of the pavement (*i.e.*, plan view). These figures show a complex three-dimensional state of displacements that exhibit some symmetry, but by no means resemble a plane strain state. A closer examination of Figures 6.39 and 6.40 reveals that the slabs exhibit double curvature, and are either concave (Fairbanks) or obtuse (Palmdale). These results suggest that in reality the slab would separate from the base layer and therefore the stress field may be quite different than that predicted here (the slab is taken to be fully bonded with the base layer in the current model), especially near the slab edges. For example, for the Palmdale locale, the plate would lift and rest on its four corners and therefore, large stresses may develop at those corners.

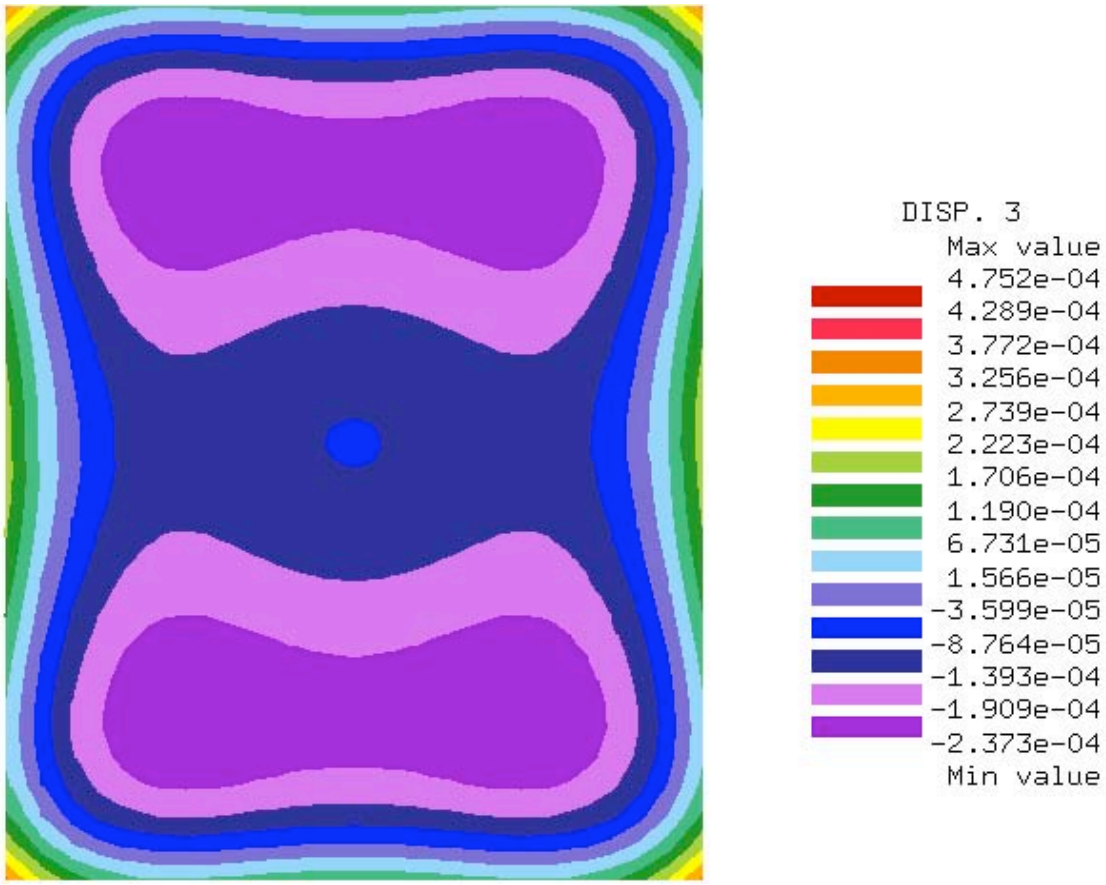

Figure 6.39: Vertical displacement contours; AC surface; thermal loading, Fairbanks locale; S3.

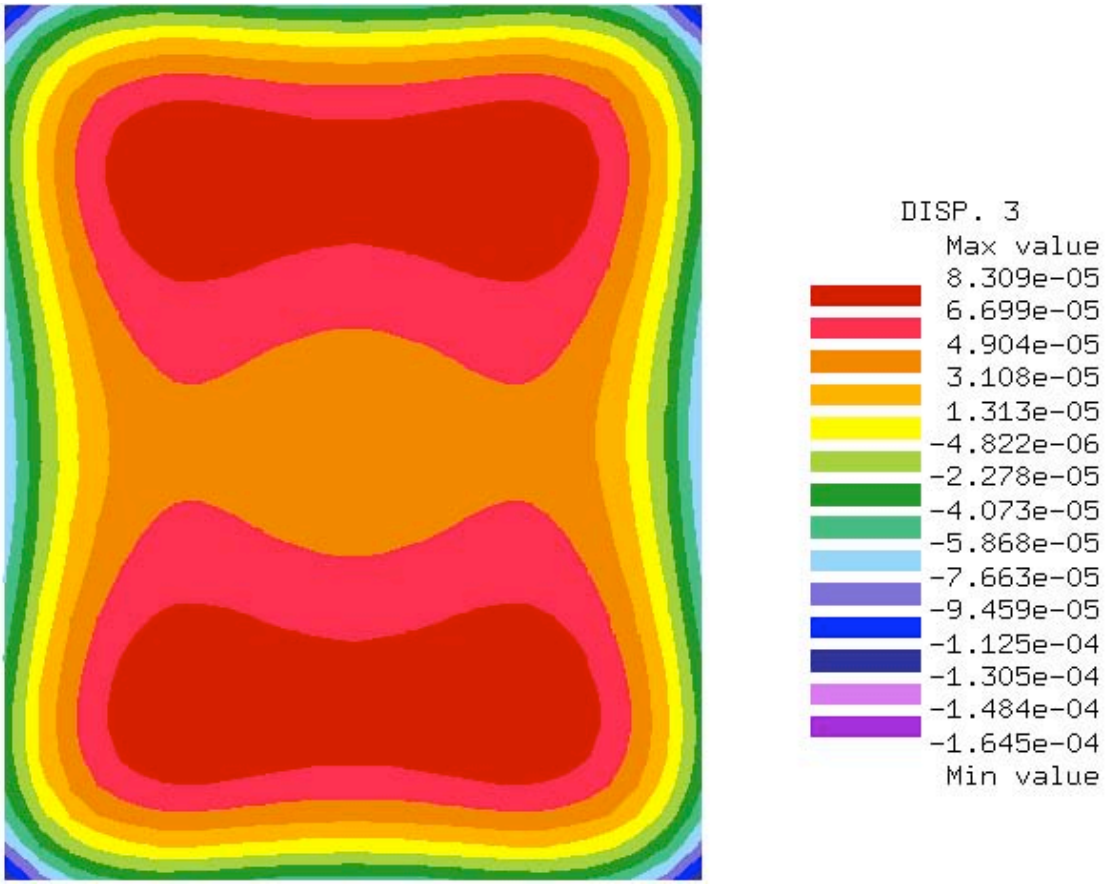

Figure 6.40: Vertical displacement contours; AC surface; thermal loading, Palmdale locale; S3.

Figures 6.41 through 6.48 provide line plots of I_1 and J_2 stress invariants along the cavity walls (PCC side). The locations along the circumference are the same as those used for the S1 and S2 pavements above. The plots for the traffic loading (both locales) are based on cases S23 because the J_2 attains its highest value for that case (see the Excel spreadsheet resSum.Exe in the accompanying CD). Finally, much more information on the S3 pavement simulation results can be found on the accompanying CD.

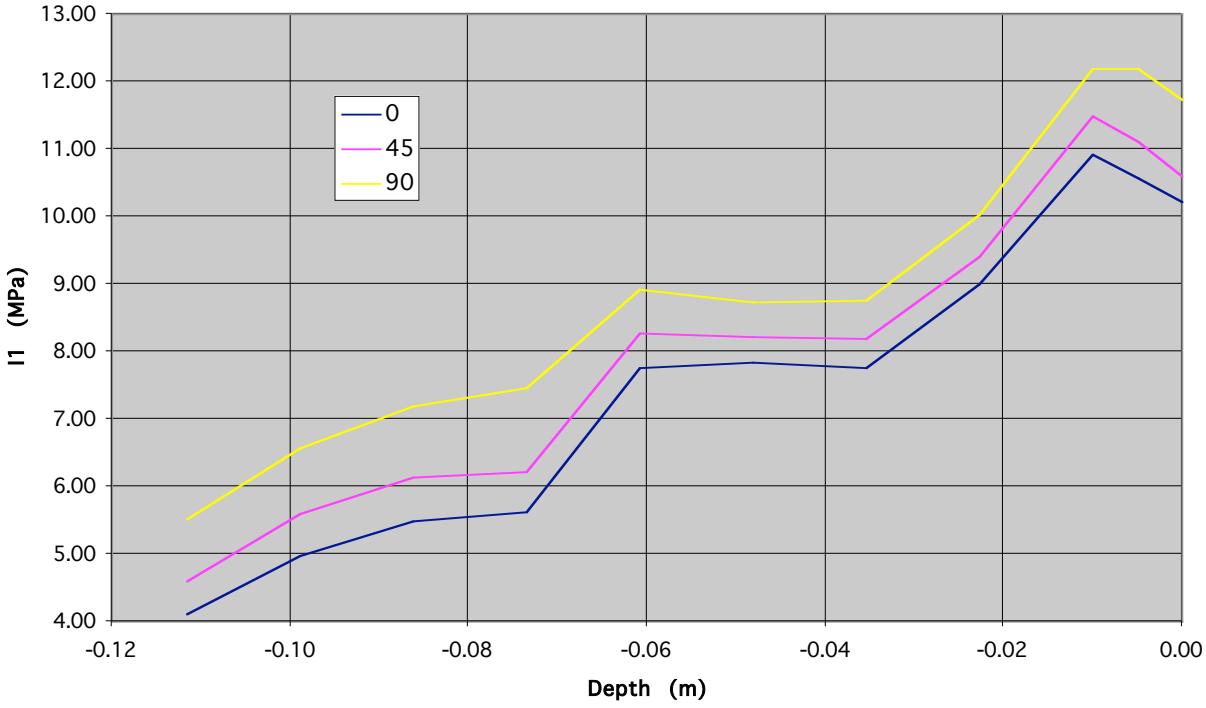

Figure 6.41: I_1 vs. depth; thermal loading; Fairbanks locale; S3.

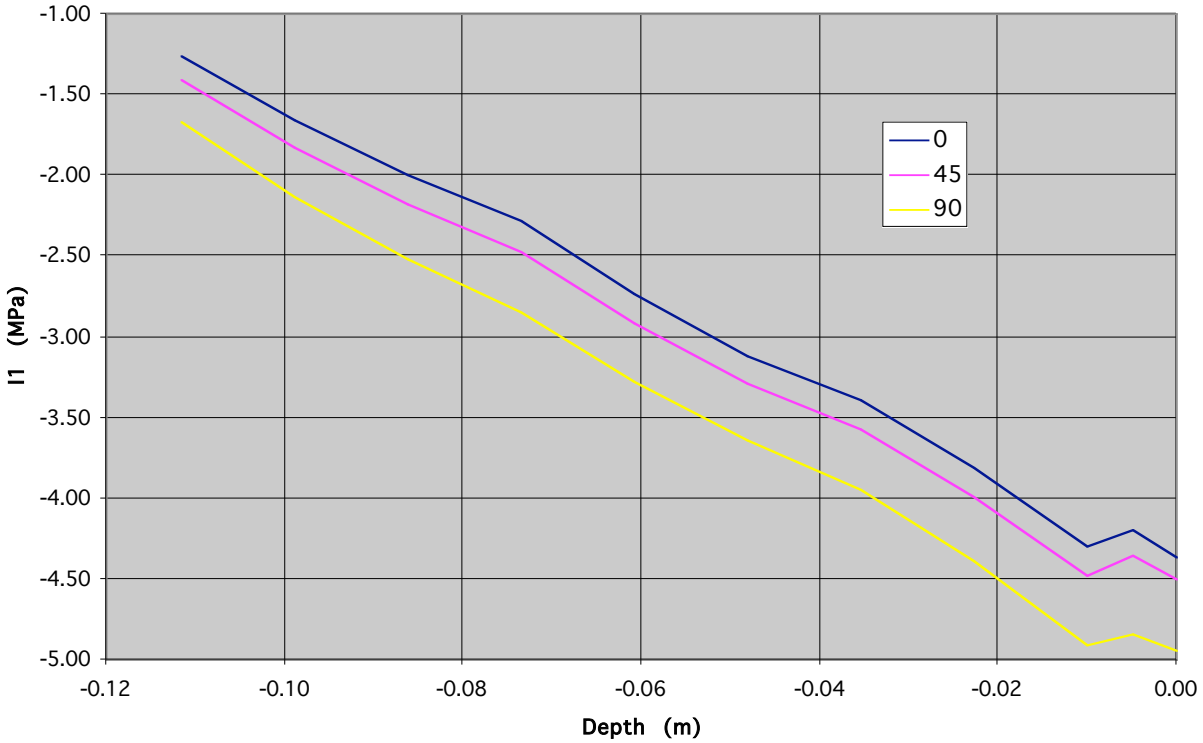

Figure 6.42: I_1 vs. depth; thermal loading; Palmdale locale; S3.

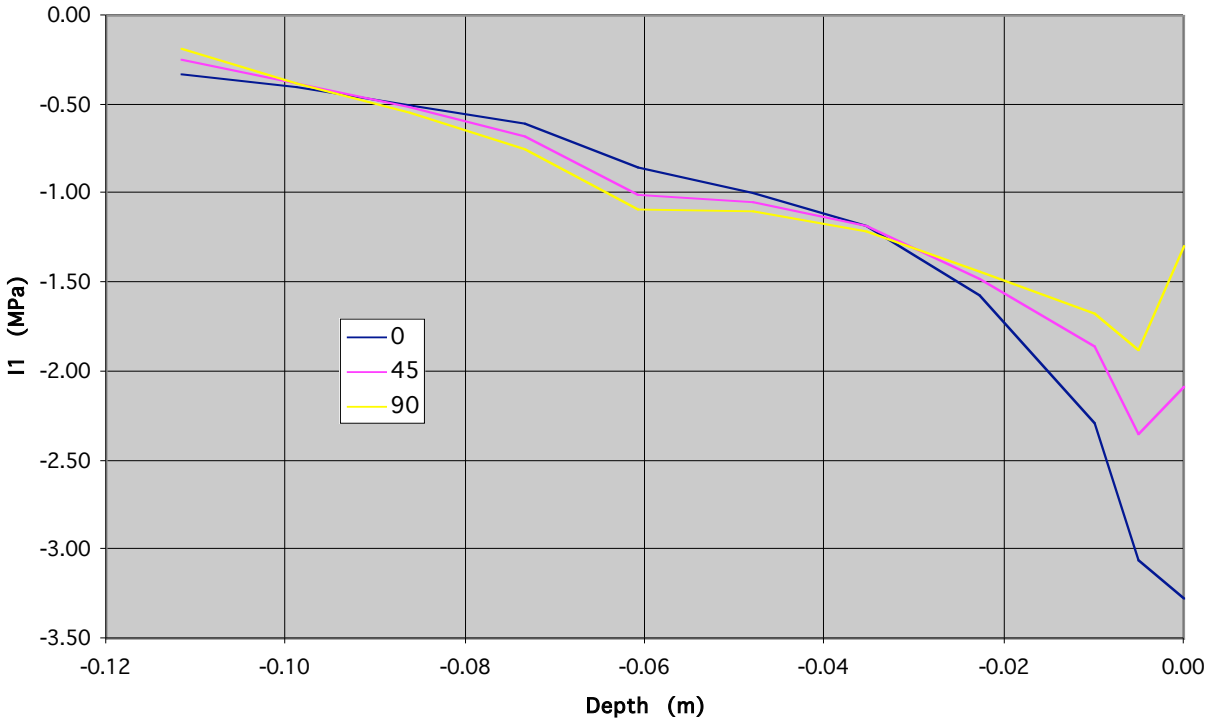

Figure 6.43: I_1 vs. depth; traffic loading (S23); Fairbanks locale; S3.

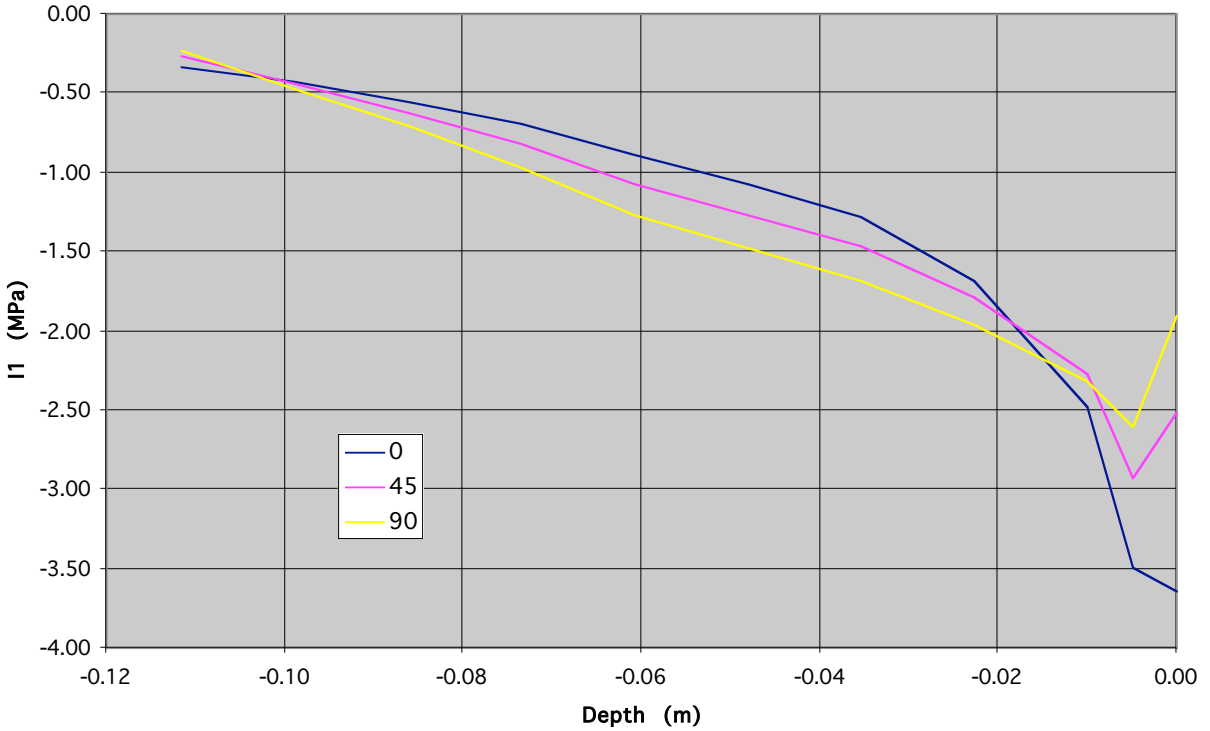

Figure 6.44: I_1 vs. depth; traffic loading (S23); Palmdale locale; S3.

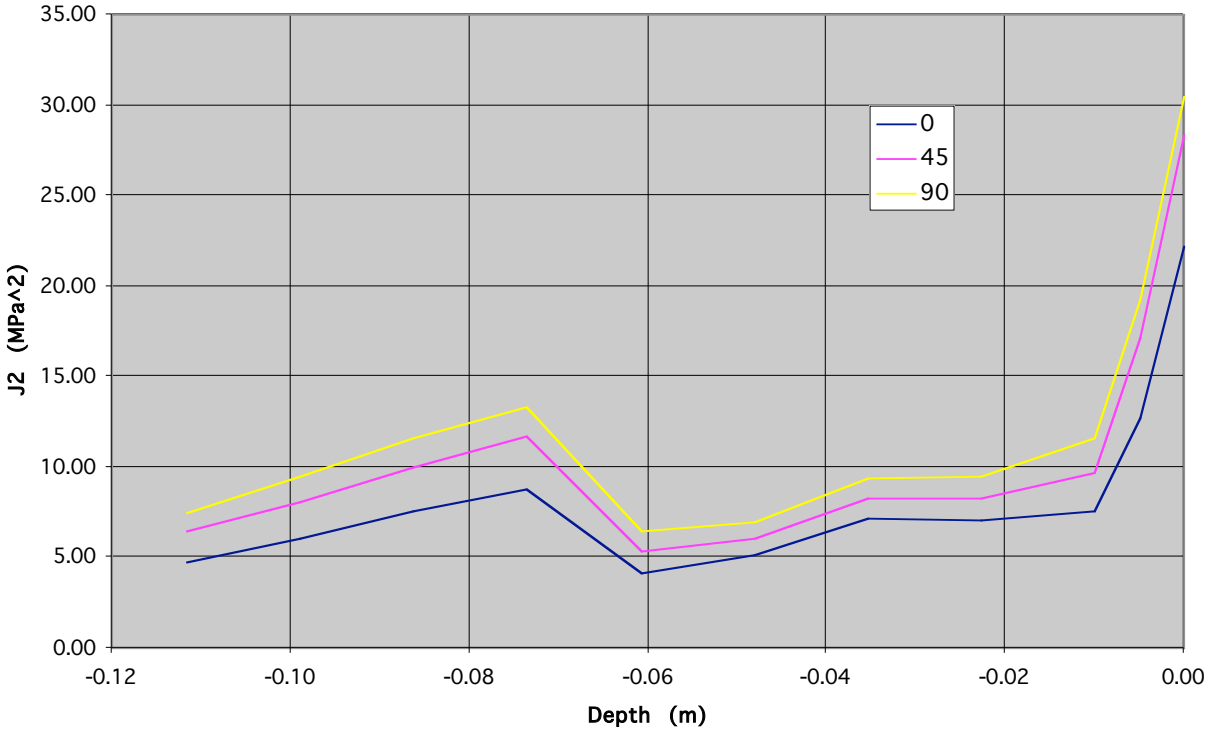

Figure 6.45: J_2 vs. depth; thermal loading; Fairbanks locale; S3.

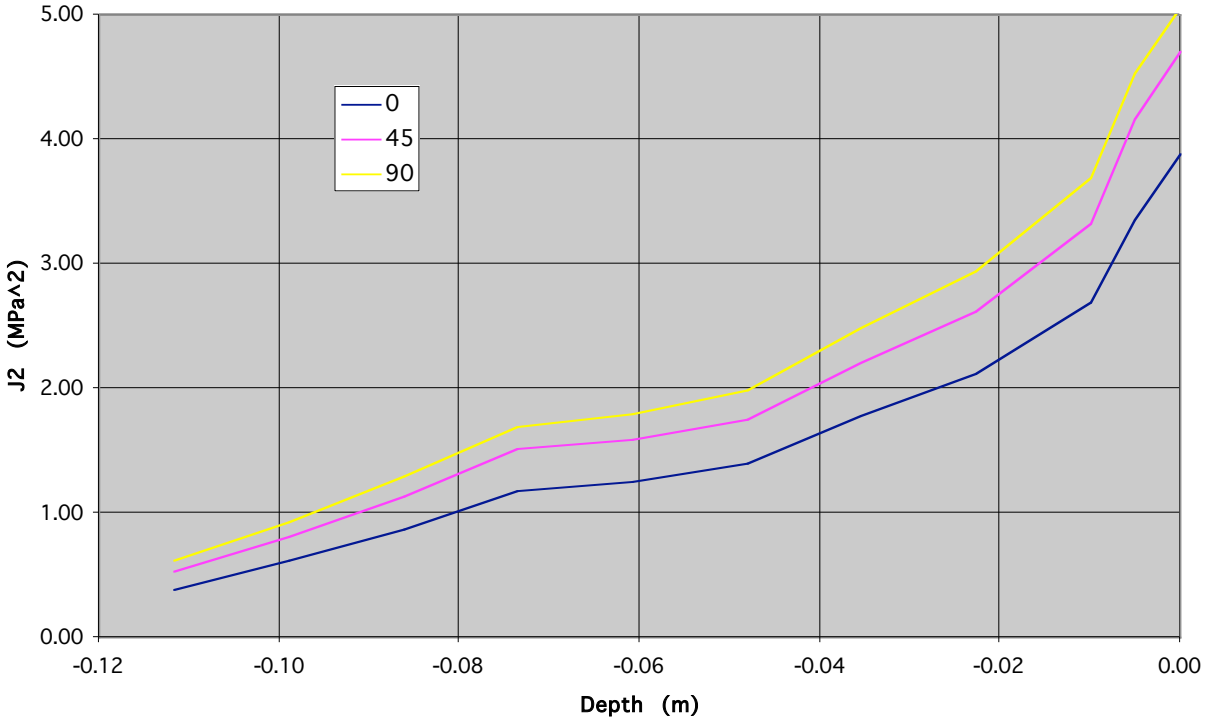

Figure 6.46: J_2 vs. depth; thermal loading; Palmdale locale; S3.

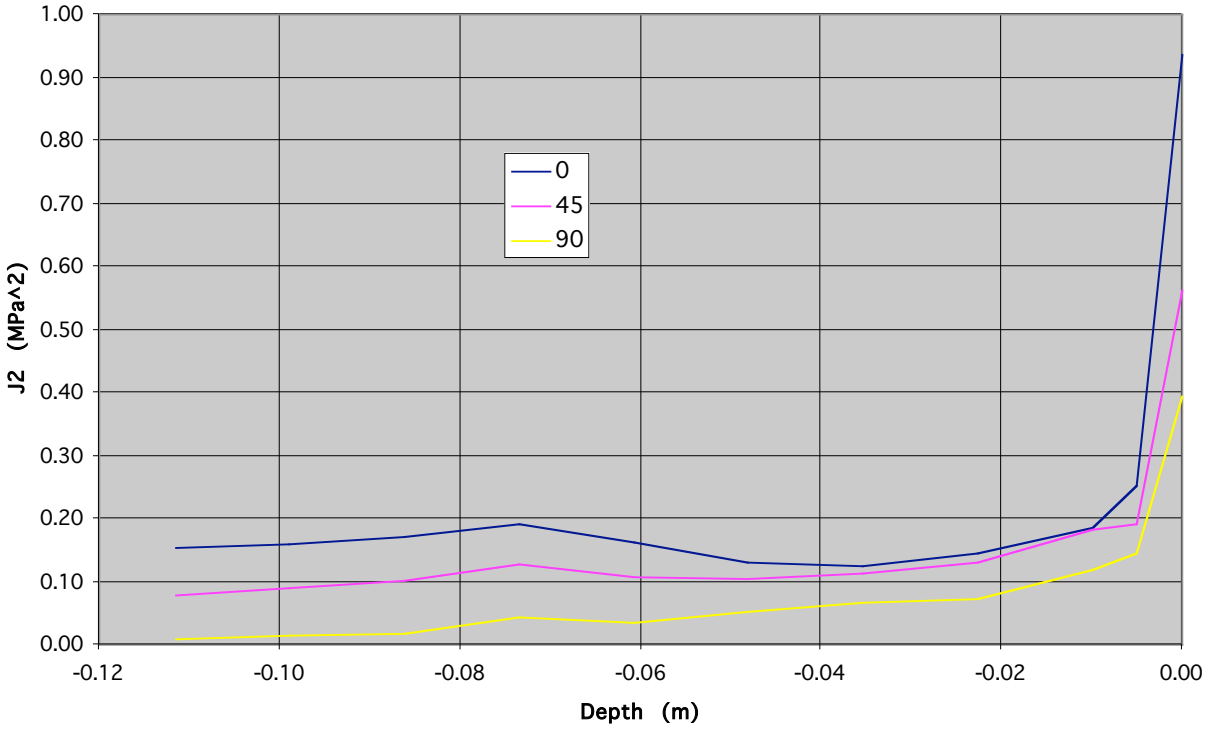

Figure 6.47: J_2 vs. depth; traffic loading (S23); Fairbanks locale; S3.

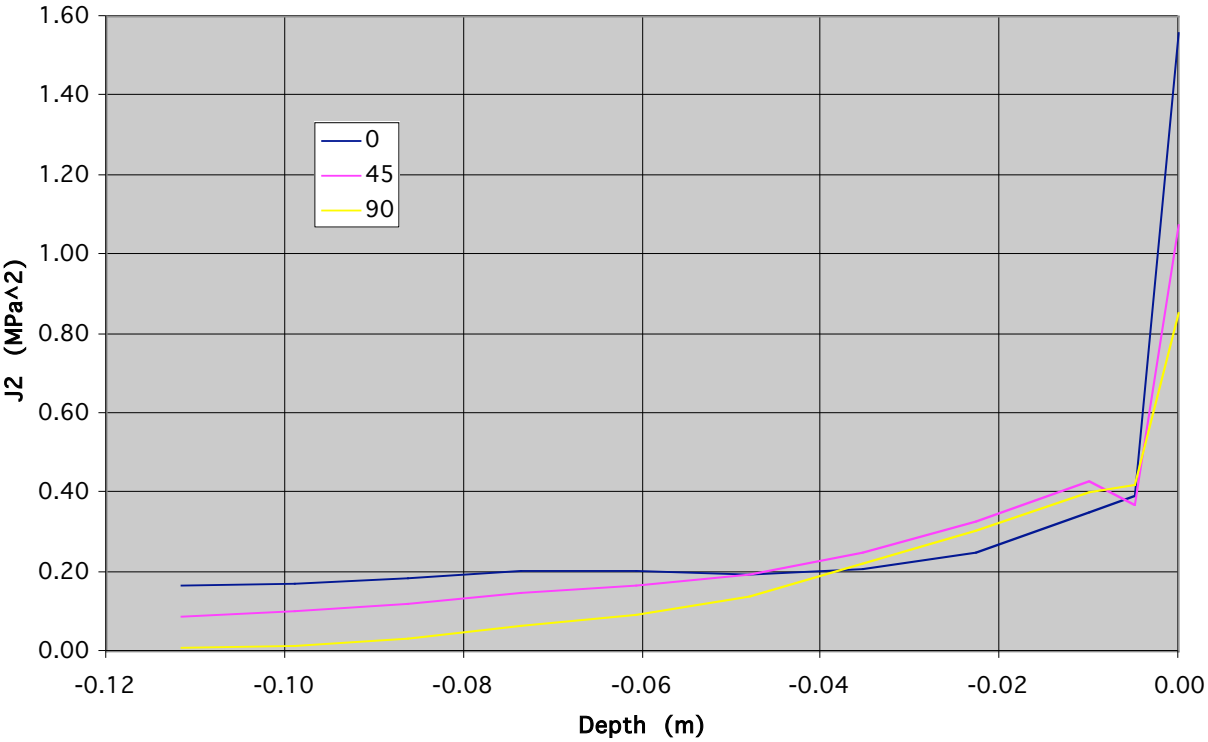

Figure 6.48: J_2 vs. depth; traffic loading (S23); Palmdale locale; S3.

6.6 S4 pavement system

The results obtained for the S4 structure are similar in nature to those discussed above for the S3 structure. Therefore, only I_1 and J_2 line plots are reported for this case. These plots are shown in Figures 6.49 through 6.56. The reader is referred to the accompanying CD for contour plots of different stress components and stress invariants.

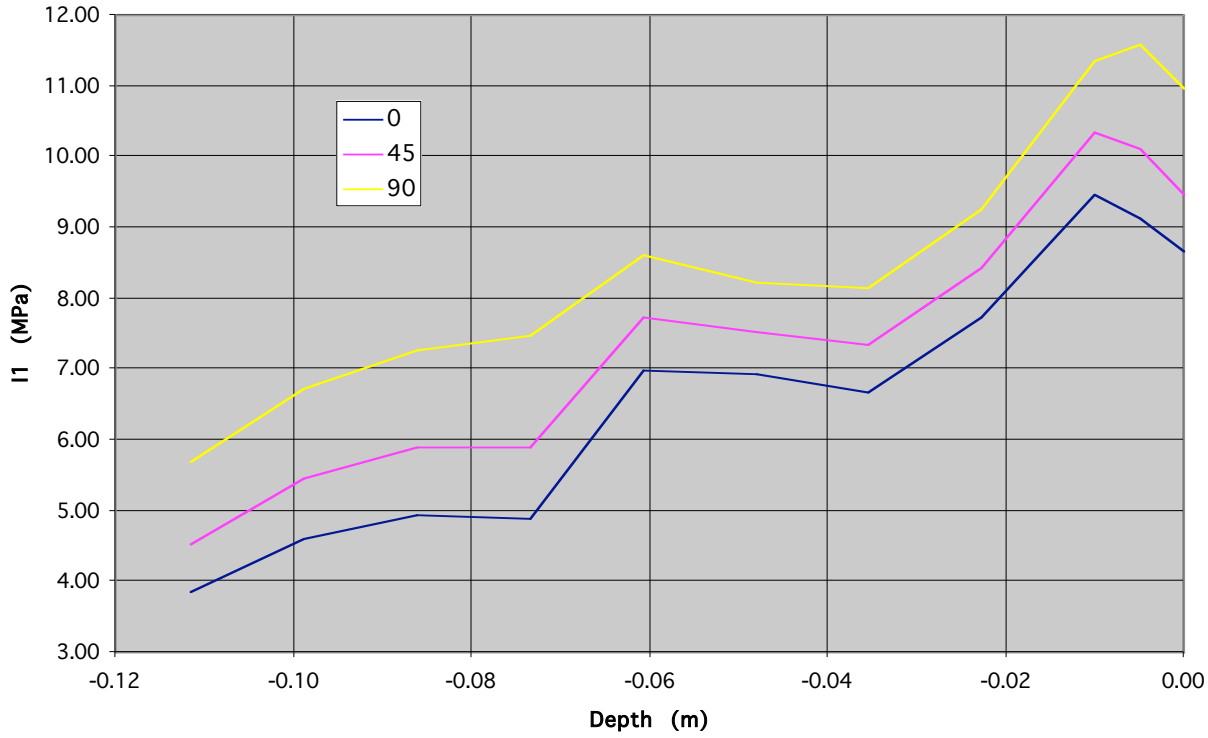

Figure 6.49: I_1 vs. depth; thermal loading; Fairbanks locale; S4.

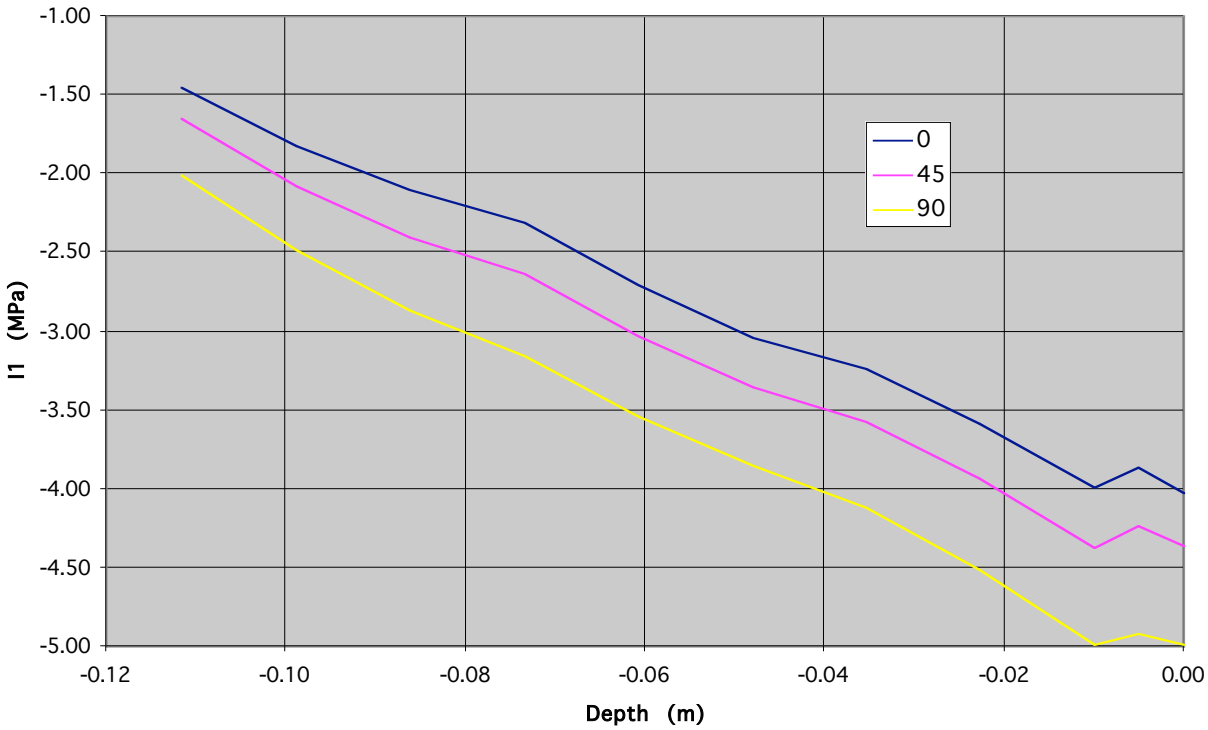

Figure 6.50: I_1 vs. depth; thermal loading; Palmdale locale; S4.

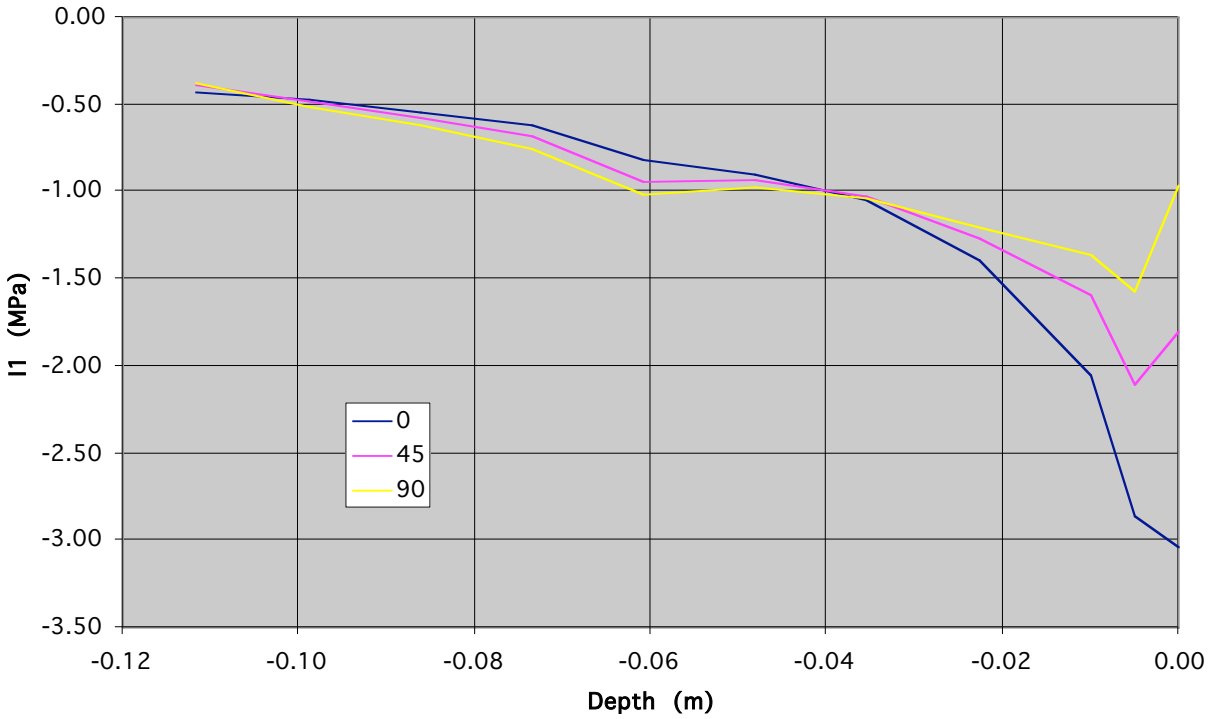

Figure 6.51: I_1 vs. depth; traffic loading (S23); Fairbanks locale; S4.

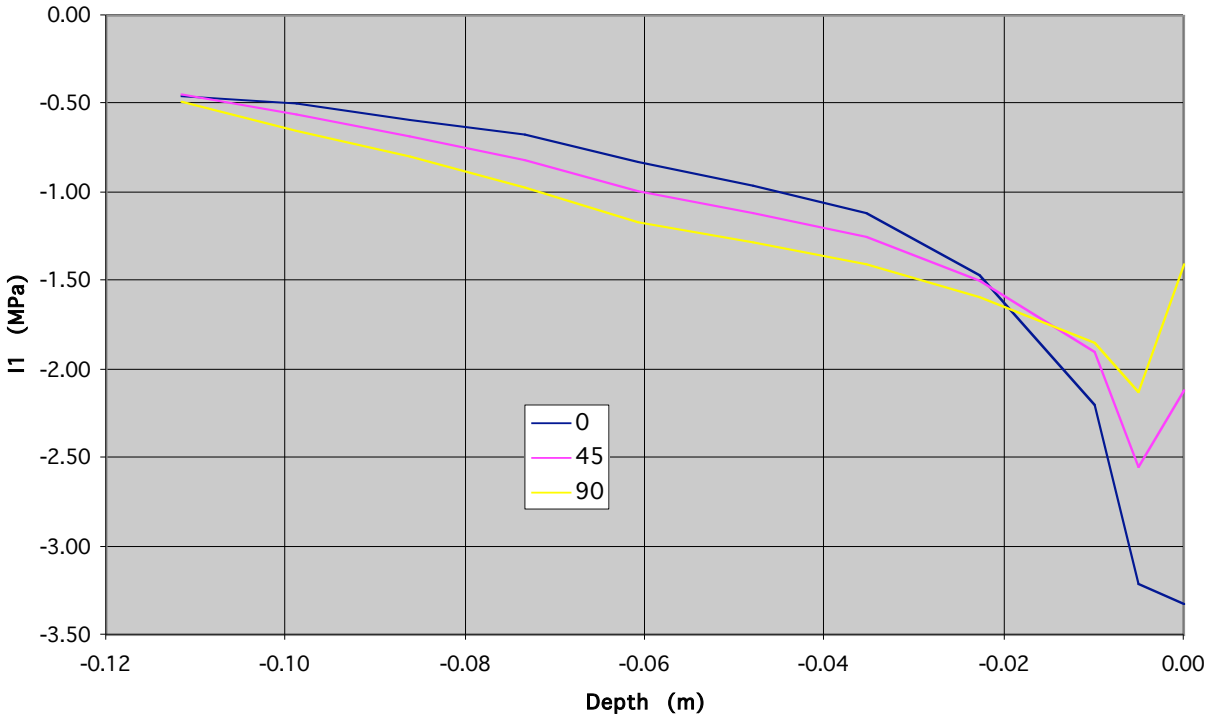

Figure 6.52: I_1 vs. depth; traffic loading (S23); Palmdale locale; S4.

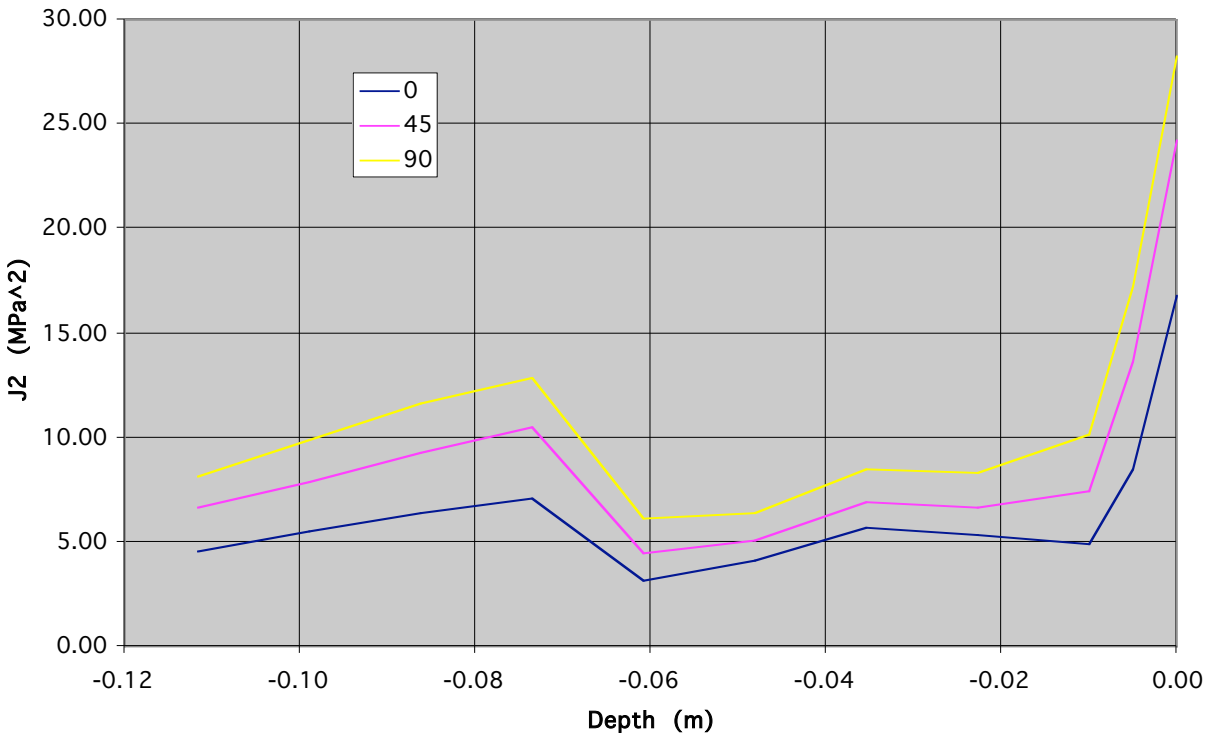

Figure 6.53: J_2 vs. depth; thermal loading; Fairbanks locale; S4.

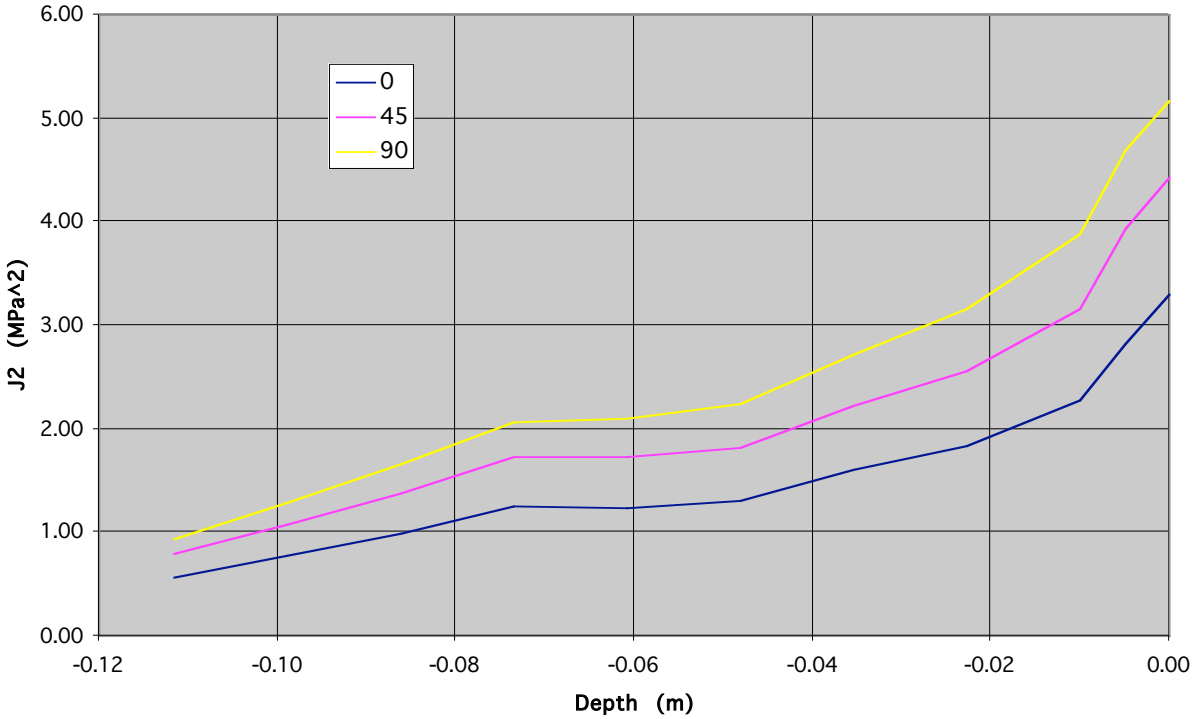

Figure 6.54: J_2 vs. depth; thermal loading; Palmdale locale; S4.

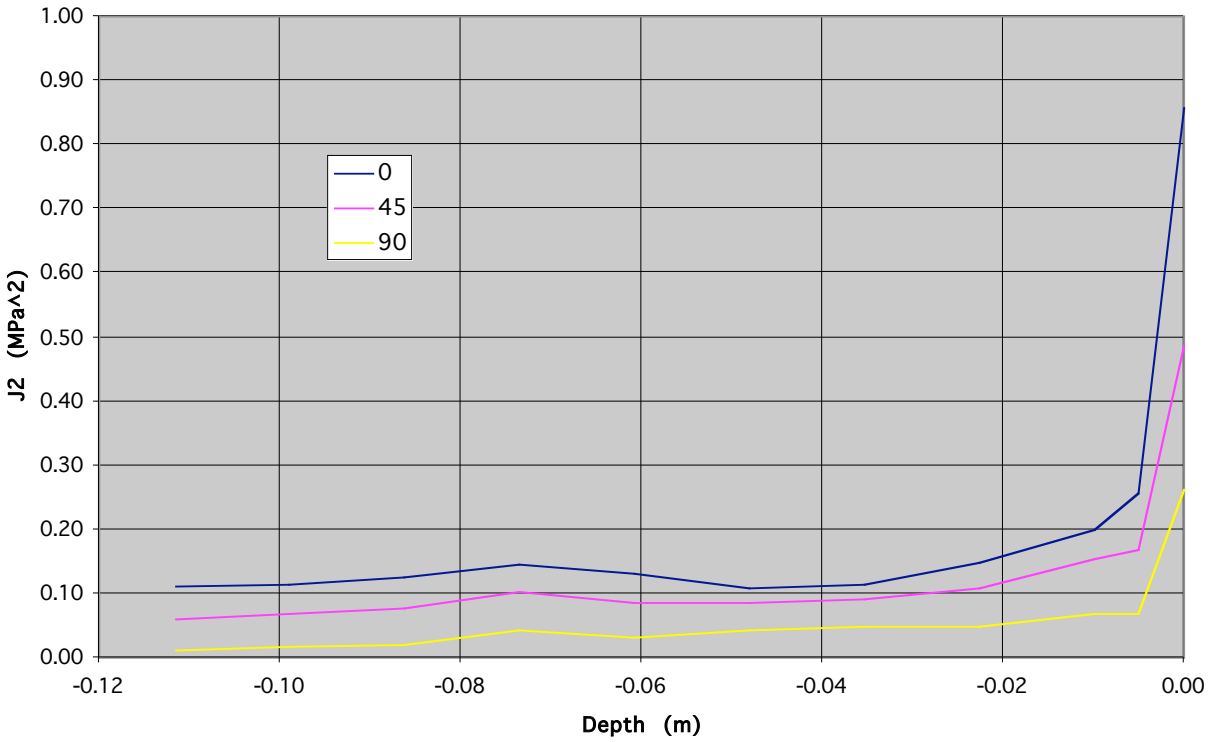

Figure 6.55: J_2 vs. depth; traffic loading (S23); Fairbanks locale; S4.

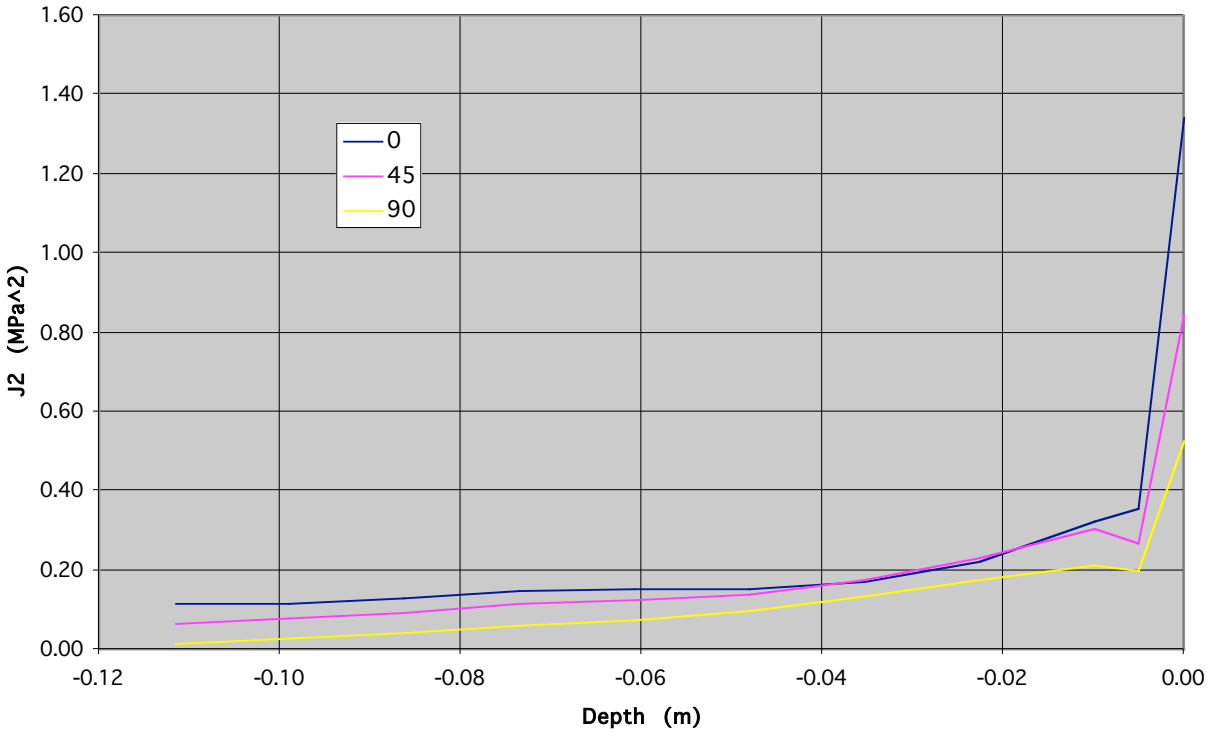

Figure 6.56: J_2 vs. depth; traffic loading (S23); Palmdale locale; S4.

6.7 S5 pavement system

S5 pavement is very different from the previous four pavements discussed above in two crucial ways. First, the magnetic plugs are not located at the surface. Because the magnitude of all stress components diminishes with the distance from the location where the loads are applied, stresses due to traffic loading are smaller for the current configuration compared with placing the magnets near the surface, as was the case for pavements S1 through S4.

Second, the AC overlay acts as a bridge over the thermal joints. The continuity of the slabs leads to two important outcomes. First, the deformed geometry is concave in the lateral direction, and convex in the longitudinal direction for the Fairbanks locale (Figure 6.57), and the reverse for the Palmdale locale (Figure 6.58). This geometry contrasts with that observed for structures of type S3/S4 where the same curvature was observed in both directions (see Figures 6.39 and 6.40), and with that observed for the S1/S2 pavements where the pavement had no curvature in the longitudinal direction.

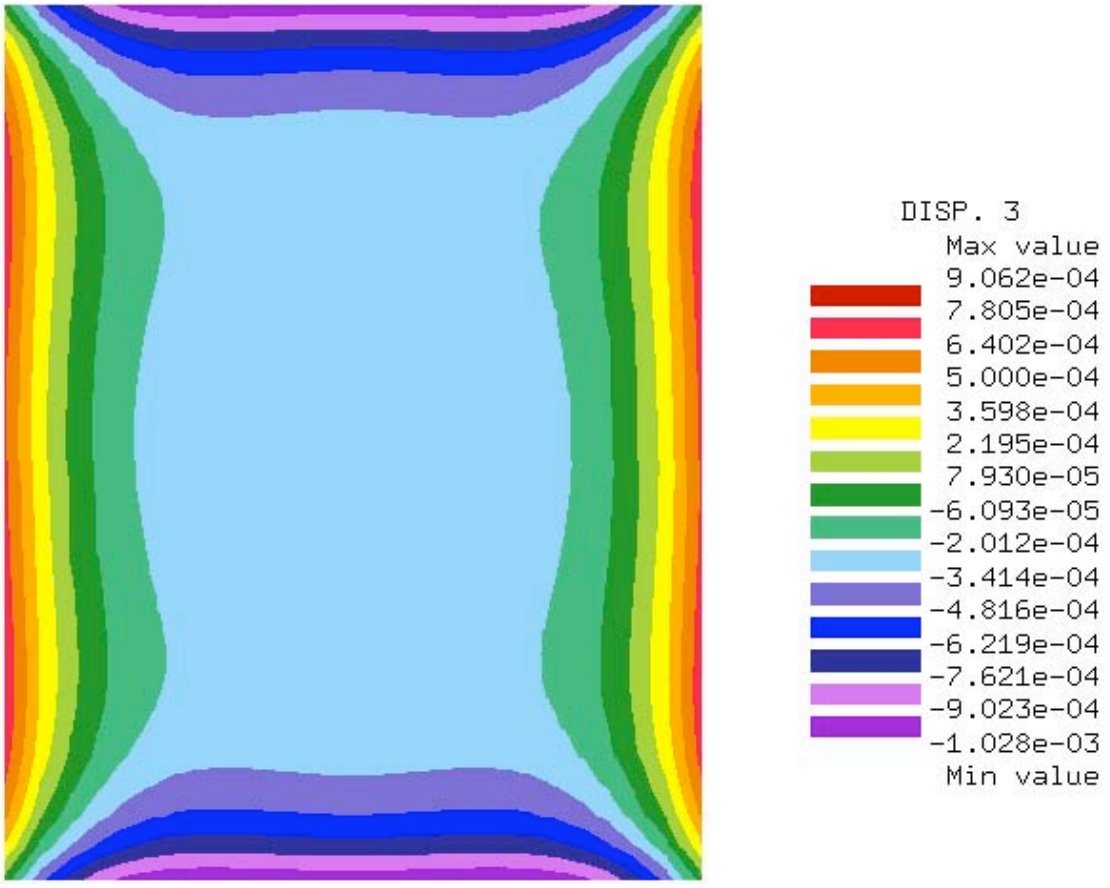

Figure 6.57: Vertical displacement contours; plan view (AC surface); S5; Fairbanks locale.

A second outcome of the slab continuity is that the thermal stresses for the S5 pavement are considerably higher than those for the original PCC pavement (*i.e.*, S3 and S4 pavements). Moreover, maximal thermal stresses in the S5 pavement develop near the thermal joints, and not near the magnetic plug as is the case for the pavements discussed above. To illustrate this point,

Figures 6.59 through 6.62 show I_1 and J_2 contour plots in plan view for both Fairbanks and Palmdale locales.

Figures 6.63 through 6.70 showing line plots of I_1 and J_2 at three locations along the circumference complete the review of the S5 pavement. Finally, as with the previous pavements, more information is available on the accompanying CD.

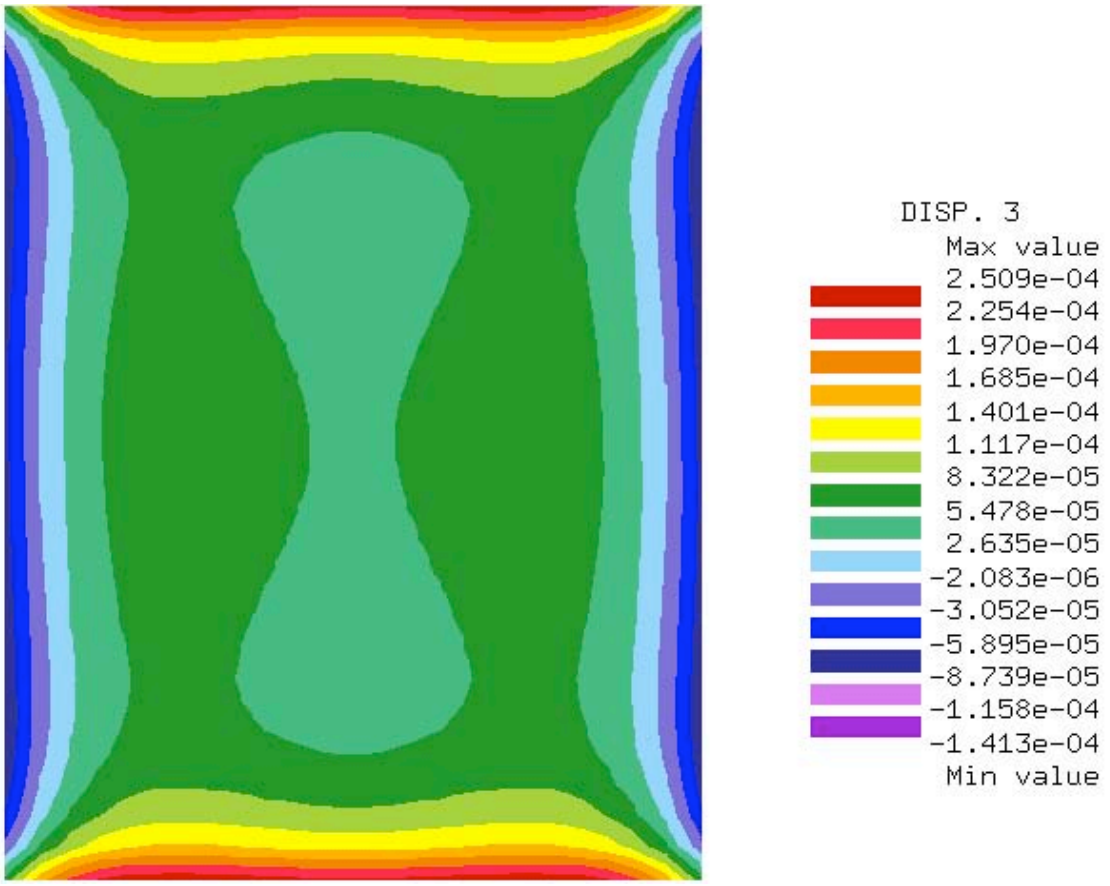

Figure 6.58: Vertical displacement contours; plan view (AC surface); S5; Palmdale locale.

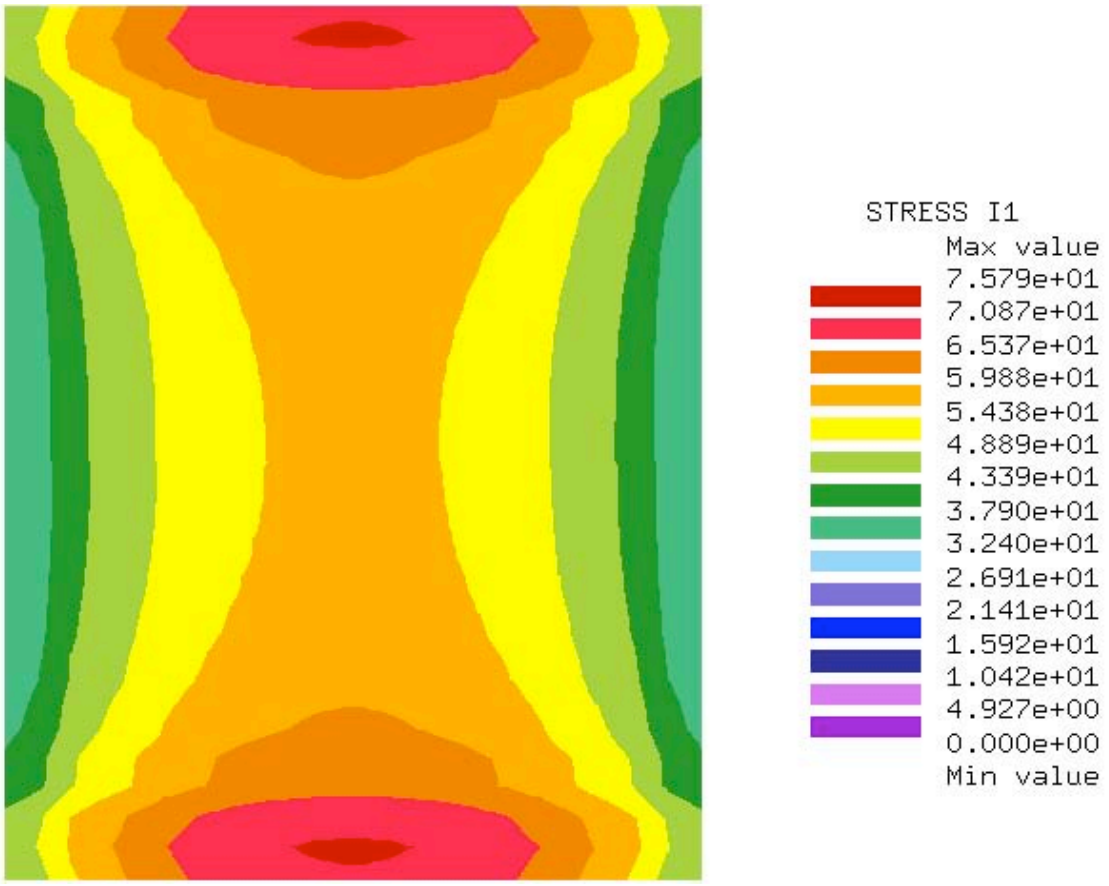

Figure 6.59: Contours of I_1; plan view (AC surface); S5; Fairbanks locale.

Figure 6.60: Contours of I_1 in plan view (AC surface); S5; Palmdale locale.

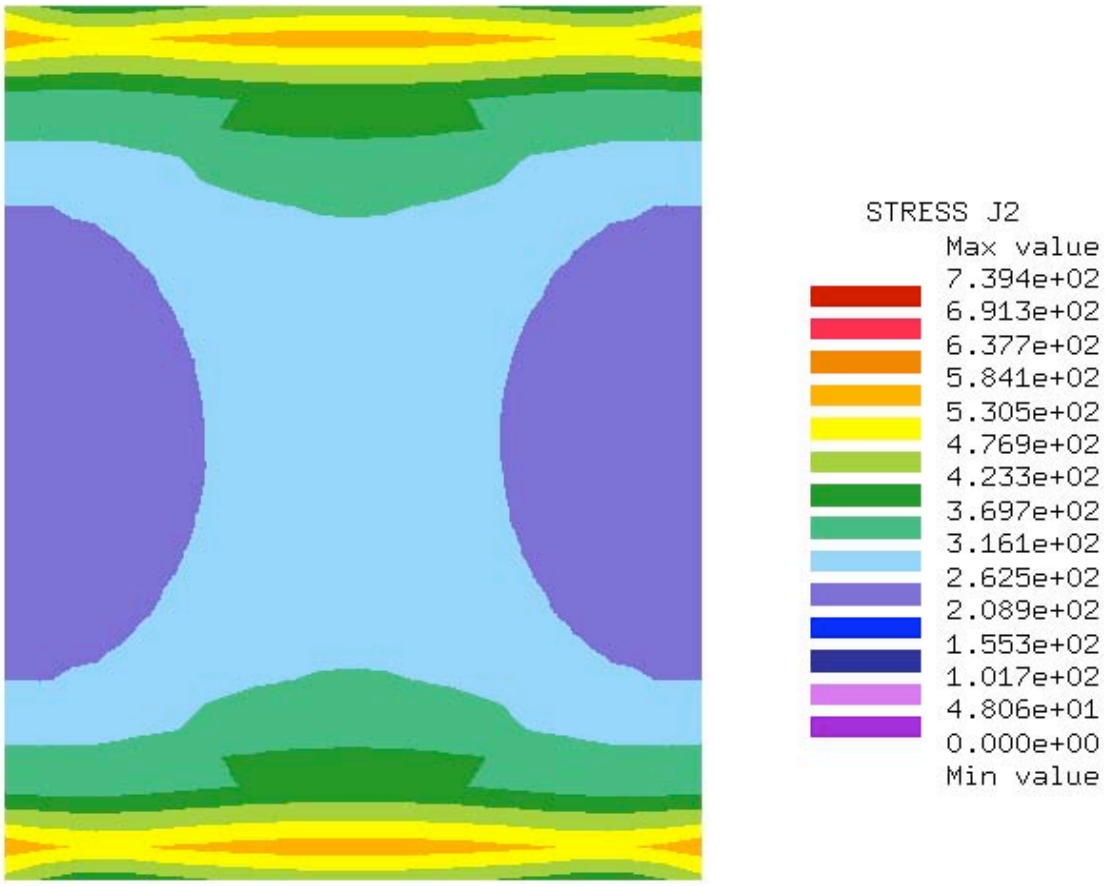

Figure 6.61: Contours of J_2 in plan view (AC surface); S5; Fairbanks locale.

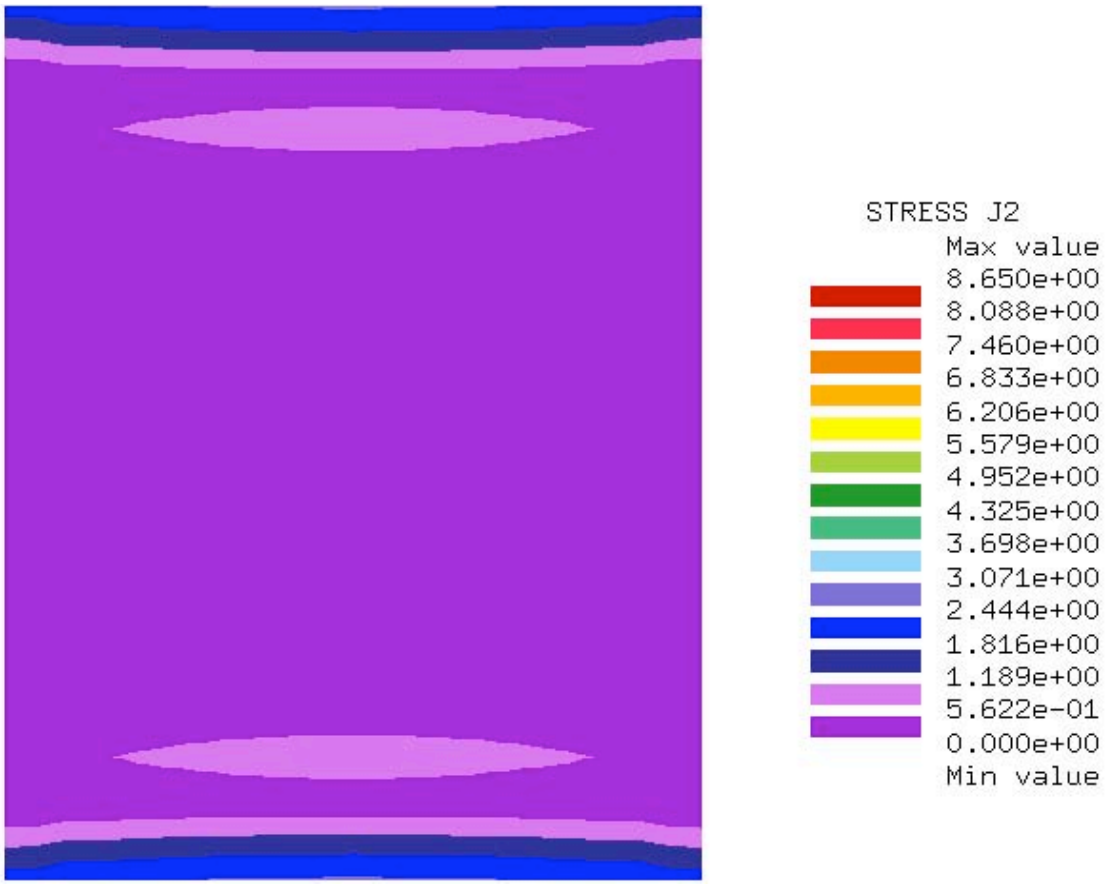

Figure 6.62: Contours of J_2 in plan view (AC surface); S5; Palmdale locale.

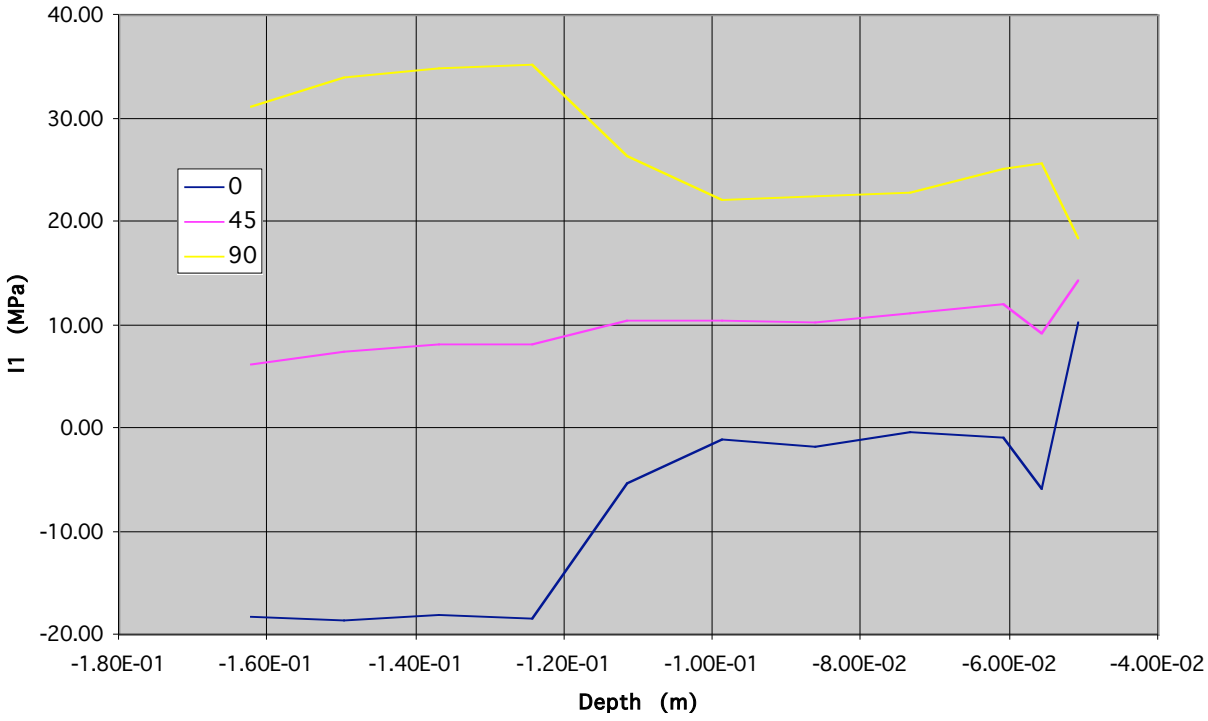

Figure 6.63: I_1 vs. depth; thermal loading; Fairbanks locale; S5.

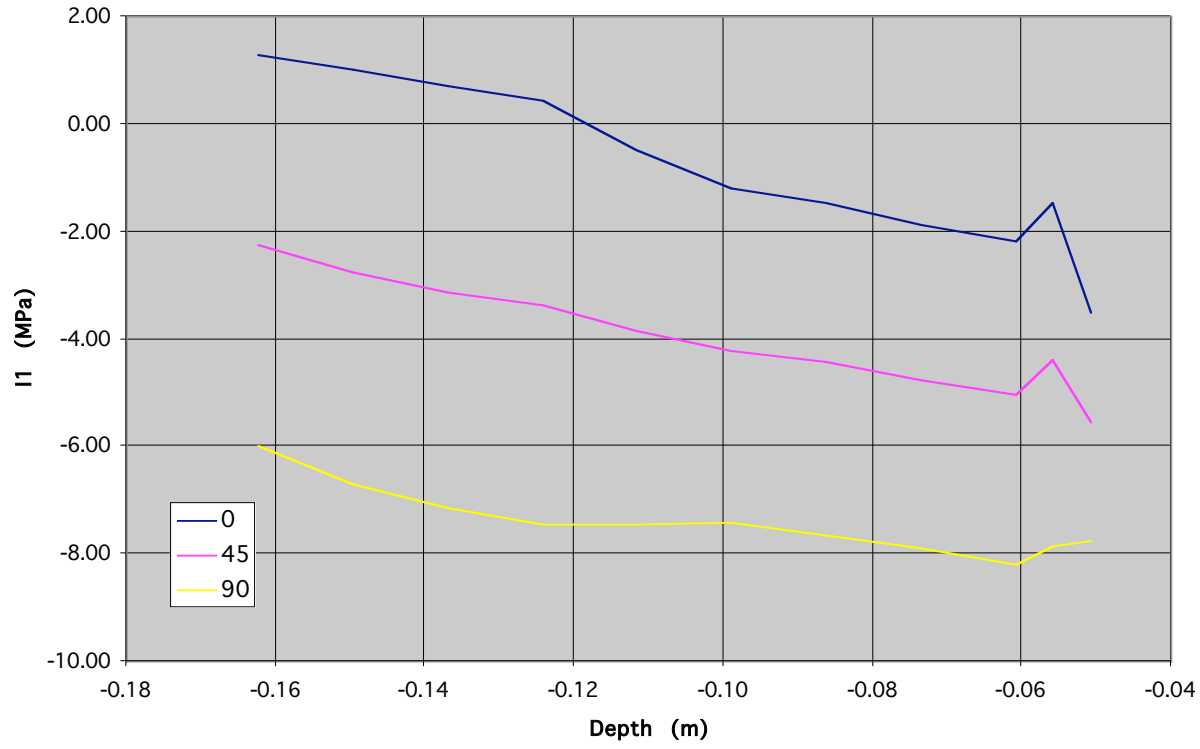

Figure 6.64: I_1 vs. depth; thermal loading; Palmdale locale; S5.

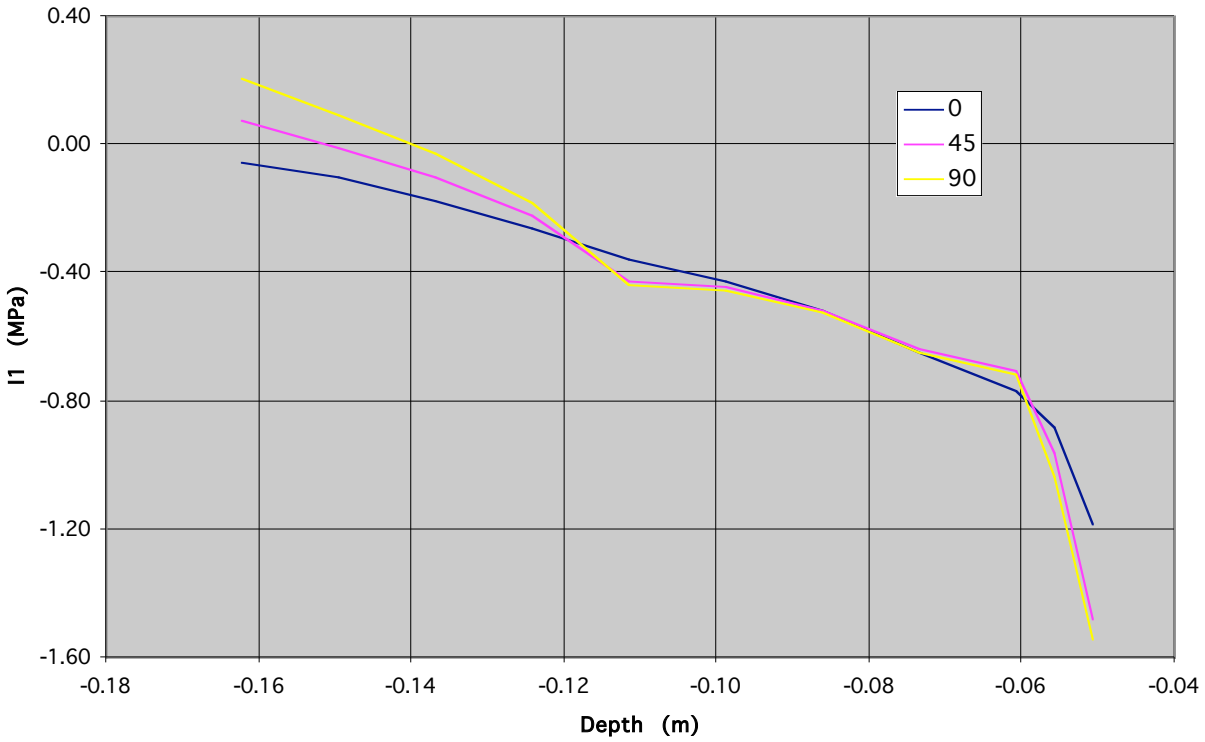

Figure 6.65: I_1 vs. depth; traffic loading (S23); Fairbanks locale; S5.

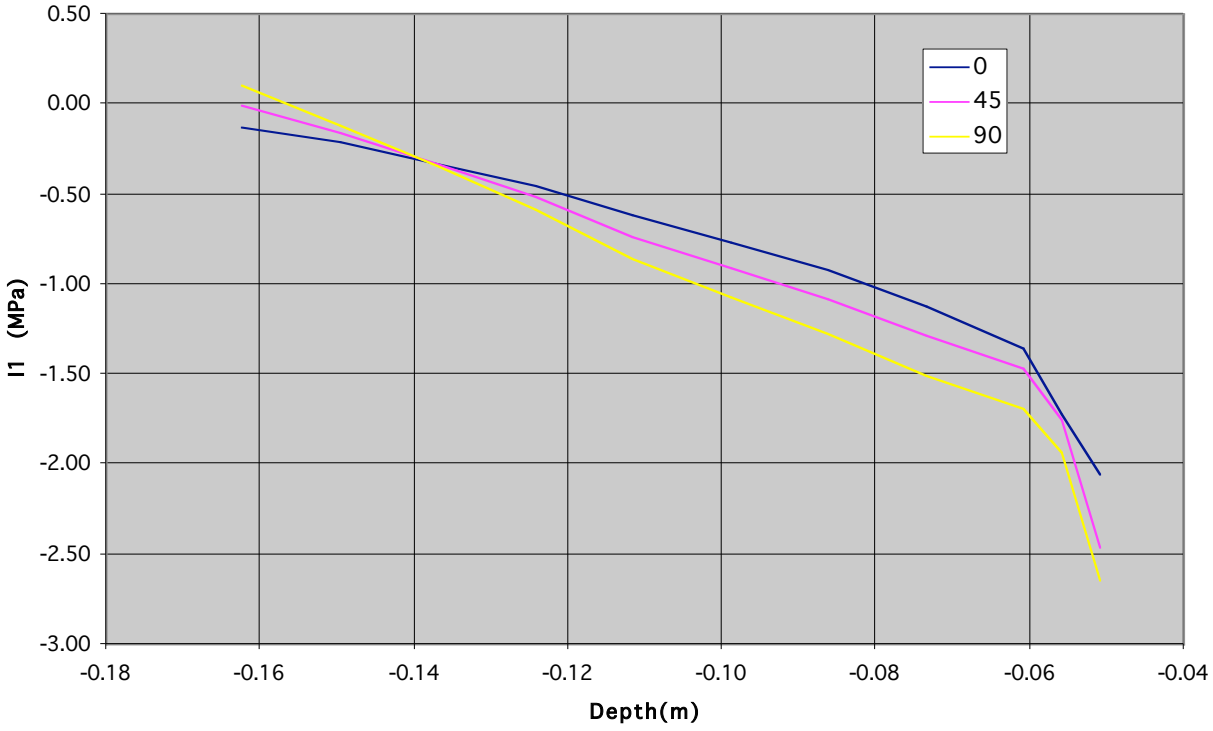

Figure 6.66: I_1 vs. loading; traffic loading (S23); Palmdale locale; S5.

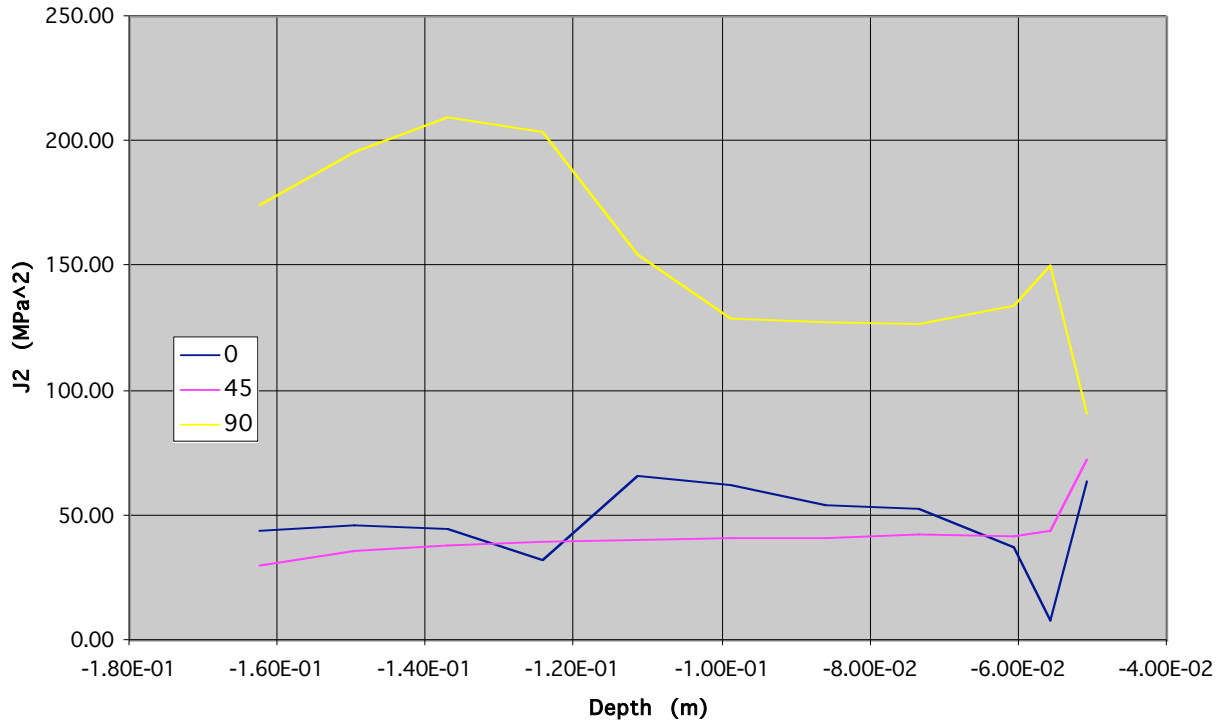

Figure 6.67: J_2 vs. depth; thermal loading; Fairbanks locale; S5.

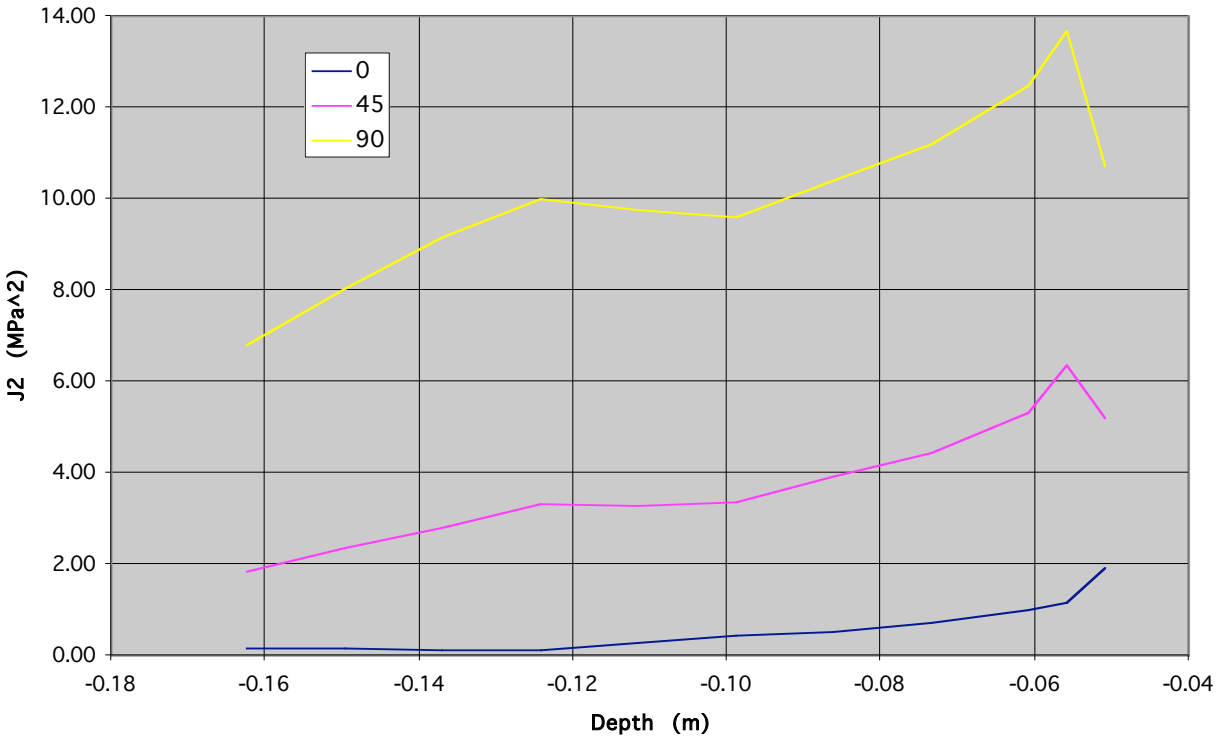

Figure 6.68: J_2 vs. depth; thermal loading; Palmdale locale; S5.

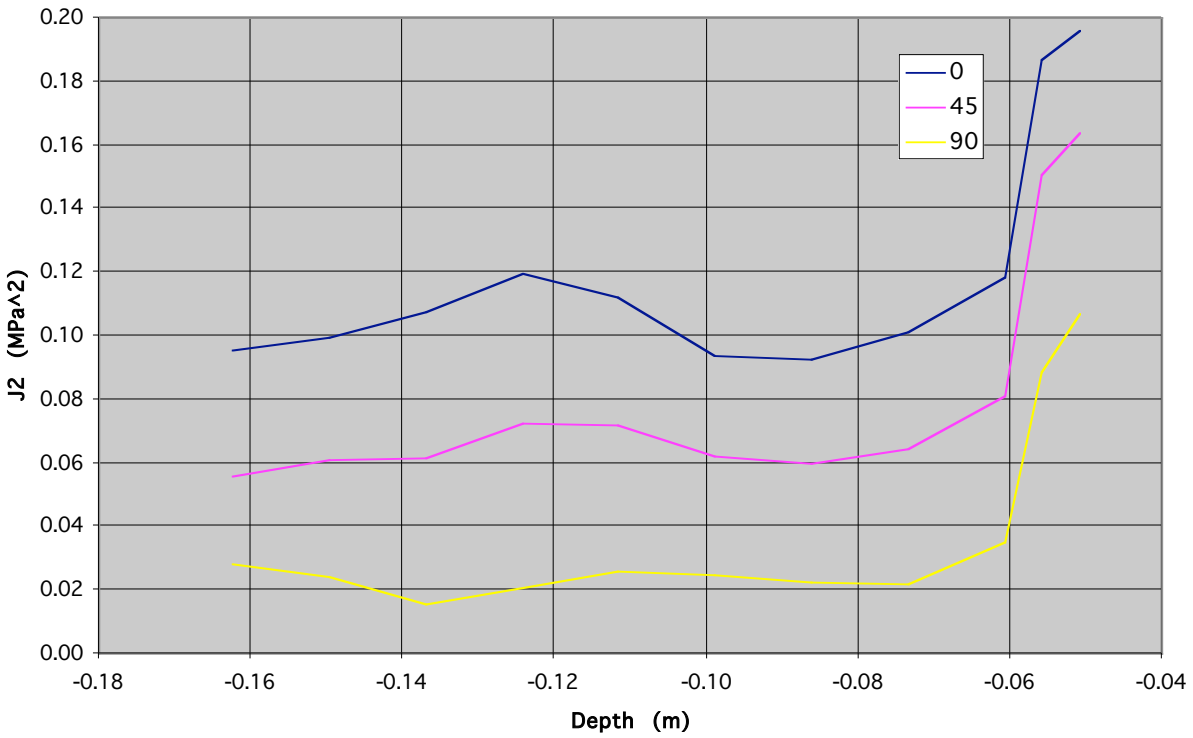

Figure 6.69: J_2 vs. depth; traffic loading (S23); Fairbanks locale; S5.

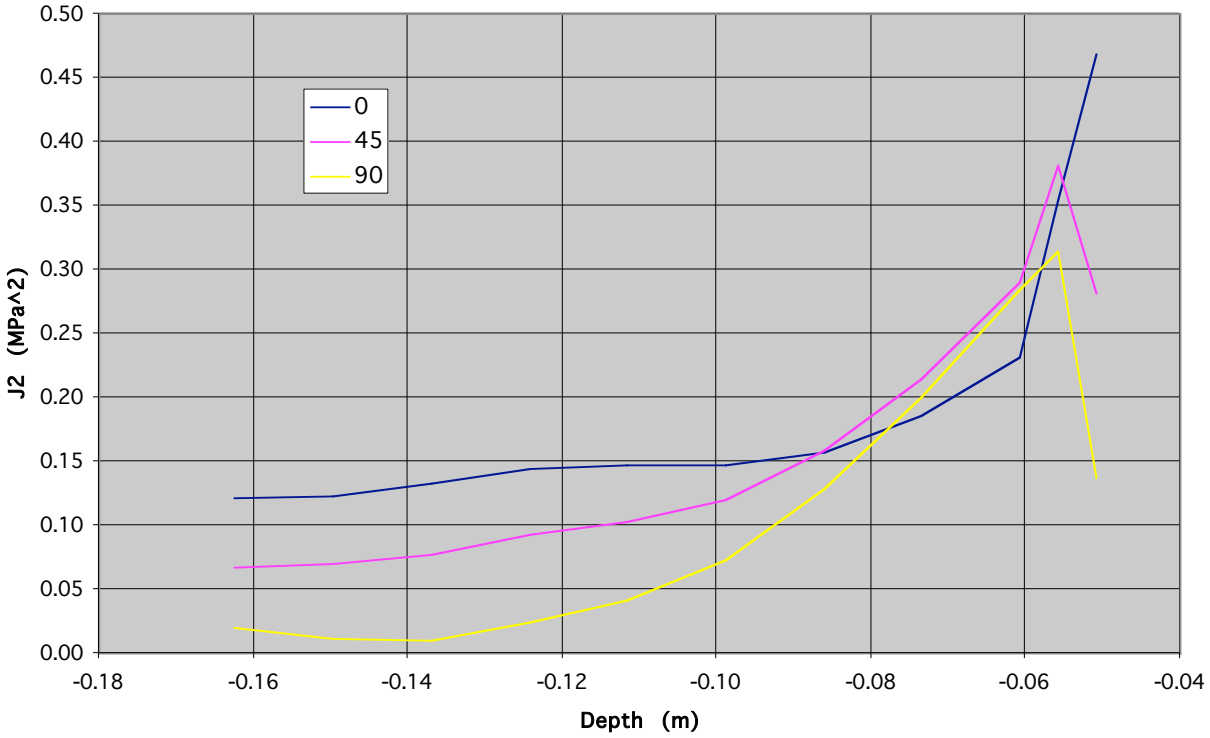

Figure 6.70: J_2 vs. depth; traffic loading (S23); Palmdale locale; S5.

7. Conclusions and Recommendations

This study evaluates the effect of inserting magnetic plugs into the surface layer of pavements. Specifically, the objective is to quantify the stress concentrations that are introduced into the pavement in the vicinity of the plugs. Knowing the stress levels induced is essential in order to be able to determine the service life of the pavements. The results of the finite element simulations detailed in this report indicate that the stresses near the plugs may be as much as three times as high as the levels away from the plugs. This result is consistent with classical results of stress concentrations near a circular hole. Therefore, the presence of the magnetic plugs may have an adverse impact on the service life of pavements.

Two types of loading are considered in the report: traffic loading and thermal loading. With respect to traffic loading, it was determined that for a vehicle traveling in a lane (*i.e.*, the plugs are aligned with the transverse center of the vehicle), the stresses near the plugs are significantly smaller then those in the vicinity of the tires. Consequently, even when the stress concentration resulting from the presence of magnetic plugs is considered, the magnetic plugs do not affect the projected service life of pavements. However, when a vehicle is changing lanes, one set of tires may come close to the magnetic plug, and the higher stresses may adversely affect the pavement. With this respect it is important to note that damage to pavements is a function of the number of load repetitions, and therefore some statistical analysis should be undertaken to assess the relevance of the higher stress during lane-changing on the longevity of the pavement service life.

The presence of magnetic plugs is much more relevant to the analysis of the effect of thermal loading. With the exception of the S5 pavement, the highest stresses are recorded at the interface between the pavement and the magnetic plugs (*i.e.*, along the walls of the drilled cavity). Consequently, it is likely that thermal cracking would initiate near the plugs. This suggests the need to better optimize the plugs-epoxy cap installation in terms of their geometry and materials. Moreover, the pavement-plugs system should be analyzed for each climate zone, and the "optimal" designs may vary from one locale to the next.

This report focuses primarily on the pavement side. However, the results of the simulations can also be used to investigate both the magnetic plugs and epoxy. To this end, animations of stresses on the surfaces of the plug and epoxy cap are provided in the accompanying CD.[18]

Under the limitations of the current study, a single geometry of the magnetic plugs and their installation is considered. This case may not be representative of what is happening in the field because the assumption taken regarding the depth to which the epoxy penetrates may not reflect true installations. Therefore, Symplectic Engineering proposes a finite element study to try and identify an "optimal" magnetic plug shape and installation. In this study, the shape of the magnetic plug (*i.e.*, height and radius), the shape of the drilled cavity, and the way the magnets are kept in place (*i.e.*, the epoxy layer) would be varied in a parametric study to achieve an optimized design. As was already noted above, the optimal design may depend on the climate in which the system resides and therefore, the optimization should be done for each climate zone where installing plugs is considered.

[18] Extreme stresses for both the magnetic plugs and epoxy caps appear on their surfaces.

One aspect that was not included at all in the present study is the presence of freezing water, and the stresses that the expanding ice may locally induce in the pavement, the magnetic plug, and epoxy cap. Moreover, because of the cyclic nature of freezing and thawing, the presence of water may result in fatigue failure. Additionally, the presence of moisture may affect the mechanical properties of the epoxy and thus, change the pavement-plug interface. Therefore, the effect of moisture should be considered as part of the finite element study proposed above.

Another issue that was ignored in the current study is aging. This issue may be of great importance because stress concentrations at the interface between the plug and the pavement critically depend on the properties of the plug, pavement, and epoxy. For example, if the epoxy stiffens with time, then the stresses at the interface between a PCC pavement and the plug will diminish because the difference between the stiffness of the PCC and epoxy will have diminished. Thus, aging effects should also be included in the finite element study proposed above.

Finally, a case where the plug is removed from the drilled cavity should also be studied. Such a case could represent a worst-case scenario, and is definitely an effect during the, hopefully short period, between the time of drilling and the time the plugs are installed.

References

De Beer, M. and C. Fisher, [1997], "Contact Stresses of pneumatic Tires Measured with the Vehicle-Road Surface Pressure Transducer Array (VRSPTA) system for the University of California at Berkeley (UCB) and the Nevada Automotive Test Center (NATC)," CSIR report No. CR-97/053.

Monismith, C.L., [2002], private communications.

Timoshenko, S.P. and J.N. Goodier, [1970], Theory of Elasticity, McGraw-Hill Book Company, New York.